

**UNIVERSITAT POLITÈCNICA DE VALÈNCIA**

**INSTITUTO INTERUNIVERSITARIO DE RECONOCIMIENTO  
MOLECULAR Y DESARROLLO TECNOLÓGICO**



**New nanostructured supports with signal  
amplification features for the detection of  
molecules and biomolecules of interest**

**PhD. THESIS**

Submitted by

**Luis Pla Blasco**

PhD. Supervisors:

**Prof. Ramón Martínez Máñez**

**Prof. Félix Sancenón Galarza**

València, Enero 2021

La tesis está sujeta a convenio de confidencialidad y limitación de difusión de resultados, autorizado por la COMISIÓN PERMANENTE del COMITÉ DE DIRECCIÓN de la ESCUELA DE DOCTORADO con fecha 04/11/2020.

Por ello, el capítulo 5 y toda mención a los resultados de este trabajo han sido eliminados.

The thesis is subject to a confidentiality agreement and limitation of dissemination of results, authorized by the PERMANENT COMMITTEE of the DIRECTING COMMITTEE of the DOCTORAL SCHOOL on 11/04/2020.

For this reason, chapter 5 and any mention of the results of this work have been eliminated.

La tesi està subjecta a conveni de confidencialitat i limitació de difusió de resultats, autoritzat per la COMISSIÓ PERMANENT del COMITÈ DE DIRECCIÓ de l'ESCOLA DE DOCTORAT amb data 2020.11.04.

Per això, el capítol 5 i tot esment als resultats d'aquest treball han estat eliminats.



UNIVERSITAT  
POLITÈCNICA  
DE VALÈNCIA

RAMÓN MARTÍNEZ MÁÑEZ, PhD in Chemistry and Professor at the *Universitat Politècnica de València*, and FÉLIX SANCENÓN GALARZA, PhD in Chemistry and Professor at the *Universitat Politècnica de València*.

CERTIFY:

That the work ***“New nanostructured supports with signal amplification features for the detection of molecules and biomolecules of interest”*** has been developed by LUIS PLA BLASCO under their supervision in the Instituto Interuniversitario de Investigación de Reconocimiento Molecular y Desarrollo Tecnológico (IDM) at *Universitat Politècnica de València*, as a Thesis Project in order to obtain the degree of PhD in Chemistry at the *Universitat Politècnica de València*.

València, 05 Octubre 2020.

Prof. Ramón Martínez Máñez

Prof. Félix Sancenón Galarza



*“No reconocer como verdadero sino lo evidente,  
dividir cada dificultad en cuantas porciones sea  
preciso para mejorar atacarlas,  
comenzar el análisis por el examen de los objetos  
más simples y más fáciles de ser comprendidos,  
para remontarse gradualmente al conocimiento de  
los más complejos”*

*Descartes*



## Agraïments:

Arribar a escriure els agraïments d'una tesi doctoral implica la imminent finalització d'aquesta. Nervis i goig es mesclen, com si d'una dissolució es tractara (un poc de pedanteria no queda mai malament), per demostrar la valia del treball realitzat durant tant de temps i per llevar-te el pes de damunt, tot siga dit.

En primer lloc, voldria agrair a Ramón, com a cap de grup i director de tesis, que comptara amb mi fa tant de temps per participar en el seu grup d'investigació i que confiara amb mi per a dur a terme totes les tasques que m'ha encomanat. El treball al llarg d'aquests quasi 6 anys m'ha permès aprendre molt sobre ciència, però també sobre altres temes de gran importància en el món laboral com la gestió de projectes i les relacions laborals. Totes les coses tenen les seues llums i les seues ombres, però en termes general, estic molt orgullós del tracte que he rebut i el que he professat a totes les persones en què m'he creuat en aquest viatge. Gràcies per aquesta oportunitat.

Félix, moltes gràcies pel teu recolzament i consell 24 hores durant els 365 dies de l'any, i per la teua infinita disposició a ajudar-nos sempre en tot allò que estava al teu abast, especialment realitzant correccions ràpides i eficaces. La teua ajuda facilita enormement el treball i es cosa d'agrair.

Moltes gràcies a Elena pel seu consell i ajuda per publicar els resultats que s'han obtingut. Gràcies també a la gent de la tercera planta Eva, Arantxa i Tania per l'ajuda que he tingut d'elles en els tràmits burocràtics que han fet falta i per la divertida gestió de compres (*nótese la ironia*) que hem compartit els darrers anys.

Com que la llista de persones que han passat pel laboratori és infinita, vull agrair de forma general a tota la gent en què m'he creuat al laboratori 2.6, la CPI i el CIPF, tant si hem col·laborat professionalment o no, perquè de segur hem tingut un moment de conversació i companyerisme que es mantindrà en el record. De forma més especial per l'amistat que hem forjat i l'estima que ens uneix, vuic agrair als meus companys Irene, Bea, Alba, JuanFran, Adrián, Elisa, Cristina de la Torre e Iris tots els moments que hem compartit dins i fora del

laboratori, de tot el que ens hem rist, ballat, cantat i gaudit. Espere que continuem sumant molts més moments com aquests any rere any. Gràcies per tot!

Aquesta tesis, sens dubte, no haguera resultat sense el **COMANDO FE**. Sara i M<sup>a</sup> Carmen, vos agraiisc enormement la vostra inestimable ajuda, intel·ligència, professionalitat i perseverança incansable, però sobretot l'estima i els valors que m'heu transmés. Us dessitge la millor de les fortunes, personals i professionals, perquè a la gent com vosaltres sols deuen passar-los coses bones. Ojalà haja sigut capaç de transmetre-vos tot el respecte i estima que us professe.

A les noves incorporacions al COMANDO, Isa, Marina y Nieves, teniu molt de treball per davant però una bona base sobre la que treballar. Ànim, ho aconseguireu!

Com no podia ser d'altra manera, vull agrair a la meua família la seua ajuda i estima. Moltes gràcies per donar-me el vostre suport en totes les decisions i accions que he emprés al llarg de la meua vida, laboral i professional. Em sent afortunat de tindre-vos i orgullós de tot el que he fet gràcies a la vostra ajuda i estima. No podria tindre una família millor.

Lorena, tu eres el pilar fonamental que em suporta, el far que il·lumina el camí a seguir i l'amor que dona sentit a la meua vida. Gràcies per ser, estar, comprendre, valorar, ajudar i estimar. Com fa uns mesos et vaig dir, t'estimaré fins que el món s'acabe i no quede res per estimar.

I finalment, vull dedicar aquest treball a Pablo, Lucas, Martín i especialment, a Arnau. Gràcies per omplir-nos de felicitat!. Que aquesta tesi doctoral siga un exemple per a vosaltres del treball, diligència, dedicació i perseverança que ha d'estar present en les vostres vides.



## Resum:

La present tesi doctoral, titulada “*New nanostructured supports with signal amplification features for the detection of molecules and biomolecules of interest*”, es centra en el disseny i preparació de nous materials híbrids orgànics-inorgànics constituïts per portes moleculars suportades sobre alúmina mesoporosa amb l’objectiu de desenvolupar nous sistemes sensors amb potencials aplicacions en el camp de la diagnosi i del control alimentari.

En el primer capítol de la tesi s’introdueixen els conceptes en què estan basats els estudis realitzats i els materials preparats. D’aquesta forma es comenten les bases de la química supramolecular i del reconeixement molecular, la síntesi y la funcionalització de la alúmina mesoporosa, els materials híbrids orgànic-inorgànics i l’aplicació d’aquests en processos de reconeixement. A continuació, en el segon capítol es descriuen els objectius generals de la tesi que seran abordats en els següents apartats.

En el tercer capítol es presenta en detall el disseny i optimització d’un nanodispositiu per a la detecció de la bactèria *Mycoplasma fermentans*. Aquesta bactèria pot produir infeccions en l’ésser humà, i és un contaminant habitual en cultius cel·lulars. Primerament, els porus d’una placa d’alúmina mesoporosa són carregats amb un indicador fluorescent (rodamina B). Seguidament, la superfície és funcionalitzada amb una seqüència d’ADN complementaria a una regió altament conservada de la subunitat ribosomal 16S de la bactèria *Mycoplasma fermentans*. L’impediment estèric generat per les seqüències d’ADN ancorades a l’exterior dels porus impedeix l’alliberament de l’indicador encapsulat. Únicament en presència d’ADN de la bactèria *Mycoplasma fermentans*, es produeix l’obertura dels porus permetent la difusió de la càrrega (rodamina B) que és posteriorment mesurada mitjançant espectroscòpia de fluorescència.

En el capítol quatre es porta a terme el disseny i optimització d’un nanodispositiu capaç de detectar de forma ràpida, sensible i selectiva la bactèria *Staphylococcus aureus*. Per a la preparació del material sensor, el suport d’alúmina mesoporosa és, primerament, carregat amb l’indicador fluorescent rodamina B. A continuació, els porus del suport són tapats

mitjançant l'ancoratge d'un aptàmer que reconeix de forma específica a la bactèria. Solament en presència de *Staphylococcus aureus* es produeix l'alliberament de l'indicador encapsulat, que és posteriorment mesurat mitjançant espectroscòpia de fluorescència. El dispositiu desenvolupat permet reduir els temps de detecció de *Staphylococcus aureus*. Mentre que els mètodes estàndard necessiten entre 48-72 hores, el mètode que nosaltres proposem tarda 1 hora. A més a més, la resposta obtinguda és específica per *Staphylococcus aureus*. Aquest sistema ha sigut validat mitjançant l'anàlisi de mostres reals provinents del servei de microbiologia de l'Hospital Politècnic i Universitari La Fe de València.

En el sisè capítol, es detalla el disseny i optimització d'un nanodispositiu híbrid orgànic-inorgànic consistent en un material d'alúmina mesoporosa cobert amb una seqüència d'ADN específica per a la detecció de l'ADN del fong *Pneumocystis jirovecii*, principal causant de la pneumònia *Pneumocystis*. En aquest cas, el suport d'alúmina carregat amb l'indicador fluorescent rodamina B és recobert amb una seqüència d'ADN específica per al reconeixement d'aquest fong i que presenta una conformació en forma de forquilla que inhibeix l'alliberament del indicador. En presència de l'organisme, la forquilla híbrida amb l'ADN del fong, resultant en una conformació *triplex* amb elevada afinitat i estabilitat, que indueix, al mateix temps, el desplaçament d'aquest complex de la superfície. Com a conseqüència d'aquest reconeixement la càrrega és alliberada i quantificada mitjançant espectroscòpia de fluorescència. El sistema ha sigut satisfactòriament validat com a mètode diagnòstic mitjançant l'anàlisi de mostres reals de pacients provinents del Servei de microbiologia de l'Hospital Politècnic i Universitari de La Fe de València.

En el seté capítol, l'interès de la tesi gira cap al sector de la seguretat i control alimentari mitjançant el disseny i desenvolupament d'un sistema sensor amb la capacitat de detectar gluten de forma ràpida i senzilla en extractes d'aliments processats i no processats. Per a això, un suport d'alúmina mesoporosa es carrega amb indicador fluorescent rodamina B i posteriorment és recobert amb un aptàmer específicament dissenyat per a la detecció de la proteïna gliadina, que constitueix el 50 % del total del clúster d'elements que formen el gluten. L'elevada afinitat i especificitat entre l'aptàmer i la proteïna

en qüestió fa que en presència d'aquesta es produeix un desplaçament de la porta molecular que permet la difusió de la càrrega encapsulada i que serà finalment monitoritzada mitjançant espectroscòpia de fluorescència.

Finalment, en el capítol vuité es discuteixen de manera conjunta els resultats obtinguts en els capítols anteriors i la potencial aplicació dels sistemes desenvolupats en l'actual sistema sanitari i de control alimentari.

Els sistemes desenvolupats en aquesta tesi pretenen avançar en el camp dels sensors aplicats a la diagnosi i a la seguretat alimentaria. Es tracta de sistemes amb elevada sensibilitat i especificitat, són ràpids i econòmics, y no requereixen mans experimentades a la volta que poden ser fàcilment transportats per a realitzar els assajos en el lloc de mostreig. Tots els sensors han sigut validats en mostres reals, reflectint la robustesa dels sistemes desenvolupats. Alguns dels materials descrits han sigut patentats i s'espera serveixen de model pel desenvolupament de nous mètodes d'anàlisi.

## Resumen:

La presente tesis doctoral titulada “*New nanostructured supports with signal amplification features for the detection of molecules and biomolecules of interest*” se centra en el diseño y preparación de nuevos materiales híbridos orgánicos-inorgánicos constituidos por puertas moleculares soportadas sobre alúmina mesoporosa con el objetivo de desarrollar nuevos sistemas sensores con aplicaciones potenciales en el campo de la diagnosis y del control alimentario.

En el primer capítulo de la tesis se introducen los conceptos en los que están basados los estudios realizados y los materiales preparados. De esta forma se comentan las bases de la química supramolecular y del reconocimiento molecular, la síntesis y funcionalización de la alúmina mesoporosa, los materiales híbridos orgánico-inorgánicos y la aplicación de estos en procesos de reconocimiento. A continuación, en el segundo capítulo se describen los objetivos generales de la tesis que serán abordados en los siguientes apartados.

En el tercer capítulo se presenta en detalle el diseño y optimización de un nanodispositivo para la detección de la bacteria *Mycoplasma fermentans*. Esta bacteria puede producir infecciones en el ser humano, y es un contaminante habitual en cultivos celulares. En primer lugar, los poros de una placa de alúmina mesoporosa se cargan con un indicador fluorescente (rodamina B). Seguidamente, la superficie es funcionalizada con una secuencia de ADN complementaria a una región altamente conservada de la subunidad ribosomal 16S de la bacteria *Mycoplasma fermentans*. El impedimento estérico generado por las secuencias de ADN ancladas al exterior de los poros impide la salida del indicador encapsulado. Únicamente en presencia de DNA de la bacteria *Mycoplasma fermentans*, se produce la apertura de los poros permitiéndose la difusión de la carga (rodamina B) que es posteriormente medida mediante espectroscopía de fluorescencia.

En el capítulo cuatro se lleva a cabo el diseño y optimización de un nanodispositivo capaz de detectar de forma rápida, sensible y selectiva la bacteria *Staphylococcus aureus*. Para la preparación del material sensor, un

soporte de alúmina mesoporosa es, en primer lugar, cargado con el indicador fluorescente rodamina B. A continuación, los poros del soporte son tapados mediante el anclaje de un aptámero que reconoce de forma específica la bacteria. Solamente en presencia de *Staphylococcus aureus* se produce la liberación del indicador encapsulado, que es posteriormente medido mediante espectroscopía de fluorescencia. El dispositivo desarrollado permite reducir los tiempos de detección de *Staphylococcus aureus*. Mientras que métodos estándar empleados necesitan entre 48-72 horas, nuestro método propuesto tarda 1 hora. Además, la respuesta obtenida es específica para *Staphylococcus aureus*. Este sistema ha sido ensayado en muestras reales provistas por el servicio de microbiología del Hospital Politècnic i Universitari La Fe de València.

En el sexto capítulo, se detalla el diseño y optimización de un nanodispositivo híbrido orgánico-inorgánico consistente en un material de alúmina mesoporosa cubierto con una secuencia de ADN específica para la detección de ADN del hongo *Pneumocystis jirovecii*, principal causa de la neumonía *Pneumocystis*. En este caso, el soporte de alúmina cargado con rodamina B se recubre con una secuencia de ADN específica para el reconocimiento de este hongo y que presenta una conformación en forma de horquilla que inhibe la liberación del indicador. En presencia del organismo, la horquilla híbrida con el ADN del hongo, lo que resulta en una conformación *triplex* con elevada afinidad y estabilidad que induce, al mismo tiempo, el desplazamiento de este complejo de la superficie. Como consecuencia de este reconocimiento la carga se libera y es cuantificada mediante espectroscopía de fluorescencia. El sistema ha sido satisfactoriamente validado como método de diagnóstico mediante el análisis de muestras reales de pacientes provenientes del Servicio de Microscopía del Hospital Politècnic i Universitari La Fe de València.

En el séptimo capítulo, el interés de la tesis gira hacia el sector de la seguridad y control alimentario mediante el diseño y desarrollo de un sistema sensor con la capacidad de detectar gluten de forma rápida y sencilla en extractos de alimentos procesados y no procesados. Para ello, un soporte de alúmina mesoporosa se carga con rodamina B y los poros se recubren con un aptámero específicamente diseñado para la detección de la proteína gliadina,

que constituye el 50 % del total del clúster de elementos que forman el gluten. La elevada afinidad y especificidad entre el aptámero y la proteína en cuestión hacen que en presencia de ésta se produzca un desplazamiento de la puerta molecular que permite la difusión del colorante encapsulado que es finalmente monitorizado mediante espectroscopía de fluorescencia.

Finalmente, en el capítulo octavo se discuten de forma conjunta los resultados obtenidos en los capítulos anteriores y la potencial aplicación de los sistemas desarrollados en el actual sistema sanitario y de control alimentario.

Los sistemas desarrollados en esta tesis pretenden avanzar en el conocimiento en el campo de los sensores aplicados a la diagnosis y a la seguridad alimentaria. Se trata de sistemas con elevada sensibilidad y especificidad, son rápidos y económicos, y no requieren manos experimentadas para su manejo, a la vez que pueden ser fácilmente transportados para realizar los ensayos en el lugar de muestreo. Todos los sensores han sido validados con muestras reales, reflejando la robustez de los sistemas desarrollados. Algunos de los materiales descritos se han patentado y se espera que sirvan de modelo para el desarrollo de nuevos métodos de análisis.

## Abstract:

The PhD thesis hereby presented and entitled “*New nanostructured supports with signal amplification features for the detection of molecules and biomolecules of interest*”, focuses in the design and preparation of new hybrid organic-inorganic materials constituted by molecular gates supported over mesoporous alumina with the aim of developing new sensor probes of potential applications in the fields of diagnosis and food control.

In the first chapter, the concepts in which studies and prepared materials are based, are introduced. In this way, the bases of supramolecular chemistry and molecular recognition, the synthesis and functionalization of mesoporous alumina, the concept of hybrid organic-inorganic materials and their applications for recognition processes, are commented. Next, the second chapter describes the general objectives of this thesis, which will be approached in the following sections.

In the third chapter, it is presented in detail the design and optimization process of a nanodevice applied for the detection of *Mycoplasma fermentans* bacterium. This bacterium may cause infections in humans and is a habitual contamination in cell cultures. First of all, mesoporous alumina porous films are charged with a fluorescent indicator (rhodamine B). Then, the surface is functionalized with a DNA sequence complementary to a highly conserved region of the 16S ribosomal subunit of the bacterium *Mycoplasma fermentans*. Steric hindrance generated by DNA sequences on the surface inhibits the release of the encapsulated indicator. Only in the presence of bacterium *Mycoplasma fermentans* DNA, molecular gates open, allowing payload diffusion to the solution, which is measured by fluorescence spectroscopy.

In chapter four, it is carried out the design and optimization of a nanodevice able to detect *Staphylococcus aureus* bacterium in a fast, sensitive and selective way. For the sensor preparation, alumina mesoporous support is, first, loaded with the rhodamine B fluorescent dye. Then, the mesoporous are blocked through the attachment of an aptamer that recognises specifically this bacterium. Exclusively in the presence of *Staphylococcus aureus* it is accomplished the release of the encapsulated dye, which is later monitored by

fluorescence spectroscopy. The developed nanodevice allows diminishing the time for *Staphylococcus aureus* detection. While employed standardized methodologies require 48-72 hours, our proposed method takes 1 hour. Moreover, the response obtained is specific for *Staphylococcus aureus*. This system has been validated in real samples provided by the microbiology department of Hospital Politècnic I Universitari La Fe de València.

In the sixth chapter, it is detailed the design and optimization process of a hybrid organic-inorganic nanodevice based on a capped mesoporous alumina material for the detection of *Pneumocystis jirovecii* fungus DNA, which is the main cause of *Pneumocystis* pneumonia. In this case, the mesoporous alumina support is loaded with a fluorescent dye and decorated with a specific oligonucleotide sequence designed for the recognition of *Pneumocystis* fungus, which presents a fork-like conformation that inhibits indicator releasing. In the presence of the target organism, the fork-like oligonucleotide hybridises with the DNA of the fungus, which results in the adoption of a *triplex* conformation with high affinity and stability that induces, at the same time, the displacement of this complex from the surface. Consequently, the payload diffused to the solution is quantified through fluorescence spectroscopy. The system has been successfully validated as a diagnostic method through the analysis of samples provided by the microbiology department of Hospital Politècnic I Universitari de La Fe of València.

In the seventh chapter, the focus turns to security and food control applications by means of designing and developing a sensor system for gluten detection, in a quick and easy way, in processed and non-processed food extracts. For this, a mesoporous alumina support is loaded with the fluorescent dye rhodamine B, and later was functionalized with an aptamer specifically designed for the detection of *gliadin*, a protein that constitutes 50 % of average cluster elements that forms gluten. The protein-aptamer high affinity and specificity induce the displacement of the capping aptamer and cargo delivery, which is monitored through fluorescence spectroscopy.

Finally, in the eighth chapter, the results obtained in the previous chapters and the potential application of the systems developed as health and food control system are discussed.



The developed systems exposed in this thesis aim to advance knowledge in the field of sensors for diagnosis and food control applications. These are systems with high sensitivity and specificity, they are fast and inexpensive, and do not require experienced hands to handle, while they can be easily transported to carry out the tests at the sampling site. All of them have been validated with real samples, which account for the robustness of the developed systems. Some of these reported works have been protected by patents, and it is expected that they became models for the developing of new analytical methods.



## Publications:

The results presented in the thesis set out below, as well as other contributions have given rise to the following scientific publications:

**Luis Pla**, Elisabet Xifré-Pérez, Àngela Ribes, Elena Aznar, M. Dolores Marcos, Lluís F. Marsal, Ramón Martínez-Máñez and Félix Sancenón; A *Mycoplasma* Genomic DNA Probe using Gated Nanoporous Anodic Alumina. *ChemPlusChem*, **2017**, *82*, 337-341.

Eva Garrido, **Luis Pla**, Beatriz Lozano-Torres, Sameh El Sayed, Ramón Martínez-Máñez and Félix Sancenón; Chromogenic and Fluorogenic Probes for the Detection of Illicit Drugs. *ChemistryOpen*, **2018**, *7*, 401-428. (Review)

**Luis Pla**, Beatriz Lozano-Torres, Ramón Martínez-Máñez, Felix Sancenón and Jose V. Ros-Lis; Overview of the Evolution of Silica-Based Chromo-Fluorogenic Nanosensors. *Sensors*, **2019**, *19*, 5138-5151. (Review)

**Luis Pla**, Sara Santiago-Felipe, María Ángeles Tormo-Mas, Javier Pemán, Félix Sancenón, Elena Aznar and Ramón Martínez-Máñez. Aptamer-capped nanoporous anodic alumina for *Staphylococcus aureus* detection. *Sensors & Actuators: B. Chemical*, **2020**, *320*, 128281.

**Luis Pla**, Anna Aviñó, Ramón Eritja, Alba Ruiz-Gaitán, Javier Pemán, Vicente Friaza, Enrique J. Calderón, Elena Aznar, Ramón Martínez-Máñez and Sara Santiago-Felipe. Triplex hybridization-based nanosystem for the rapid screening of *Pneumocystis pneumonia* in clinical samples. *Journal of Fungi*, **2020**, *6*, 292.

### Submitted publications:

**Luis Pla**, M. Ángeles Tormo-Mas, Alba Ruiz-Gaitán, Javier Pemán, Eulogio Valentín, Félix Sancenón, Elena Aznar, Ramón Martínez-Máñez and Sara Santiago-Felipe. Oligonucleotide-capped nanoporous anodic alumina biosensor for the rapid detection of *Candida auris* infection. Submitted to *Emerging Microbes and Infections*.

**Luis Pla**, M. Carmen Martínez-Bisbal, Elena Aznar, Félix Sancenón, Ramón Martínez-Máñez and Sara Santiago-Felipe. A fluorogenic capped

mesoporous aptasensor for Gluten detection. Submitted to *Analytica Chemical Acta*.

Iris Garrido-Cano, **Luis Pla**, Sara Santiago-Felipe, Soraya Simón, Belen Ortega, Begoña Bermejo, Ana Lluch, Juan Miguel Cejalvo, Pilar Eroles and Ramón Martínez-Máñez. Nanoporous anodic alumina-based sensor for miR-99a-5p detection as an effective early breast cancer diagnostic tool. Submitted to *ACS Sensors*.

**Luis Pla**, Félix Sancenón, M. Carmen Martínez-Bisbal, Celia Bañuls, Nuria Estañ, Guillermo Sáez, Ramón Martínez-Máñez and Sara Santiago-Felipe. New 8-oxo-7,8-2'-deoxyguanosine nanoporous anodic alumina aptasensor for colorectal cancer diagnosis in blood and urine. Submitted to *Nanoscale*.

**Luis Pla**, Félix Sancenón, M. Carmen Martínez-Bisbal, Ricardo Prat-Acín, Inma Galeano Senabre, Sarai Palanca-Suela, Elena Aznar, Ramón Martínez-Máñez and Sara Santiago-Felipe. A Nanoporous Anodic Alumina immunosensor for in-tissue detection of IDH1-R132H mutation in gliomas. Submitted to *ACS Sensors*.

Patent application:

**Luis Pla Blasco**, Sara Santiago-Felipe, Elena Aznar Gimeno, Ramón Martínez Máñez, Juan Salvador Frasquet Artes, Amparo Valentín Martín, Javier Pemán García, María Ángeles Tormo Mas. "Método para la detección y diagnóstico rápido de *Staphylococcus aureus*". Presentado el 27-04-2020. En fase de evaluación por la OEPM (P202030356).

Sara Santiago Felipe, **Luis Pla Blasco**, María Ángeles Tormo Mas, Elena Aznar Gimeno, Alba Cecilia Ruiz Gaitán, Eulogio Valentín Gómez, Javier Pemán García, Ramón Martínez Máñez. "Método para la detección rápida de *Candida auris* y el diagnóstico de la infección causada por este patógeno". Presentado el 27-04-2020. En fase de evaluación por la OEPM (P20203057).

## Abbreviations and Acronyms:

### A

AAO	Aluminium anodic oxide
ALD	Atomic layer deposition
ATP	Adenosine 5'-triphosphate
APTES	(3-Aminopropyl)triethoxysilane
AuNPs	Gold anoparticles

### B

BAL	Bronchoalveolar lavage
BET model	Brunauer, Emmet and Teller model
BG	(1,3)- $\beta$ -D-glucan
BJH model	Barret, Joyner and Halenda model
BPA	Bisphenol A
BPC	Bisphenol C
BPE	Bisphenol E
BHI	Brain heart infusion

### C

CD	Celiac disease
CD-GOx	Cyclodextrin-modified glucose oxidase
CE	European comission
CIBER-BBN	Centro de Investigación Biomedical En Red de Bioingeniería, Biomateriales y Nanomedicina
CPG	Controlled pore glass
CTABr	Cetyltrimethylammonium bromide
CRS	Cozart® rapid scan
c.a.	Approximately
CSF	Cerebrospinal fluid
CVD	Chemical vapour deposition

### D

Dint	Interpore distance
------	--------------------

DNA	Deoxyribonucleic acid
DLS	Dinamyc light scatering
DNP	1,5-Dioxynaphthalene
Dp	Nanopore diameter
DTAB	Dodecyltrimethylammoniuym bromide
DOPC	1,2-Dioleoyl-sn-glycero-3-phosphocholine
<b>E</b>	
EXC	Excitation
EDTA	Ethylendiaminetetraacetic acid
ELISA	enzyme-linked immunosorbent assay
<b>F</b>	
FDA	Food and drug administration
FESEM	Field emission scanning electronic microscopy
FITC	Fluorescein isothiocyanate
FT-IR	Fourier transform infrared radiation
<b>G</b>	
GC	Gas chromatography
GO	Graphene oxide
Gox	Glucose oxidase
<b>H</b>	
H	Hours
HA	Hard anodisation
HPLC	High pressure liquid chromatography
<b>I</b>	
ICMUV	Institut de Ciència dels Materials, Universitat de València
ICPTS	3-(Triethoxysilyl)propyl isocyanate
IDM	Instituto de Reconocimiento Molecular y Desarrollo Tecnológico
i.e.	In essence

IUPAC	International union pure ans applied chemistry
ITS	Internal transcriber spacer
<b>L</b>	
LC	Liquid chromatography
LDH	Lactate deshydrogenase
LOD	Limit of detection
<b>M</b>	
MA	Mild anodisation
Min	Minutes
MCM	Mobil cristallyne material
ME	Mercaptoethanol
mRNA	Micro RNA
MS	Mass spectrometry
MSNs	Mesoporous silica nanoparticles
MALDI-TOF	Matrix-assisted laser desorption/Ionization time-Of-flight
<b>N</b>	
NAA	Nanoporous anodic alumina
NMOF	Nano-metal-organic framework
NPA	Nasopharyngeal aspirate
<b>O</b>	
OTA	Ochratoxin A
OD	Optical dichroism
<b>P</b>	
P	Pression
PCP	<i>Pneumocystis</i> pneumonia
PEG	Polyethylene glycol
PLGA	Polylactic-co-glycolic acid
PMOs	Periodic mesoporous organosilicas
PNIPAAm	N-Isopropylacrylamide polymer

P0	Absolute pression
Ppm	Parts per million
PXRD	Power X-Ray diffraction
PBS	Phosphate buffer saline
PCR	Polymerase chain reaction
PTI	Photon technology international
PWG	European prolamin working group

## Q

QCM	Quartz crystal microbalance
-----	-----------------------------

## R

RNA	Ribonucleic acid
SELEX	Systematic evolution of ligands by exponential enrichment
Rpm	Revolutions per minute

## S

SAM	Adenosylmethionine
SAMs	Self-assembled monolayers
STDA	Structure-directing agent
SMS	Silica mesoporous support
RhB	Rhodamine B
SDS	Sodium dodecyl sulfate
SPR	Surface plasmon resonance

## T

T	Temperature
TATP	Triacetone triperoxide
TCEP	Tris (2-carboxyethyl)phosphine
TEA	Triethylamine
TEM	Transmission electron microscopy
TEOS	Tetraethylorthosilicate
TGA	Thermogravimetric analysis



TLCT	True liquid crystal
TMOS	Tetramethylorthosilica
TRIS	Tris(hydroxymethyl)aminomethane
TE	TRIS-EDTA
TSA	Tryptic soy agar

**U**

UV	Ultraviolet
UVM	Universidad Valencia material
UFC	Unite forming colony

**V**

V	Volt
---	------

**Y**

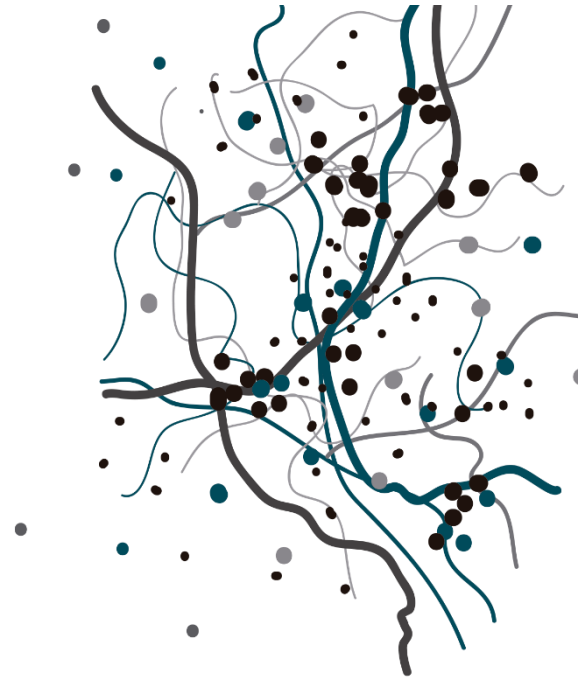
YPD	Yast extract peptone dextrose
-----	-------------------------------



## Table of contents

<b>Resum</b>	<b>i</b>
<b>Resumen</b>	<b>iv</b>
<b>Abstract</b>	<b>vii</b>
<b>Publications</b>	<b>xi</b>
<b>Table of Contents</b>	<b>1</b>
<b>1. General Introduction</b>	<b>5</b>
1.1. Supramolecular chemistry	<b>5</b>
1.2. Molecular recognition	<b>6</b>
1.3. Nanotechnology: A step forward towards future molecular sensors	<b>13</b>
1.4. Organic-inorganic hybrid porous materials	<b>15</b>
1.4.1. Types of porous materials	<b>17</b>
1.4.1.1. Nanoporous anodic alumina	<b>18</b>
1.5. Gated materials	<b>33</b>
1.5.1. Sensing applications	<b>42</b>
1.5.2. Pathogens: Problems & perspectives	<b>56</b>
1.5.3. Food control. Bringing security to consumer	<b>59</b>
<b>2. Objectives</b>	<b>63</b>
<b>3. A <i>Mycoplasma</i> genomic DNA probe using gated nanoporous anodic alumina</b>	<b>67</b>
<b>4. Aptamer-capped nanoporous anodic alumina for <i>Staphylococcus aureus</i> detection</b>	<b>89</b>
<b>5. Oligonucleotide-capped nanoporous anodic alumina biosensor for the rapid detection of <i>Candida auris</i> infection</b>	<b>113</b>
<b>6. Triplex hybridization-based nanosystem for the rapid screening of <i>Pneumocystis pneumonia</i> in clinical samples</b>	<b>117</b>
<b>7. A fluorogenic capped mesoporous aptasensor for gluten detection</b>	<b>149</b>
<b>8. Summary of Results and General Discussion</b>	<b>175</b>





# 1

## General Introduction



## 1.1 Supramolecular Chemistry.

Everything we have around us, all we can see, hear, taste, smell, or even touch, is chemistry or imply some chemical process. Indeed, our most primary senses are a final result of millions of complex and intricate chemical reactions inside our body. Thus, if we want to know the world we live in and how we interact with it, we must immerse into the deep sea of chemistry and dive from the simple certainties in the surface to the un-knowledge of the bottom.

Chemistry is based on the construction and/or destruction of molecular entities with the aim of reach a more stable state. The force that set the direction of whole chemical processes is the achievement of the state with the lowest energy, and this may consist on the formation of new chemical bonds or in the break of the existent ones.

In 1960, researchers Pedersen, Cram and Lehn introduced for the first time the concept of “*Supramolecular Chemistry*”, whose development was rewarded in 1987 with the Nobel Prize. This new area of knowledge is colloquially defined as “*chemistry beyond the molecule*” because it focuses on the behaviour of “*supermolecules*”, a new term coined by Dr Lehn himself, to name organized chemical entities of higher complexity that result from the association of two or more chemical species held together by intermolecular forces.<sup>1</sup> Between these forces are included hydrogen bonding, hydrophobic forces, metal coordination, van der Waals forces, electrostatic effects and  $\pi$ - $\pi$  stacking interactions,<sup>2</sup> which are weak, noncovalent and reversible interactions that may be modulated.

Inspiration for the continuous development of supramolecular chemistry is nature itself. Some examples of complex nanostructures essential for life and with biological origin that have been the basis of mimicked synthetic systems are enzymatic reactions, proteins interactions with substrates, immunological antigen-antibody associations, signal neurotransmission, intermolecular

---

<sup>1</sup> J. M. Lehn, *Supramolecular Chemistry*, Ed. VCH, Weinheim, **1995**; J. M. Lehn, Nobel lecture, **1987**.

<sup>2</sup> J. L. Atwood, J.L. Steed, *Encyclopaedia of Supramolecular Chemistry*, 1<sup>st</sup> Ed. Taylor & Francis Group, New York, **2004**.

reading, translation and transcription of the genetic code, oxygen transport, etc.<sup>3</sup> But, not only the inspiration by nature has led to a rapid development of this field. From the beginning, potential applications such as sensor nanotechnology and medical diagnosis have been associated with supramolecular chemistry and molecular recognition,<sup>4</sup> which have definitely contributed to its study.

Supramolecular chemistry applications are deeply related to the size of the target molecular system. Generally, systems designed for sensing applications are small, relatively simple and require the interaction of limited number of molecules, while those for the construction of complex molecular assemblies might be made from countless numbers of molecules, and therefore, interactions.<sup>5</sup> This is the case of the synthesis of sophisticated structures such as mesoporous materials.

Supermolecules are special because they have abilities and/or properties that cannot be provided individually by the entities that form them, thus, their integration, for example with mesoporous materials, may contribute to the development of new functional materials that can be really useful in a wide range of fields.

## 1.2 Molecular Recognition.

Supramolecular chemistry is generally based on the interaction between two or more molecules which formed a supramolecular aggregate through the use of non-covalent forces. Taking into account this fact, "*molecular recognition*" is a crucial concept that deserves attention. Long before supramolecular chemistry was defined, there existed a branch of knowledge commonly known as host-guest chemistry that focused on the study of molecules that could recognize other molecules. At this respect, a "*host*" molecule is a chemical entity able to recognize other species which are called "*guest*". The interaction between a host and a guest (molecular recognition) is

---

<sup>3</sup> K. Ariga, T. Kunitake, *Supramolecular Chemistry – Fundamentals and application*, 1<sup>st</sup> Ed., Springer-Verlag, Heidelberg, 2006.

<sup>4</sup> D. N. Reinhoudt, Reference Module in Chemistry, *Molecular Sciences and Chemical Engineering*, 2013.

<sup>5</sup> K. Ariga, Supermolecules, *Biomaterials Nanoarchitectonics*, 2016.



mainly driven by the formation of a supramolecular ensemble (or supermolecule) with a lower energy state than that of the individual components. Besides, host and guest must have mutual spatial and electronic complementary binding sites, following the key-lock principle (Figure 1). This principle indicates that host binding site must be thoroughly complementary in size and shape to the guest site. As Jean-Marie Lehn said in his Nobel lecture, “*Mere binding is not recognition, although it is often taken as such. Recognition is binding with a purpose, like receptors are ligands with a purpose. It implies a structurally well-defined pattern of intermolecular reactions*”.<sup>6</sup>



**Figure 1:** Scheme of molecular recognition event by a specific host-guest interaction.

One of the main applications of molecular recognition, and also of supramolecular chemistry, is the development of “*molecular sensors*”. According to their definition, a “*sensor*” is a device that detects, record, and indicates a physical or chemical property. Hence, a “*molecular sensor* or *chemosensor*” are chemical entities with the ability of detecting molecules of interest (analytes) at very low concentrations. Analogously to supramolecular chemistry, the design of molecular sensors and their main components are sometimes inspired on natural reactions and processes undertaken by living organisms. In a biological environment, these living beings can report the presence of analytes through biomolecular recognition, and so have been set as the basis of molecular sensors. Those organisms show specialized recognition mechanisms to detect a broad range of molecules, such as nutrients and toxins, as well as biomolecular interactions such as metabolic activities,

<sup>6</sup> J.-M. Lehn, *Supramolecular Chemistry – Scope and perspectives – Molecules, Supermolecules and Molecular Devices. Nobel Lecture*, 8 December 1987.

glucose levels and hormones.<sup>7</sup> The resulting sensors are a technology with truly high potential, as witnessed by the annual multibillion-dollar investment from both small and medium-sized enterprises (SMEs) as well as large pharmaceutical and chemicals companies for the development of chemosensors. Some of their main applications are summarized in Table 1.<sup>8</sup>

**Table 1:** Application areas of sensors.

---

»	Biomedical, diagnostic ( <i>in vivo</i> ):
•	Glucose monitoring in diabetes patients.
•	Body fluids screening for disease detection.
•	Other physical parameters that are related to activities of molecules (temperature, voltage, pressure, light intensity).
»	Biomedical ( <i>ex vivo</i> ):
•	Blood screening.
•	Drug discovery and evaluation.
•	Protein engineering in biosensors.
»	Environmental and safety:
•	River water (detection of pesticides, heavy metal ions).
•	Air pollution (gas, particulate matter).
•	Explosive detection.
•	Gas monitoring.
»	Food related:
•	Drinking water.
•	Allergens (egg, wheat, gluten, milk, tree, nuts, shellfish, soy).
•	Determination of drug residues (antibiotic, growth promoters).

---

---

<sup>7</sup> J. Zhang and K. Hoshino, *Molecular Sensors and Nanodevices*, Elsevier Inc., **2014**.

<sup>8</sup> E.L. Que, D.W. Domaille, C.J. Chang, *Chem. Rev.*, **2008**, *108*, 1517–1549.

Chemical sensors (or chemosensors) combine both molecular recognition events with the generation of a readable signal to sense the presence of the guest,<sup>9</sup> and are generally composed by, at least, two subunits (Figure 2):

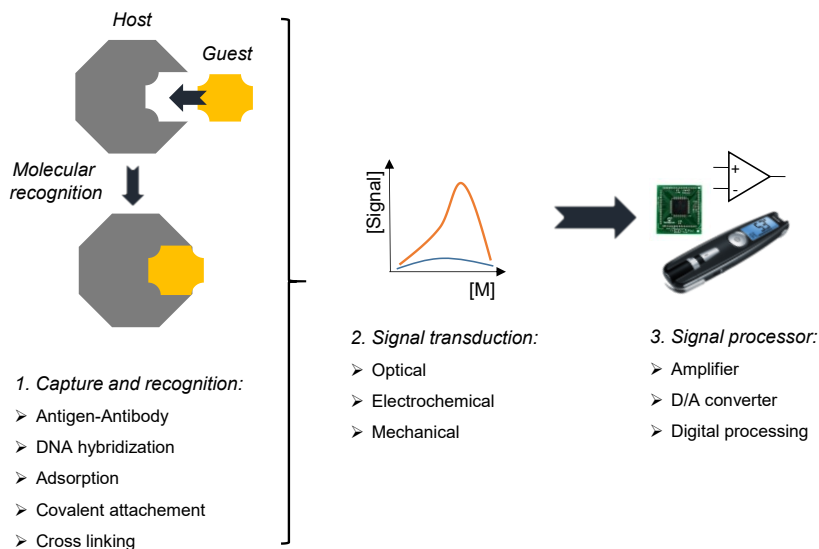


**Figure 2:** Elements of a chemosensor.

- » **Recognition subunit:** This is the part designed for the interaction between molecules and is responsible of the specificity and sensitivity of the recognition process. This interaction, or binding, induces the sensing event, thus, requiring a high degree of complementarity between both receptor and target in terms of size, shape, electrostatic charge, etc. Ideally, this subunit must provide: (a) interaction only with the target analyte (selectivity), (b) induce marked changes in the signalling unit in the presence of the lowest amount of target (sensitivity), (c) these changes must be directly related with the amount of target analyte (resolution) and (d) in a broad range of concentrations (dynamic range).

<sup>9</sup> W.C Rogers, M.O. Wolf, *Coord. Chem. Rev.*, **2002**, 233, 341-350; b) S. Akine, F. Utsuno, S. Piao, H. Orita, S. Tzusuki, T. Nabeshima, *Inorg. Chem.*, **2006**, 55, 810-821.

- » **Signalling subunit:** This part refers to the transduction or conversion of the detection event (microscopic level) into a measurable signal (macroscopic output), and may be a change in physical or chemical parameters such as absorption or fluorescence variations, redox processes or electrochemical reactions. The best chemical sensors are those with high sensitivity and resolution.

Among the different transduction methodologies applied for the development of chemical sensors, chromo-fluorogenic (optical) changes are appealing and, for this reason, deserved special attention. In these chromo-fluorogenic sensors, the recognition event induces changes in the absorption or emission spectra of the signalling subunit (shifts of the wavelengths or changes in the intensity of the bands).<sup>10</sup> Taking into account these facts, optical chemosensors can be described either as colorimetric (ground-state energy, absorption) or luminescent (excited-state energy, fluorescent or phosphorescent). In both cases, the use of spectrophotometers to record the generated signals are required. On the other hand, these are easy to handle and are extended in most of scientific institutions. In addition, limits of detection achieved using fluorescence are truly competitive, being below  $10^{-6}$  M for most of the chemosensors described. Besides, fluorogenic sensors are usually more sensitive and specific since they allow the selection of absorption and emission bands and show lower limits of detection when comparing with colorimetric techniques.

There are myriads of optical chemosensors described in the literature combining different binding sites (selective for cations, anions or neutral molecules) and signalling units (dyes and/or fluorophores) but most of them are constructed using three well-known paradigms (which are showed in Figure 3) namely (a) *the binding site-signalling subunit* approach, (b) the *displacement* approach and (c) the *chemodosimeter* approach.<sup>11</sup> The three approaches differ in the form in which binding/reactive sites and signalling subunits are integrated.

---

<sup>10</sup> a) N.J. Turro, *Modern Molecular Photochemistry. University Science Books, 1991*; b) V. Balzani, *Supramolecular photochemistry, New York: Ellis Horwood, 1990*.

<sup>11</sup> R. Martínez-Máñez, F. Sancenón, *Coord. Chem. Rev.*, **2006**, *250*, 3081–3093.

- » **Binding site – signalling subunit approach:** This approach is the most commonly used for the preparation of optical chemosensors and the binding site and the signalling subunit are linked through covalent bonds. When the target analyte coordinates with the binding site, it induces changes in the electronic features of the signalling subunit that can be adequately monitored. These changes may be a modulation of fluorescence/absorption intensity, as well as changes in the bands wavelengths.<sup>12</sup> In spite of the fact that this approach is the most used for the construction of optical chemosensors, it presents some drawbacks which limit its application in real settings (a) required complex synthetic procedures and (b) the interaction between the binding site and the target analyte relies only in weak supramolecular interactions. These bonds are highly influenced by the polarity of the environment in which the recognition takes place and most of this chemosensors do not work in water or in aqueous mixtures.
- » **Displacement approach:** In this approach, the binding site and the signalling subunit are not covalently grafted but formed a complex ensemble. Addition of target analyte disruptes this complex due to its preferential coordination with the binding site. As a consequence, the signalling subunit is released to the solution. These chemosensors are designed in such a way that the optical features of the signalling unit are different when coordinated with the binding site or when free in solution, achieving a colour and/or an emission change in the presence of the target analyte.<sup>13</sup>
- » **“Chemodosimeter” approach:** This third approach takes advantage of specific chemical reactions, between the chemosensor and the target analyte, which generates fluorescence or colorimetric changes.<sup>14</sup> The use of chemodosimeters in sensing protocols present

---

<sup>12</sup> a) T. Gunnlaugsson, M. Glynn, G.M. Tocci, P.E. Kruger, F.M. Pfeffer, *Coord. Chem. Rev.*, **2006**, 250, 3094-3117; b) V. Amendola, D. Esteban-Gómez, L. Fabbrizzi, M. Licheli, *Acc. Chem. Res.*, **2006**, 39, 343-353; c) T. Gunnlaugsson, H.D.P. Ali, M. Glynn, P.E. Kruger, G.M. Hussey, F.M. Pfeffer, C.M.G. Dos Santos, J. Tierney, *J. Fluoresc.*, **2005**, 15, 287-299.

<sup>13</sup> a) S. L. Wiskur, H. Ait-Haddou, J.J. Lavigne, E.V. Anslyn, *Acc. Chem. Res.*, **2001**, 34, 963-972; b) B. T. Nguyen, E.V. Anslyn, *Coord. Chem. Rev.*, **2006**, 250, 3118-3127.

<sup>14</sup> Z. Xu, X. Chen, H.N. Kim, J. Yoon, *Chem. Soc. Rev.*, **2010**, 39, 127-137.

clear advantages, when compared with the other two approaches, which are (a) enhanced selectivity due to the fact that only the selected analyte is able to react with the designed probe and (b) the ability to work in water or in aqueous environment which allows their application for *in situ* and *at site* measurements in real settings.

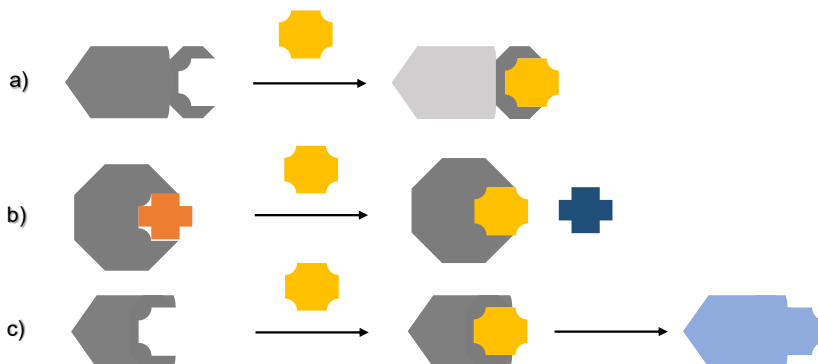


**Figure 3:** Schematic representation of three employed approaches for optical chemosensors: (a) binding site-signalling subunit approach; (b) displacement approach; (c) chemodosimeter approach.

Taking into account the above mentioned facts, the design and development of optical chemosensors for the detection of target analytes in several research fields (such as health, food industry, environmental control) has boosted in the last years. Nowadays, chemosensors for identification of target bioanalytes, such as pathogens, amino acids and enzymes, are considered a potential application for a rapid exploration and monitorization of pathogenesis derived of various diseases (Figure 4). New advances in the application of optical chemosensor for the point-of-care assistance of patients will be envisioned in the near future. Besides, the blending of chemical sensors with nanomaterials can lead to the preparation of new innovative sensing nanodevices with enhanced features (in the terms of selectivity, sensitivity and applicability) when compared with molecular-based probes.

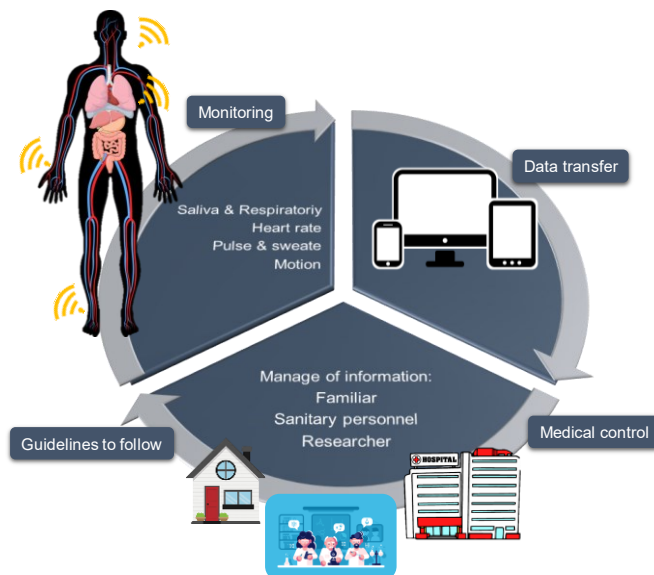


**Figure 4:** Future medical application of chemosensors in permanent and remote monitoring of diseases.

### 1.3 Nanotechnology: A step forward towards future sensors.

First known use of the term *Nanotechnology* is attributed to Professor Norio Taniguchi in 1974, who defined it as “*production technology to extra high accuracy and ultra-fine dimensions, that is, the preciseness and fineness on the order of 1 nm, 10<sup>-9</sup> m, in length*”.<sup>15</sup>

Since then, the study and application of nanotechnology have grown constantly at an amazing speed, just like their definition, that have evolved to “*the construction and use of functional structures designed from atomic or molecular size scale with at least one characteristic dimension measured in nanometers*”.<sup>16</sup> That is, definitely, managing matter at 1-100 nm scale (Figure 5).

<sup>15</sup> N. Taniguchi, in *Proc. Intl. Conf. Prod. Eng. Tokyo, Part II, Japan Society of Precision Engineering, 1974*.

<sup>16</sup> K. Narendra, S. Kumbhat, *Essentials in Nanoscience and Nanotechnology, John Wiley & Sons, 2016*.

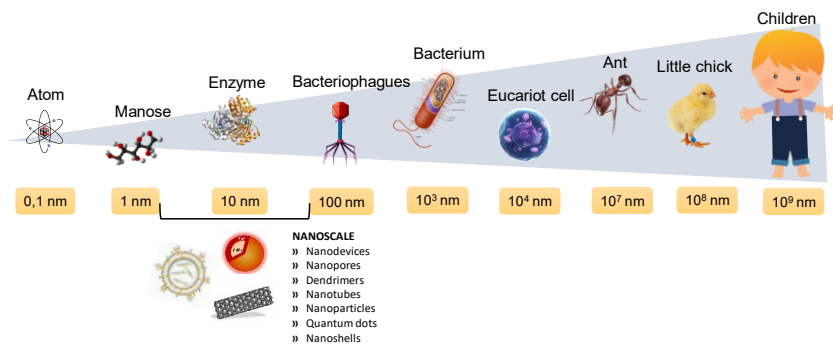


**Figure 5:** Scale illustration of common objects range of sizes.

This particular range of size provides significant advantages due to the appearance of quantum mechanical effects and, as a consequence, nanotechnology presents several outstanding applications in almost all scientific fields that range from materials science, electric and electronic engineering, catalysis, metallurgy and powder engineering, chemical engineering, drug delivery, polymer science and engineering, medicine, biotechnology, forensic, environmental and food control, etc.

Next, and for a better understanding of the scope of this research, this thesis focus on one of the most relevant elements within nanotechnology: nanomaterials.

Nanomaterials are defined as materials in which a single unit is sized (in at least one dimension) in the nanoscale range, and they include among others nanoparticles, nanofibers, nanotubes, nanocomposites, nanofoams and *nanoporous materials*. Inside the vast realm of nanomaterials, nanoporous materials are nanostructured systems that contain porous networks in which pores sizes range from 1 to 100 nm. A number of systems based on nanoporous materials are being developed and applied on almost every research field and industrial area. Their applications are predetermined by their structural features; hence, tailored fabrication techniques are essential. Some structural parameters such as pore size, porosity, functionalization and specific



surface area determine the final properties like hydrophilicity/hydrophobicity, conductivity, charge distribution and also catalytic activity.<sup>17</sup>

Very recently, the use of nanoporous materials for the development of reliable, miniaturized and portable sensing devices was explored. For this purpose, the pores of the nanoporous support are loaded with a suitable signalling reporter and the external surface functionalized with (supra)molecular or biochemical architectures yielding systems that remain closed until the presence of a certain molecule induces the delivery of the signalling reporter. In the next sections we introduce these concepts and the different porous inorganic supports used for the preparation of hybrid sensing materials.

#### **1.4 Organic-inorganic hybrid porous materials.**

Since the beginning of industrial era, mixing organic and inorganic products with the aim of obtaining unique materials with properties from both of the components was a challenge. However, the term “*hybrid organic-inorganic material*” was recently coined, only once this field of research was able to manifest its broad bunch of applications. Nowadays, it is considered an expanding and dynamic research discipline.

Hybrid materials combines their two constituents in a synergic way, that is, not only summing the properties they already present in their isolated way, but showing new characteristics that only can be afforded when they are together.<sup>18</sup> This is supported by professor Clément Sanchez, who said that “*hybrid organic-inorganic materials are not simple mixtures. They can be broadly defined as molecular or nano-composites with (bio)organic and inorganic components, intimately mixed where at least one of the component domains has a dimension ranging from a few Å to several nanometers. Consequently, the properties of hybrid materials are not only the sum of the individual contributions of both phases, but the role of their inner interfaces could be predominant*”.<sup>19</sup> The final

---

<sup>17</sup> S. Ameen, M. Shaheer-Akhtar, R. Godbole, H.-S. Shin, *An Introduction to Nanoporous Materials*. Nanoporous Materials, IntechOpen.

<sup>18</sup> a) *Coord. Chem. Rev.*, Ed. P. A. Gale, **2006**, 250; b) J.F. Callan, A.P. de Silva, D.C. Magri, *Tetrahedron*, **2005**, 61, 8551-8588; c) G.J. Mohr, *Sens. Actuators B*, **2005**, 107, 2-13.

<sup>19</sup> C. Sánchez, *J. Mater. Chem.*, **2005**, 15, 3559-3592.

structure and properties of the nanocomposite are obviously determined by the selected inorganic support, by the organic moieties anchored onto its surface and, in particular, by the reaction conditions used in its synthesis.<sup>20</sup>

Some of these materials can be prepared by the anchoring of functional (organic) groups into nanoscopic materials mainly composed by inorganic structures as scaffolds.<sup>21</sup> Indeed, this thesis focuses in the design and development of new hybrid organic-inorganic materials following this strategy.

Anchoring or functionalization of solids supports by covalent bonding offers interesting advantages for molecular recognition processes that are summarized below.

- » Receptors are organized in the surface in compact monolayers (depending on functionalization degree) which generates new collective processes.
- » Subsequent functionalization with different organic molecules can be undertaken, providing the material different properties depending on the organic molecules anchored.
- » Leaching processes involving receptors are avoided.
- » Reversible reactions can be performed when organic molecules anchored to the surface allows it.

According to the nature of the interface between organic and inorganic components, these materials can be divided in two classes: In class I, weak bonds (hydrogen, van der Waals or ionic bonds) cohesion the whole structure. In contrast, organic-inorganic interfaces in class II are linked through strong chemical bonds (covalent or ionic-covalent bonds), although simultaneously they can also interact through weak bonds that define class I. All the examples of hybrid materials described in this PhD thesis will correspond to class II.

Within this strategy, improved sensing ensembles in terms of sensibility and/or selectivity have been designed for targets that are difficult to specifically

---

<sup>20</sup> J. Livage, M. Henry, C. Sánchez, *Prog. Solid. State. Chem.*, **1988**, *18*, 259-341.

<sup>21</sup> K. Rurack, R. Martínez-Máñez, *The supramolecular chemistry of organic-inorganic hybrid materials*, **2010**, Ed. John Wiley & Sons.

be detected by conventional methods.<sup>22</sup> These improvements are even greater when supported on 3D-architected inorganic supports, i.e. nanoporous inorganic scaffolds, whose properties are enhanced compared with their planar analogues. Some examples of these new characteristics provided are control of access to certain region, flux control inside channels, double functionalization in the inner and outer regions of the material, among others.

A deeper description of these nanostructured materials will be developed below.

#### 1.4.1 Types of porous materials:

Porous materials exist widely around us and play important roles in many aspects of our daily lives. *International Union of Pure and Applied Chemistry* (IUPAC) classified porous materials into three main categories: *micro*-porous (<2 nm), *macro*-porous (>50 nm) and, those within our interest, known as *meso*-porous, which sizes are comprised between 2 and 50 nm. Porous materials can be made of several and different solids both oxides and non-oxides, crystalline and also amorphous, and their pores may consist on cavities, channels or also interstices.

Microporous scaffolds, such as zeolites and metallophosphates, were synthesized for the first time almost two centuries ago, and still nowadays are indispensable in plenty of industrial processes, especially in catalysis, filtration and separation, and also in biomedical regeneration, enzyme immobilization, drug delivery and sensing, among others.<sup>23</sup> Macroporous materials

---

<sup>22</sup> a) A. Verma, V.M. Rotello, *Chem. Commun.*, **2005**, 3, 303-312; b) U. Drechsler, B. Erdogan, V.M. Rotello, *Chem. Eur. J.*, **2004**, 10, 5570-5579; c) A.B. Descalzo, R. Martínez-Máñez, F. Sancenón, K. Hoffmann, K. Rurack, *Angew. Chem. Int. Ed.*, **2006**, 45, 5924-5948; d) F. Mancin, E. Rampazzo, P. Tecilla, U. Tonellato, *Chem. Eur. J.*, **2006**, 12, 1844-1854; e) I. Willner, B. Basnar, B. Willner, *Adv. Funct. Mater.*, **2007**, 17, 702-717.

<sup>23</sup> a) F. Schülth, W. Schmidt, *Adv. Eng. Mater.*, **2002**, 4, 269-279; b) D.E De Vos, M. Dams, B.F. Sels, P.A. Jacobs, *Chem. Rev.*, **2002**, 102, 3615-3640; c) S. Cavenati, C.A. Grande, F.V.S. Lopes, A.E. Rodrigues, *Micropor. Mesopor. Mater.*, **2009**, 121, 114-120; d) N. Carlsson, H. Gustafsson, C. Thörn, L. Olsson, K. Holmberg, B. Akerman, *Adv. Colloid Interface Sci.*, **2014**, 205, 339; e) M. Vallet-Regí, M. Colilla, I. Izquierdo-Barba, *J. Biomed. Nanotechnol.*, **2008**, 4, 1-15; f) I.I. Slowing, B.G. Trewyn, S. Giri, V.S.-Y. Lin, *Adv. Funct. Mater.*, **2007**, 17, 1225-1236; g) K.A. Killian, T. Böcking, K. Gaus, M. Gal, J.J. Gooding, *ACS Nano*, **2007**, 4, 335-361; h) A. Jane, R. Dronov, A. Hodges, N. H. Voelcker, *Trends Biotechnol.*, **2009**, 27, 230-239.

implementation in industry, in contrast, have emerged drastically during the last decade.

Mesoporous materials were developed more recently, but, as well as microporous, have attracted much attention due to their large specific surface area and their wide range of application in diverse scientific and technological fields. Typical synthesis processes include the presence of organized self-assembly organic molecules or polymers, micellar solutions, lyotropic liquid crystals, or also microemulsions, all of them committed to serve as structure-directing agents. Their synthesis is especially relevant, since pore geometry is directly related to the resulting properties and final application.<sup>24</sup> Thanks to the knowledge developed through continuous experimentation, it has been possible to gain certain degree of control over the desirable architecture and on the final features, governing synthetic parameters and reagents.

This thesis focuses on the use of *nanoporous anodic alumina* (NAA) as mesoporous solid scaffold. For this reason, the following sections described the synthesis and functionalization of NAA supports.

#### 1.4.1.1 Nanoporous anodic alumina (NAA).

Porous anodic alumina was discovered in the 1930s<sup>25</sup> but it was from 1950s to 1970s when efforts resulted, finally, in its development.<sup>26</sup> From the beginning, scientists worked in the development of new routes of synthesis and applications, with results that were consequently patented.<sup>27</sup> Then, in 1995, the formation of NAA with highly ordered 2D hexagonal porous structure was confirmed and since then, their interest for R+D applications has been growing up exponentially (75% increase of *aluminium anodic oxide* (AAO)-related publications in 1990-2005 period).

Keller characterized NAA by electron microscopy for the first time, and described it as: "*hexagonally arranged arrays of nanometric pores, in which the*

---

<sup>24</sup> X. Wang, X. Bu, P. Feng, *Porous Inorganic Materials. An Encyclopaedia of Inorganic and Bioinorganic Chemistry*, R. A. Scott (Ed.). **2011**.

<sup>25</sup> S. Setch, A. Miyata, *Sci. Pap. Inst. Phys. Chem. Res.*, **1932**, 19, 237.

<sup>26</sup> a) F. Keller, M.S. Hunter, D. L. Robinson, *J. Electrochem. Soc.*, **1953**, 100, 411-419; b) J. P. O'Sullivan, G.C. Wood, *Proc. Roy. Soc. Lond. A.*, **1970**, 317, 511-543.

<sup>27</sup> a) British Patent 223994 (1923); b) Italian Patent 741753 (1936); c) A. Smith, (Nov 26, 1974), *Process for producing an anodic aluminum oxide membrane*.

*interpore distance* (distance measured between centres of adjacent pores) is *directly proportionate to the anodization voltage*.<sup>26</sup> Over the time, it has been confirmed that controlling shape and geometry depends mostly on anodization voltage or current intensity. Other synthetic parameters that affect the resulting material are anodization time, type/concentration of the electrolyte, pH, and temperature.<sup>28</sup>

NAA has emerged as a useful tool for nanotechnology because of its wide diversity of applications. Among them, energy, nanofabrication, biotechnology, and in particular biosensing, are the most important. Given the orientation of this thesis, sensing and biosensing will be widely explained. NAA is an optimal scaffold for the implementation of selected (bio)molecules due to its unique mechanical, electrical and chemical features. Also its high surface, thermal stability, hardness, biocompatibility as well as transparency in the visible range make this material an optimal scaffold for the development of hybrid materials with applications in the field of molecular recognition and sensing.<sup>29</sup>

In general terms, NAA structure can be described as an alumina matrix with hexagonally-arranged cells with cylindrical pore that grows perpendicularly to the substrate surface.<sup>30</sup>

Roughly, NAA is obtained by controlled anodization of aluminium surfaces in aqueous acids (sulfuric, oxalic and phosphoric acids).<sup>31</sup> Pore size and shape geometry are determining in many applications, thus, controlling the anodization procedure is vital. Masuda and Fukuda reported their findings of optimal anodization process in 1995.<sup>32</sup> The nanoimprint process, two years

---

<sup>28</sup> a) W. Chen, J.S. Wu, X.H. Xia, *ACS Nano*, **2008**, *5*, 959–965; b) L. Zaraska, W.J. Stepniowski, M. Jaskuła, G.D. Sulka, *Appl. Surf. Sci.*, **2014**, *305*, 650–657; c) W. Lee, S.J. Park, *Chem. Rev.*, **2014**, *114*, 7487–7556; d) L. Zaraska, A. Brudzisz, M.E. Wierzbicka, G.D. Sulka, *Electrochim. Acta*, **2016**, *198*, 259–267.

<sup>29</sup> A.M. Md Jani, I.M. Kempson, D. Losic, N.H. Voelcker, *Angew. Chem. Int. Ed.*, **2010**, *49*, 7933–7937.

<sup>30</sup> W. Lee, R. Ji, U. Gösele, K. Nielsch, *Nat. Mater.*, **2006**, *5*, 741–747.

<sup>31</sup> a) A.M. Md. Jani, D. Losic, H.N. Voelcker, *Prog Mater Sci.*, **2013**, *58*, 636–704; b) G. Patermarakis, K. Masavetas, *J. Electroanal. Chem.*, **2006**, *588*, 179–189; c) K. Ersching, E. Dorico, R.C. da Silva, V.C. Zoldan, E.A. Isoppo, A.D.C. Viegas, A.A. Pasa, *Mater. Chem. Phys.*, **2012**, *137*, 140–146.

<sup>32</sup> H. Masuda, K. Fukuda, *Science*, **1995**, *268*, 1466–1468.

later, revolutionized NAA exploitation.<sup>33</sup> A two-step anodization procedure was proposed. In the first step, an irregular oxide layer is formed, which is consecutively removed to use the nanocaves remaining as nucleation sites for the second anodization. According to Zaraska et al.<sup>34</sup> this way allows the formation of better hexagonal pore rearrangement. This process offers large advantages comparing to other techniques, such as lithography, which are time consuming and expensive. It is a simple and cost-competitive fabrication, allows controllable pore structure within nanometric scale, and moreover, is easily scalable for industrial production.<sup>35</sup>

Several theoretical models have been undertaken to explain pore nucleation and growth in NAA,<sup>36</sup> however, a clear and complete explanation is still under debate. It is agreed that pore nucleation is originated in the oxide thin film generated during the first seconds of anodization process, but great differences can be observed in the numerous explanations reported. Models may be divided in two main groups, the ones that regard electric field<sup>37</sup> as the driving force, and those who regard mechanical stress.<sup>38</sup> According to the first ones, that are supported by the most scientific community, instability produced by electric field at certain sites (nucleating centres) generate localized enhancement of temperature and ionic conduction that results in the preferential dissolution of oxide and formation/growth of pores. In contrast,

---

<sup>33</sup> H. Masuda, H. Yamada, M. Satoh, H. Asoh, M. Nakao, T. Tamamura, *Highly Appl. Phys. Lett.*, **1997**, *71*, 2770-2772.

<sup>34</sup> L. Zaraska, A. Brudzisz, M.E. Wierzbicka, G.D. Sulka, *Electrochim. Acta*, **2016**, *198*, 259–267.

<sup>35</sup> a) A.P. Li, F. Müller, A. Birner, K. Nielsch, U. Gösele, *J. Appl. Phys.*, **1998**, *84*, 6023-6026; b) A. Eftekhari, *Nanostructured Materials in Electrochemistry*, Wiley-VCH Verlag GmbH & Co. KGaA, Germany, **2008**.

<sup>36</sup> a) T.P. Hoar, N.F. Mott, *J. Phys. Chem. Solids*, **1959**, *9*, 97-99; b) G. Patemarakis, N. Papandreadis, *Electrochim. Acta*, **1993**, *38*, 2351-2361; c) C. Cheng, A.H.W. Ngan, *Nanoporous Alumina Fabrication, Structure, Properties and Applications*; D. Losic, A. Santos (Eds.), **2015**.

<sup>37</sup> a) G.C. Wood, in *Oxide and Oxide Films*, Ed. by J.W. Diggle (Marcel Dekker), New York, **1973**. b) J.P. O'Sullivan, G.C. Wood, *Proc. R. Soc. London, Ser. A*, **1970**, *317*, 511; c) T.P. Hoar, N.F. Mott, *J. Phys. Chem. Solids*, **1959**, *9*, 97-99; d) Q. Van Overmeere, F. Blaffart, J. Proost, *Electrochem. Commun.*, **2010**, *12*, 1174-1176.

<sup>38</sup> a) O. Jessensky, F. Müller, U. Gosele, *Appl. Phys. Lett.*, **1998**, *72*, 1173-1175; b) K.R. Hebert, J.E. Houser, *J. Electrochem. Soc.*, **2009**, *156*, C275-C281; c) J.E. Houser, K.R. Hebert, *Nat. Mater.*, **2009**, *8*, 415-420; d) S.J. Garcia-Vergara, L. Iglesias-Rubianes, C.E. Blanco-Pinzon, P. Skeldon, G.E. Thompson, P. Campestrini, *Proc. R. Soc. A*, **2006**, *462*, 2345-2358.

mechanical stress supporting models explains that the significant expansion of volume observed when the oxide layer is formed, induces a mechanical stress that favours an oxide flow from the bottom to the pore walls. Others base its explanation on hybrid electric-mechanical driven process. This is pore formation driven by the electric field from the pore bottom and through the barrier layer, resulting in the formation of aluminium oxide; but, at the same time, this is also dependent of the plasticity of the barrier layer and the stress relief generated while formed.<sup>39</sup>

» Synthesis:

Fabrication of NAA supports is accomplished by an anodization process. According to its general definition, this is an electrochemical process that provides an anodic oxide finish to metallic surfaces. The process gets its name due to the fact that metal support constitutes the anode electrode in the electrolytic cell that encompasses the electrochemical process.

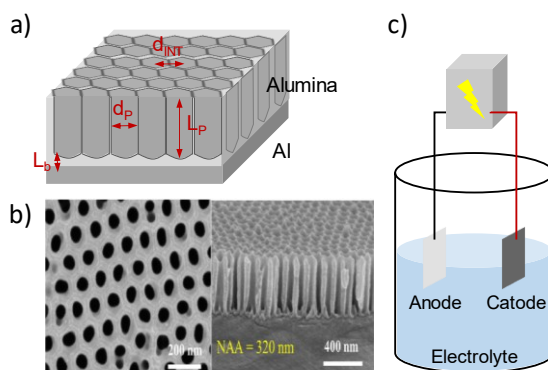


**Figure 6:** a) Illustrative scheme with the most representative geometric parameters of NAA, b) top and cross-section scanning electron microscopy (SEM) images of NAA,<sup>40</sup> c) illustration describing a basic electrochemical anodization cell used to produce NAA.

<sup>39</sup> a) S. Lee, D. Kim, E. Gillete, J. Oh, S.W. Han, *Phys. Chem.*, **2013**, *15*, 10659-10665; b) B. He, S.J. Son, S.B. Lee, *Langmuir*, **2006**, *22*, 8263-8265.

<sup>40</sup> Y. Li, W.J. Yue, Z.X. Chen, B.Q. Cao, X.Q. Fu, C.W. Zhang, Z.M. Li, *Nanoscale Res. Lett.*, **2018**, *13*, 217.

Within the anodization process, there are some key structural parameters that are dependent on the reaction conditions. These are, pore size ( $D_p$ ), inter-pore distance ( $D_{int}$ ), pore length ( $L_p$ ) and oxide barrier layer thickness ( $L_b$ ) (Figure 6). In one hand,  $D_p$  and  $D_{int}$  can vary even hundreds of nanometres just modulating anodization voltages, and it has also been reported that pore, inter-pore and barrier thickness linear relationship with anodization voltage may vary with temperature and acid concentration in the electrolyte cell. Resulting NAA scaffolds present two distinguishable regions in terms of chemical composition. A pure aluminium oxide inner layer close to the interface with aluminium, and the outer alumina layer contaminated with anionic species from electrolytes (i.e. phosphate, sulphate, oxalate, etc.).<sup>41</sup>

Anodization voltage, electrolyte type and concentration, and also temperature have been recognized as the most crucial parameters to control NAA pore distribution and geometry.<sup>42</sup> Regarding the electrolyte, sulphuric acid ( $H_2SO_4$ ), oxalic acid ( $H_2C_2O_4$ ) and phosphoric acid ( $H_3PO_4$ ) are the most representative. However, others such as citric, malic, malonic, tartaric and sulfamic acids have also been employed in several publications although the resulting alumina showed poor organization.<sup>43</sup>

Average ordered zone size has been established as factor for evaluating NAA ordering quality prepared under different anodization conditions, which have permitted to determine the best anodization conditions. Two different conditions regime have been classified: (i) mild anodization with moderate voltages and temperatures, and (ii) hard anodization with higher voltage

---

<sup>41</sup> J. Lee, S. Nigo, Y. Nakano S. Kato, H. Kitazara, G. Kido, *Sci. Tech. Adv. Mater.*, **2010**, *11*, 1-4; b) F. Le Coz, L. Arurault, S. Fontorbes, V. Vilar, L. Datas, P. Winterton, *Surf. Interface Anal.*, **2010**, *42*, 227-233; c) K. Nielsch, J. Choi, K. Schwim, R.B. Wehspohn, U. Gösele, *Nano Lett.*, **2002**, *2*, 677-680.

<sup>42</sup> a) A.P. Li, F. Müller, A. Bimer, K. Nielsch, U. Gösele, *J. Appl. Phys.*, **1998**, *84*, 6023–6026; b) S. Ono, M. Saito, H. Asoh, *Electrochim. Acta*, **2005**, *51*, 827–833; c) D. Losic, L. Velleman, K. Kant, T. Kumeria, K. Gulati, J.G. Shapter, D.A. Beattie, S. Simovic, *Aust. J. Chem.*, **2011**, *64*, 294–301.

<sup>43</sup> a) V. Surganov, P. Morgen, J. Nielsen, G. Gorokh, A. Mozalev, *Electrochim. Acta*, **1987**, *32*, 1125–1127; b) V. Surganov, G. Gorokh, *Mater. Lett.*, **1993**, *17*, 121–124; c) S. Chu, K. Wada, S. Inoue, M. Isogai, Y. Katsuta, A. Yasumori, *J. Electrochem. Soc.*, **2006**, *153*, B384–B391; d) S. Ono, M. Saito, M. Ishiguro, H. Asoh, *J. Electrochem. Soc.*, **2004**, *151*, B473–B478.



conditions but lower temperatures. Acid electrolyte chosen will determine the conditions that are summarised in Table 2.

**Table 2.** Summary of the most representative fabrication conditions for NAA produced by the mild anodization (MA) or hard anodization (HA) protocols.

Acid electrolyte	Anodization Regime	V (V)	T (°C)	$d_p$ (nm)	$d_{int}$ (nm)	Growth rate ( $\mu\text{m}\cdot\text{h}^{-1}$ )	Ref.
H <sub>2</sub> SO <sub>4</sub> 0.3 M	MA	25	5-8	25	63	7.5	44
H <sub>2</sub> SO <sub>4</sub> 0.3 M	HA	40	0-1	30	78	85	45
H <sub>2</sub> C <sub>2</sub> O <sub>4</sub> 0.3 M	MA	40	5-8	30	100	3.5	46
H <sub>2</sub> C <sub>2</sub> O <sub>4</sub> 0.3 M	HA	140	0-1	50	280	50	47
H <sub>3</sub> PO <sub>4</sub> 0.1 M	MA	195	0-1	160	500	2	48

According on the distribution of electric potential within the alumina, electric potential drop is concentrated in concaved regions (Figure 7), which results in a much higher electric field intensity compared with a flat region.<sup>49</sup> Thus, in the second stage, pore channels are constructed as a consequence of the different rates of oxide growth, which penetrates preferentially into concavities. Within time, initial pores that show larger depths will grow faster than their flatter neighbours, including expansion in the horizontal plane. However, pore growth will be mainly in the elongation direction since electric field intensity is concentrated in the pore bottom and reduces significantly in the walls while penetrating deeper.

Finally, current reaches a steady-state value and geometry of pore bottom tends to stabilize. Self-origination of pores continues, and it is during this stage

<sup>44</sup> G. Patermarakis, P. Lenas, C. Karavassilis, G. Papayiannis, *Electrochim. Acta*, **1991**, *36*, 709–725.

<sup>45</sup> S.K. Thamida, H.C. Chang, *Chaos*, **2002**, *12*, 240–251.

<sup>46</sup> V.P. Parkhutik, V.I. Shershulsky, *Appl. Phys.*, **1992**, *25*, 1258–1263.

<sup>47</sup> J.W. Diggle, T.C. Downie, C.W. Coulding, *Chem. Rev.*, **1969**, *69*, 305–405.

<sup>48</sup> G. Patermarakis, N. Papandreadis, *Electrochim. Acta*, **1993**, *38*, 2351–2361.

<sup>49</sup> C. Cheng, A.H.W. Ngan, *Electrochim. Acta*, **2011**, *56*, 9998–10008.

that disordered porous evolve to a better organization porous distribution in a process that may take from hours to days of anodization time.

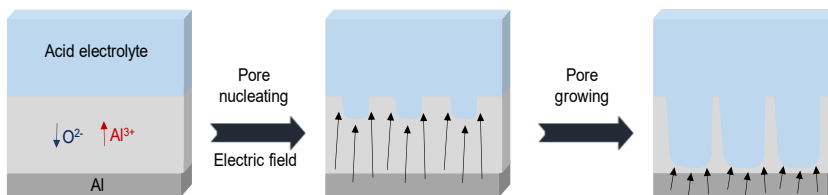


**Figure 7:** Schematic representation of aluminium oxide growth process under constant voltage condition.

More particularly and for the development of the research work hereby presented, nanostructured NAA scaffolds used were prepared through a synthesis methodology developed by Masuda and other researchers known as “two-step anodization method”.<sup>50</sup>

Highly ordered nanostructured supports are obtained through this synthetic process. The first anodization causes a non-ordered and thoroughly irregular oxide layer, however, upon being chemically removed, the remained nanocavities will act as nucleation points inducing a more homogenized and regular pore growth along the whole surface.<sup>51</sup>

During the first anodization, a long electrochemical process of about 24 hours generates a multichannel structure with disordered appearance in the surface but highly hexagonal-shape porous in the bottom. This is consequence of self-organization and pore distribution within time and in constant anodization potential. Chemical etching is applied and superficial and disordered oxide layer is removed. In this way, an organized alumina template is created in a more similar shape to the desired final pore geometry and distribution. During the second anodization, electric field is concentrated in the concavities previously formed maintaining the finally expected hexagonally arranged distribution from the beginning (Figure 8).

<sup>50</sup> a) H. Masuda, M. Satoh, *Jpn. J. Appl. Phys.*, **1996**, 35, L126–L129; b) H. Masuda, K. Fukuda, *Science*, **1995**, 268, 1466–1468; c) A.P. Li, F. Müller, U. Gösele, *Electrochem. Solid-State Lett.*, **2000**, 3, 131–134.

<sup>51</sup> S. Ateş, E. Baranb, B. Yazıcı, *Thin Solid Films*, **2018**, 648, 94–102.

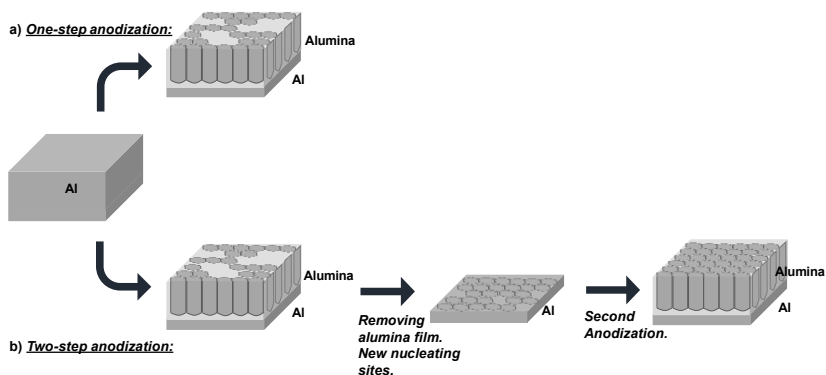


**Figure 8:** Schematic diagram describing the most widely used methods for fabricating NAA: a) One-step anodization versus b) two-step anodization.

The prepared NAA support consisted of an amorphous phase that can evolve to a purer state by thermal treatment. First transition, from amorphous to gamma alumina phase ( $\gamma$ -Alumina) starts at 700 °C and ends at 1000 °C, but if temperature increases above 1200 °C NAA phase evolves to pure  $\alpha$ -alumina.<sup>52</sup>

This developed ability to structurally engineer and control NAA internal structure and modify chemically their surface, provides new tools to improve NAA capabilities for example, for developing highly sensitive and selective biochemical sensing systems, which is the aim of this thesis.

#### » Functionalization:

According to their definition, functionalization is the process of adding new functions, features, capabilities, or properties to a material by changing the surface chemistry of the cited material.

A vast number of works have studied the methods for the functionalization of NAA surfaces for their protection from acidic environments and to impart

<sup>52</sup> a) P.P. Mardilovich, A.N. Govyadinov, N.I. Mukhurov, A.M. Rzhevskii, R. Paterson, *J. Membr. Sci.*, **1995**, *98*, 131–142; b) W.L. Xu, M.J. Zheng, S. Wu, W.Z. Shen, *Appl. Phys. Lett.*, **2004**, *85*, 4364–4366; c) A. Kirchner, K.J.D. MacKenzie, I.W.M. Brown, T. Kemmitt, M.E. Bowden, *J. Membr. Sci.*, **2007**, *287*, 264–270; d) Y Li, G.H. Li, G.W. Meng, L.D. Zhang, F. Phillip, *J. Phys. Condens. Matter*, **2001**, *13*, 2691–2699; e) N.M. Yakovleva, A.N. Yakovlev, E.A. Chupakhina, *Thin Solid Films*, **2000**, *366*, 37–42; f) L.F. Marsal, L. Vojkuvka, P. Formentín, J. Pallarès, J. Ferré-Borrull, *Opt. Mater.*, **2009**, *31*, 860–864.

them specific functionalities. Techniques can be divided in two groups depending on the medium where the process is run (Figure 9):<sup>53</sup>

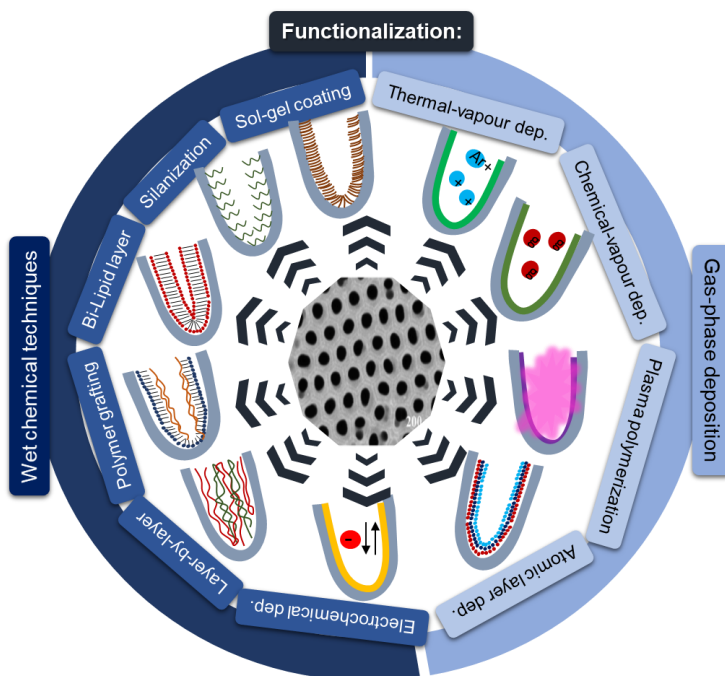


**Figure 9:** Schematic summary of typical gas phase and wet chemical functionalization techniques used to modify NAA surface.

- a) Physical/gas phase deposition: Thermal vapour deposition, chemical vapour deposition (CVD), plasma polymerization and atomic layer deposition (ALD). They are mostly employed to deposit a wide variety of materials as metals, metal oxides, nitrides, and carbon nanotubes on NAA.
- b) Wet chemical modifications: *self-assembly processes of silanes*, organic and phosphonic acids, layer-by-layer deposition, polymer grafting, sol-gel processing, electrochemical and electroless deposition. Unlike physical surface modification, chemical surface

<sup>53</sup> a) T. Kumeria, A. Santos, D. Losic, *Sensors*, **2014**, *14*, 11878-11918; b) A.M. Md Jani, D. Losic, N.H. Voelcker, *Prog. Mater. Sci.* **2013**, *58*, 636–704; c) C. Eckstein, L.K. Acosta, L. Pol, E. Xifré-Pérez, J. Pallares, J. Ferre-Borrull, L.F. Marsal, *ACS Appl. Mater. Interfaces*, **2018**, *10*, 10571-10579.

modification result in no noticeable change in the structural properties of the NAA substrate.

Chemical approaches usually rely on the formation of self-assembled structures, creating uniform and extensive monolayers over the surface. Irregularities along NAA surface, due to anionic impurities from electrolyte solutions used during their fabrication, facilitates attack by oxides, which results in the generation of surface hydroxyl groups that may act as anchorage centres for the functionalization. Main functionalization techniques are summarised below:

➤ Electrochemical and electroless deposition of metals:

Within this deposition approach, monolayer is formed over a conducting surface (electrode) through deposition of ions (anions or cations) contained in a solution into an electrolytic cell (Figure 10). Three electrodes (working, counter and reference) are required allowing electron movement and oxidation and reduction reactions responsible for carrying out the deposition.<sup>54</sup> Quality of the resulting electrodeposition is strongly affected by pre-treatment and cleaning of the metal surface, concentration of metal ions in the electrolyte, pH, agitation, voltage, temperature, electrolyte conductance and addition agents.

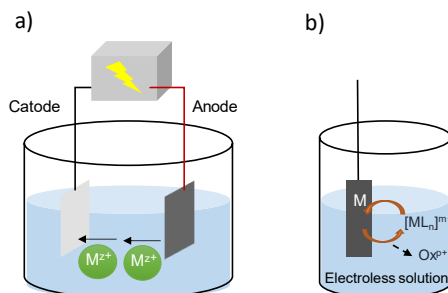


**Figure 10:** Schematic representation of a) electrochemical and b) electroless deposition for NAA surface functionalization.

Electrochemical and electroless depositions present certain advantages when compared to other functionalization procedures. At this respect, they are

<sup>54</sup> C.A.D. Rodriguez and G. Tremiliosi-Filho, Electrochemical Deposition. Encyclopedia of Tribology, 918–922, Springer, Boston, MA, 2013.

significant less expensive, more versatile because can be applied in the simultaneous coating of a large number of samples, and pieces that are large in size. Besides, NAA functionalized using these procedures presents remarkable features such as hardness, corrosion resistance, as well as excellent frictional characteristics.

➤ Sol-gel chemistry:

In this functionalization protocol a hydrolysis reaction takes place between the sol-precursor and NAA surface functional groups (Figure 11). In a first step, substrate contacts sol-precursor solution through immersion, dipping or spin coating to be followed by solvent evaporation and formation of a glassy gel over the pores.<sup>55</sup> A "sol" is a colloidal solution that gradually evolves towards the formation of a gel-like diphasic system containing both a liquid and a solid phase whose morphologies range from discrete particles to continuous polymer networks.

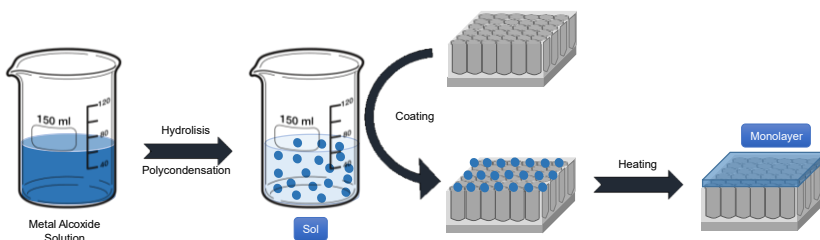


**Figure 11:** Schematic representation of sol-gel chemistry for NAA surface functionalization.

The sol-gel approach is a cheap and low-temperature technique that allows synthesis of high purity homogenous and multi-component structures, with high degree of control over their structure, thermal stability and surface reactivity.<sup>56</sup> This process makes possible the uniform deposition of small quantities of dopants (such as organic dyes and rare-earth elements) and thus, is extensively used in ceramics processing and manufacturing as a casting material, or as a means of producing very thin films of metal oxides for various

<sup>55</sup> L.L. Hench, J.K. West, *Chem. Rev.*, **1990**, *90*, 33-72.

<sup>56</sup> a) B.B. Lakshmi, C.J. Patrissi, C.R. Martin, *Chem. Mater.*, **1997**, *9*, 2544-2550; b) W.J. Hunks, G.A. Ozin, *J. Mater. Chem.*, **2005**, *15*, 3716-3724.

purposes. Sol-gel derived materials have diverse applications in optics, electronics, energy, space, (bio)sensors, medicine, reactive material, and separation technology.

➤ Layer-by-Layer deposition:

This technique is based on the alternatively dip of substrate into electrolyte solutions of contrary electrostatic charge (Figure 12).

Using this method, it is possible to obtain thin electrolyte films in the nanometric scale and with high resolution control. Among their applications tuning transport properties of NAA membranes, attaching nanoparticles and biomolecules, as well as fabrication of polyelectrolytic nanotubular structures using NAA as a template, are the most important.<sup>57</sup>

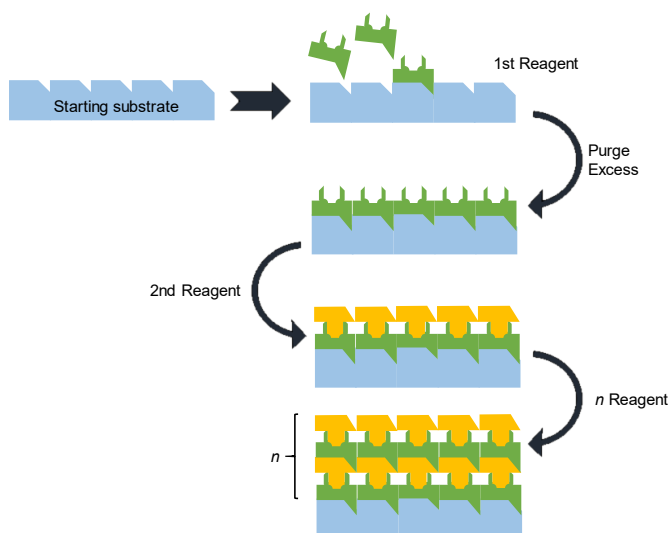


**Figure 12:** Schematic representation of layer-by-layer NAA surface functionalization.

➤ Functionalization with organic and phosphonic acids:

NAA functionalization with organic and phosphonic acids has been extensively used for its characteristic control of wettability, corrosion resistance

<sup>57</sup> A.M. Md Jani, D. Losic, N.H. Voelcker, *Prog. Mater. Sci.*, **2013**, 58, 636–704.

and homogeneity of the formed layer. Attachment is undertaken by dip-coating through the formation of a self-assembled monolayer (SAM) by chemical bonding acids with NAA surface hydroxyl groups (Figure 13).<sup>58</sup>

Within changing chain length, surface properties can be tuned. Organic and phosphonic acids show high compatibility with other organic functional groups, which allows the attachment of other organic/inorganic structures over the monolayer (such as nanoparticles, nanotubes, catalysts, biomolecules and others). Moreover, this functionalization protocol can be performed in many solvents, including water.

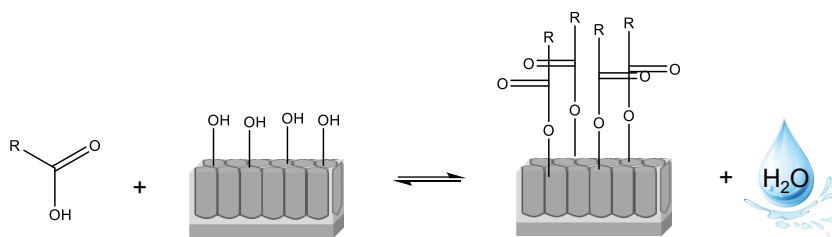


**Figure 13:** Functionalization path of NAA surfaces with *n*-alkanoic acid.

➤ Organosilane Modification of aluminium anodic oxide (AAO):

In the development of the scientific work hereby presented, silanes as functionalization tool to attach biomolecules over the NAA surface is used. The technique is thoroughly described below.

Grafting of organic molecules to NAA surface is accomplished by the spontaneous attachment and rearrangement of these molecules from a liquid phase, or in other words, by the formation of self-assembled monolayers (SAMs). Within this functionalization method, organosilanes and phosphonates (see “Functionalization with organic and phosphonic acids” section above) homogeneous layers extend over alumina surface, allowing the addition of a broad range of different and reactive terminal functional groups (such as amine, isocyanate, carboxyl, epoxy, azide, halide, alkene, alkyne).

<sup>58</sup> a) M.A. Frank, C. Meltzer, B. Braunschweig, W. Peukert, A. R. Boccaccini, S. Virtanen, *Appl. Surf. Sci.*, **2017**, *404*, 326-333; b) C. Queffelec, M. Petit, P. Javier, D. A. Knight, B. Bujoli, *Chem. Rev.*, **2012**, *112*, 3777-3807.



SAMs formation is undertaken through the reaction with superficial hydroxyl groups by simple incubation of the NAA substrate in a silane solution.<sup>59</sup> A schematic of silanization of hydroxylated NAA is provided in Figure 14.

Through changes in the carbon chain length and in its terminal group, it is possible to confer different applicability to the material. Silanes with hydrophobic terminal groups such halides (e.g. trichloro-silanes and perfluoroalkyl-silanes) provide complete hydrophobicity to the material,<sup>60</sup> while in contrast, silanes terminated with poly(ethylene glycol), amines and epoxy moieties, improve significantly NAA wettability, prevent NAA structure from biofouling and improve their biocompatibility character.<sup>61</sup>

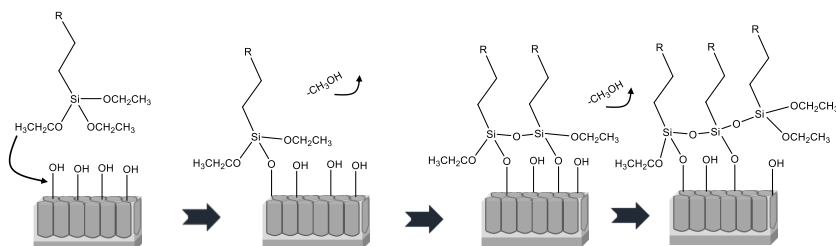


**Figure 14:** Illustration of organosilane attachment and re-arrangement over NAA surfaces.

However, the most exploited application of organosilanes for functionalization of materials is the formation of an active layer, to allow the immobilization of other molecules or biomolecules, nanoparticles, polymers, quantum dots or even lipid bilayers, and to provide functionality to the hybrid organic-inorganic material. In other words, they act as linkers in which one end of the molecule binds to the scaffold surface, while the other end immobilizes specific bio-receptor molecules. Terminal active groups determine the reaction conditions for the immobilization of receptors over the layer formed. Table 3

<sup>59</sup> V. Szczepanski, I. Vlassioug, S. Smirnov, *J. Membr. Sci.*, **2006**, 281, 587–591.

<sup>60</sup> a) Z.D. Hendren, J. Brant, M.R. Wiesner, *J. Membr. Sci.*, **2009**, 331, 1–10; b) D.J. Odom, L.A. Baker, C.R. Martin, *J. Phys. Chem. B*, **2005**, 109, 20887–20894; c) A.Y. Ku, J.A. Ruud, T.A. Early, R.R. Corderman, *Langmuir*, **2006**, 22, 8277–8280.

<sup>61</sup> a) K.C. Popat, G. Mor, C.A. Grimes, T.A. Desai, *Langmuir*, **2004**, 20, 8035–8041; b) K.E. La Flamme, K.C. Popat, L. Leoni, E. Markiewicz, T.J. La Tempa, B.B. Roman, C.A. Grimes, T.A. Desai, *Biomaterials*, **2007**, 28, 2638–2645; c) S.W. Lee, H. Shang, R.T. Haasch, V. Petrova, G.U. Lee, *Nanotechnology*, **2005**, 16, 1335–1340.

summarizes the most common organosilane reagents and the reaction required.

**Table 3.** Summary of the most common silanes used to functionalize NAA and their linking abilities.

ORGANOSILANE	TERMINAL GROUP	LINKAGE	REF.
APTES	-NH <sub>2</sub>	✓ Urea bond. ✓ Amide bond. ✓ Electrostatic interactions.	62
ICPTS	-N=C=O	Urea bond.	63
(3-azidopropyl) triethoxysilane / 3-Trimethylsiloxy-1-propyne	-N <sub>3</sub> / -≡	Huisgen cycloaddition.	64
(3-mercaptopropyl) triethoxysilane	-SH	✓ Thiol bond ✓ SH-Au bond	65
(3-iodopropyl) trimethoxysilane	-I / -Cl	Substitution reaction.	66

Silanization, which consist on the covering of a surface with organofunctional alkoxysilane molecules, is frequently performed by using the following two reactivities: (3-aminopropyl)triethoxysilane (APTES) and (3-isocyanatopropyl)triethoxysilane (ICPTS). Both share principal chemical structure with the only difference on the terminal active group, amine for APTES and isocyanate in the case of ICPTS. The mechanism reaction for the formation of the superficial monolayers are the same for both. First, hydrolysis reaction of

<sup>62</sup> H. Yan, C. Teh, S. Sreejith, L. Zhu, A. Kwok, W. Fang, X. Ma, K.T. Nguyen, V. Korzh, Y.S. Zhao, *Angew. Chem. Int. Ed.*, **2012**, *51*, 8373–8377; b) Y.-L. Sun, B.-J. Yang, S.X. Zhang, Y.-W. Yang, *Chem. Eur. J.*, **2012**, *18*, 9212–9216.

<sup>63</sup> Q. Yuan, Y.F. Zhang, T. Chen, D.Q. Lu, Z.L. Zhao, X.B. Zhang, Z.X. Li, C.H. Yan, W.H. Tan, *ACS Nano*, **2012**, *6*, 6337–6344.

<sup>64</sup> X. He, Y. Zhao, D. He, K. Wang, F. Xu, J. Tang, *Langmuir*, **2012**, *28*, 12909–12915.

<sup>65</sup> a) S.S. Wu, X. Huang, X.Z. Du, *Angew. Chem. Int. Ed.*, **2013**, *52*, 5580–5584; b) A. Schlossbauer, A.M. Sauer, V. Cauda, A. Schmidt, H. Engelke, U. Rothbauer, K. Zolghadr, H. Leonhardt, C. Bräuchle, T. Bein, *Adv. Healthcare Mater.*, **2012**, *1*, 316–320.

<sup>66</sup> P. Diez, A. Sanchez, M. Gamella, P. Martínez-Ruiz, E. Aznar, C. de la Torre, J.R. Murguía, R. Martínez-Máñez, R. Villalonga, J.M. Pingarrón, *J. Am. Chem. Soc.*, **2014**, *136*, 9116–9123.

ethoxy groups convert alcoxysilanes in silanols, that rapidly condense with NAA surface hydroxyl groups for the SAM formation (Figure 14).<sup>67</sup>

The implementation of functionality to NAA supports entails a powerful tool for the development of hybrid materials for new applications. In particular, immobilization of biomolecules over their surface, constitute a basic element for the development of sensing devices with great specificity and sensibility.

## 1.5 Gated materials.

Very recently, the blending of (supra)molecular architectures with porous inorganic supports of 2D and 3D nature has led to the preparation of smart nanodevices with plenty of scientific and technological applications. One of the most interesting examples of these smart nanodevices is the so called *gated materials*. These materials contain *gated molecular ensembles*, which are defined as “switchable entities controlling either the on-command release of confined guest or the on-command entrance of molecular species to certain sites”.<sup>68</sup> Generally, gated materials consist on two main components: (i) a switchable “gate-like” ensemble with the ability to “open” or “close” when specific stimuli are applied; and (ii) a porous inorganic support in which certain cargo can be loaded.

Gated materials are constructed through the grafting of organic molecules, biomolecules and supramolecules (different in chemical nature, size and shape) along the surface of a mesoporous inorganic scaffold, with the final objective of tuning the diffusion of a cargo from the voids of the porous material to a solution, or vice versa, in response of predefined stimuli.<sup>69</sup> In general, the inner of the pores is loaded with certain cargos while the outer surface is functionalized with(bio)molecules that modulate the release of the entrapped

---

<sup>67</sup> R. Peña-Alonso, F. Rubio, J. Rubio, J. L. Oteo, *J. Mater. Sci.*, **2007**, *42*, 595–603; b) O.J. Guy, K.A.D. Walker, *Silicon Carbide Biotechnology* (Second Edition), **2016**.

<sup>68</sup> a) E. Aznar, R. Martínez-Mañez, F. Sancenón, *Expert Opin. Drug Delivery*, **2009**, *6*, 643–655; b) K.K. Cotí, M.E. Belowich, M. Liong, M.W. Ambrogio, Y.A. Lau, H.A. Khatib, J.I. Zink, N.M. Khashab, J.F. Stoddart, *Nanoscale*, **2009**, *1*, 16–39.

<sup>69</sup> E. Aznar, M. Oroval, Ll. Pascual, J. R. Murguía, R. Martínez-Mañez, F. Sancenón, *Chem. Rev.*, **2016**, *116*, 561-718.

payload upon the application of an external stimulus. Figure 15 shows a schematic representation of a gated material and the release protocol.

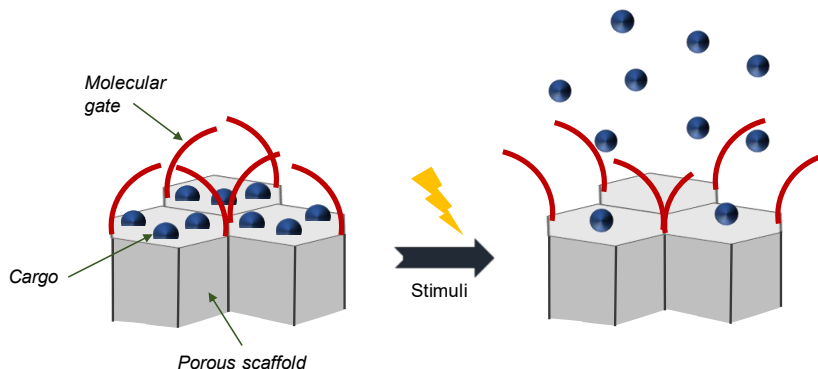


**Figure 15:** Schematic representation of a gated material.

Literature certifies that the most common applications of gated materials are related with controlled release protocols, especially for biomedical applications.<sup>70</sup> Besides, more recently, gated materials for sensing/molecular recognition events have been gaining relevance, bringing to light an interesting application full of potential.<sup>71</sup>

The most important parameters when designing a gated material are the selection of the stimulus which triggers cargo release and the molecular gate that will respond to the presence of the selected stimulus allowing mass transport. External stimuli can be divided in two main groups: (i) physical and (ii) (bio)chemical.

I. Physical stimuli have some particularities that make them interesting. In one hand, they do not require the introduction of additional substances, which simplifies their optimization. Among the common physical stimulus, light,<sup>72</sup>

<sup>70</sup> a) J.A. Barreto, W. O'Malley, M. Kubeil, B. Graham, H. Stephan, L. Spiccia, *Adv. Mater.*, **2011**, 23, H18–H40; b) W.J. Stark, *Angew. Chem. Int. Ed.*, **2011**, 50, 1242–1298; c) Z. Li, J.C. Barnes, A. Bosoy, J.F. Stoddart, J.I. Zink, *Chem. Soc. Rev.*, **2012**, 41, 2590–2605. d) T.L. Doane, C. Burda, *Chem. Soc. Rev.*, **2012**, 41, 2885–2911.

<sup>71</sup> C. Coll, A. Bernardos, R. Martínez-Máñez, F. Sancenón, *Acc. Chem. Res.*, **2013**, 46, 339–349.

<sup>72</sup> a) E. Johansson, E. Choi, S. Angelos, M. Liang, J. I. Zink, *Sol–Gel Sci. Technol.*, **2008**, 46, 313–317; b) Q. Lin, Q. Huang, C. Li, C. Bao, Z. Liu, F. Li, L. Zhu, *L. J. Am. Chem. Soc.*, **2010**, 132, 10645–10647.

temperature<sup>73</sup> and magneto-thermal effects<sup>74</sup> are the most reported. However, very limited bio-organic molecules are controllable through physical stimulus, which difficults the development of gated materials sensitive to these stimuli.

II. (Bio)chemical stimuli have, in contrast, plenty of examples and applications. Most common stimuli are protons (changes in pH),<sup>75</sup> metal cations,<sup>76</sup> oligonucleotides,<sup>77</sup> saccharides,<sup>78</sup> small molecules,<sup>79</sup> small redox active molecules,<sup>80</sup> enzymes,<sup>81</sup> and peptides<sup>82</sup> among others.

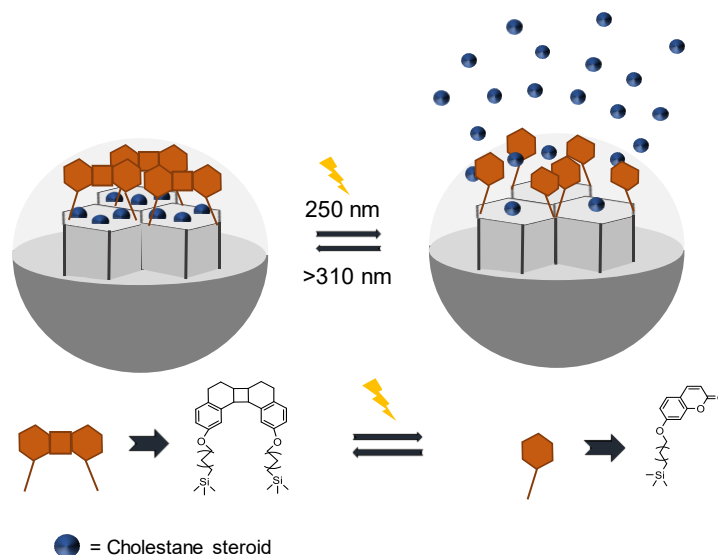


**Figure 16:** Schematic representation of a photochemically controlled gated material. Upon irradiation at 250 nm, selected cargos were released and coumarin monomers regenerated.

<sup>73</sup> a) J. Lai, X. Mu, Y. Xu, X. Wu, C. Wu, C. Li, J. Chen, Y. Zhao, *Chem. Commun.*, **2010**, 46, 7370–7372.

<sup>74</sup> C. Liu, J. Guo, W. Yang, J. Hu, C. Wang, S. Fu, *J. Mater. Chem.*, **2009**, 19, 4764–4770; b) C.R. Thomas, D.P. Ferris, J.H. Lee, E. Choi, M.H. Cho, E.S. Kim, J.F. Stoddart, J.S. Shin, J. Cheon, J.I. Zink, *J. Am. Chem. Soc.*, **2010**, 132, 10623–10625.

<sup>75</sup> a) R. Casasús, M.D. Marcos, R. Martínez-Máñez, J.V. Ros-Lis, J. Soto, L.A. Villaescusa, P. Amorós, D. Beltrán, C. Guillem, J. Latorre, *J. Am. Chem. Soc.*, **2004**, 126, 8612–8613; b) M. Ruiz-Rico, É. Pérez-Esteve, M.J. Lerma-García, M.D. Marcos, R. Martínez-Máñez, J.M. Barat, *Food Chem.*, **2017**, 218, 471–478; c) Q. Yang, S. Wang, P. Fan, L. Wang, Y. Di, K. Lin, F. S. Xiao, *Chem. Mater.*, **2005**, 17, 5999–6003; d) V. Cauda, C. Argyo, A. Schlossbauer, T.J. Bein, *J. Mater. Chem.*, **2010**, 20, 4305–4311; e) B. Tian,

Along the years, gated ensembles have been evolving from the simplest molecules or singular entities, to complex supermolecules.

In 2003, Fujiwara and co-workers reported the first example of a gated material using MCM-41 mesoporous silica nanoparticles (MSNs) loaded with steroid cholestane and in which the possibility of regulating photochemically the uptake, storage and release of the cargo was implemented (Figure 16).<sup>78</sup> For this purpose, the pores of the MSNs were loaded with cholestane and then the

---

S. Liu, S. Wu, W. Lu, D. Wang, L. Jin, Z. Quan, *Colloids Surf. B*, **2017**, *154*, 287–296; f) H. Meng, M. Xue, T. Xia, Y. L. Zhao, F. Tamanoi, J.F. Stoddart, J.I. Zink, E.A. Nel, *J. Am. Chem. Soc.*, **2010**, *132*, 12690–12697; g) A. Llopis-Lorente, B. Lozano-Torres, A. Bernardos, R. Martínez-Máñez, F. Sancenón, *J. Mater. Chem. B*, **2017**, *5*, 3069–3083; h) W. Guo, J. Wang, S.J. Lee, F. Dong, S.S. Park, C.S. Ha, *Chem. Eur. J.*, **2010**, *16*, 8641–8646; i) A. Popat, J. Liu, G. Q. Lu, S. Z. Qiao, *J. Mater. Chem.*, **2012**, *22*, 11173–11178.

<sup>76</sup> Y. Zhou, L.-L. Tan, Q.-L. Li, X.-L. Qiu, A.-D. Qi, Y. Tao, Y.-W. Yang, *Chem. Eur. J.*, **2014**, *20*, 2998.

<sup>77</sup> a) C.L. Zhu, C.H. Lu, X.Y. Song, H.H. Yang, X.R. Wang, *J. Am. Chem. Soc.*, **2011**, *133*, 1278–1281; b) A. Schossbauer, S. Warncke, P.M.E. Gramlich, J. Kecht, A. Manetto, T. Carell, T. Bein, *Angew. Chem. Int. Ed.*, **2010**, *49*, 4734–4743; c) Y. Zhang, Q. Yuan, T. Chen, X. Zhang, Y. Chen, W. Tan, *Anal. Chem.*, **2012**, *84*, 1956–1962.

<sup>78</sup> a) N.K. Mal, M. Fujiwara, Y. Tanaka, *Nature*, **2003**, *421*, 350–353; b) N.K. Mal, Y. Tanaka, T. Taguchi, M. Matsukata, *Chem. Mater.*, **2003**, *15*, 3385–3394; c) A. Bernardos, L. Mondragón, E. Aznar, M. D. Marcos, R. Martínez-Máñez, F. Sancenón, J. Soto, J. M. Barat, E. Pérez-Payá, C. Guillem, P. Amorós, *ACS Nano*, **2010**, *4*, 6353–6368.

<sup>79</sup> a) R. Casasús, E. Aznar, M. D. Marcos, R. Martínez-Máñez, F. Sancenón, J. Soto, P. Amorós, *Angew. Chem. Int. Ed.*, **2006**, *45*, 6661–6664; b) L. Zhang, Y. Li, C.Y. Jimmy, *J. Mater. Chem. B*, **2014**, *2*, 452–470; c) N. Song, Y.W. Yang, *Chem. Soc. Rev.*, **2015**, *44*, 3474–3504; d) E. Aznar, C. Coll, M.D. Marcos, R. Martínez-Máñez, F. Sancenón, J. Soto, P. Amorós, J. Cano, E. Ruiz, *Chem. Eur. J.*, **2009**, *15*, 6877–6888; e) Y. Zhao, B. G. Trewyn, I.I. Slowing, V. S.Y. Lin, *J. Am. Chem. Soc.*, **2009**, *131*, 8398–8400; f) Y.L. Choi, J. Jaworsky, M.L. Seo, S.J. Lee, J.H. Jung, *J. Mater. Chem.*, **2011**, *21*, 7882–7885; g) A. Schulz, R. Woolley, T. Tabarin, C. McDonagh, *Analyst*, **2011**, *136*, 1722–1727; h) J. Lee, J. Lee, S. Kim, C.J. Kim, S. Lee, B. Min, Y. Shin, C. Kim, *Bull. Korean Chem. Soc.*, **2011**, *32*, 1357–1358; i) I. Candel, A. Bernardos, E. Climent, M.D. Marcos, R. Martínez-Máñez, F. Sancenón, J. Soto, A. Costero, S. Gil, M. Parra, *Chem. Commun.* **2011**, *47*, 8313–8315.

<sup>80</sup> a) R. Liu, X. Zhao, T. Wu, P. Feng, *J. Am. Chem. Soc.*, **2008**, *130*, 14418–14419; b) R. Mortera, J. Vivero-Escoto, I.I. Slowing, E. Garrone, B. Onida, V.S.Y. Lin, *Chem. Commun.*, **2009**, 3219–3221.

<sup>81</sup> a) K. Patel, S. Angelos, W.R. Dichtel, A. Coskun, Y.W. Yang, J.I. Zink, J.F. Stoddart, *J. Am. Chem. Soc.*, **2008**, *130*, 2382–2383; b) A. Schlossbauer, J. Kecht, T. Bein, *Angew. Chem. Int. Ed.*, **2009**, *48*, 3092–3095; c) A. Bernardos, E. Aznar, M. D. Marcos, R. Martínez-Máñez, F. Sancenón, J. Soto, J. M. Barat, P. Amorós, *Angew. Chem. Int. Ed.*, **2009**, *48*, 5884–5887; d) C. Park, H. Kim, S. Kim, C. Kim, *J. Am. Chem. Soc.*, **2009**, *131*, 16614–16615; e) P.D. Thornton, A. Heise, *J. Am. Chem. Soc.*, **2010**, *132*, 2024–2028.

<sup>82</sup> a) C. Coll, L. Mondragón, R. Martínez-Máñez, F. Sancenón, M.D. Marcos, J. Soto, P. Amorós, E. Pérez-Payá, *Angew. Chem. Int. Ed.*, **2011**, *50*, 2138–2140; b) F. Porta, G.E.M. Lamers, J.I. Zink, A. Kros, *Phys. Chem. Chem. Phys.*, **2011**, *13*, 9982–9985.

external surface functionalized with 7-[(3-triethoxysilyl)-propoxy]coumarin. This coumarin derivative undergoes a [2+2] photodimerization reaction, when irradiated at wavelengths longer than 310 nm, yielding bulky cyclobutane dimers in anti head-to-head conformation that blocked pore entrances inhibiting cholestane release. The dimerization process is reversible and irradiation at 250 nm restored the monomer conformation allowing cholestane release. Comparable results were obtained with other cargos (pyrene, phenanthrene and progesterone), demonstrating control over the accessibility of the pores.

Other representative example of a gated material was reported by Yang et al. The authors selected a nano metal-organic framework (NMOF) mesoporous support (UMCM-1-NH<sub>2</sub>)<sup>83</sup> which was functionalized with pillar[n]arenes macrocycles sensible to both changes in pH and the presence of methyl viologen salts (Figure 17).<sup>84</sup> UMCM-1-NH<sub>2</sub> is a NMOF developed by the University of Michigan with a hexagonal mesopore distribution and containing -NH<sub>2</sub> moieties onto its surface. The pores of the support were loaded with certain cargos (rhodamine 6G and doxorubicin) and then the external surface was decorated with pyridinium moieties. Finally, pores were capped upon addition of negatively charged carboxylatopillar[5]arene (CP5) macrocycle, which formed [2]pseudorotaxanes after interaction with the grafted pyridinium salts. Addition of methyl viologen induced pore opening and cargo release because formed strong inclusion complexes with CP5 macrocycle than those formed with the grafted pyridinium salts. Besides, this gated nanodevice was also modulated by pH variations. At this respect, when solution pH is 5 or lower, the carboxylate moieties in CP5 were protonated and the electrostatic interactions with the grafted pyridinium salts were neutralised, thus leading to the uncapping of nanopores and cargo release. This pH modulation has important application for drug delivery. For this purpose, doxorubicin was successfully encapsulated into the MOF nanopores to be specifically released in zones of tumour tissues where pH is known to be more acidic than normal tissues and blood. This way, undesired drug release during transportation is

---

<sup>83</sup> Z. Wang, K. K. Tanabe, S. M. Cohen, *Inorg. Chem.*, **2009**, *48*, 296-306.

<sup>84</sup> L.-L. Tan, H. Li, Y.-C. Qiu, D.-X. Chen, X. Wang, R.-Y. Pan, Y. Wang, S.X.-A. Zhang, B. Wang, Y.-W. Yang, *Chem. Sci.*, **2015**, *6*, 1640-1644.

avoided, drug effectivity is enhanced significantly and chemotherapy adverse effects are diminished.

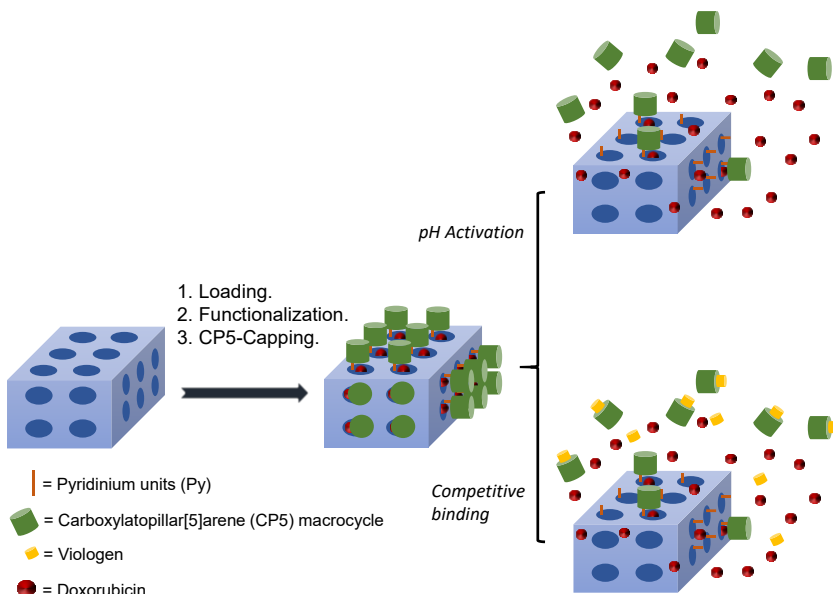


**Figure 17:** Schematic representation of NMOFs gated by pillar[5]arene-based nanovalves and response to variation in pH and competitive binding with methyl viologen.

The following example shows how the complexity in the design of the molecular gates has been increasing over time incorporating more advanced structures, with the possibility of interconnecting several nanodevices, with different gating ensembles and encapsulated cargos.

At this respect, in 2014, Martínez-Máñez and co-workers demonstrated the possibility of sharing information between three different gated MSNs. For this communication, the chemical messenger released first by the external stimulus is the key for the second cargo delivery, which is the stimulus necessary to open the third gated system.<sup>85</sup>

<sup>85</sup> C. Giménez, E. Climent, E. Aznar, R. Martínez-Máñez, F. Sancenón, M.D. Marcos, P. Amorós, K. Rurack, *Angew. Chem. Int. Ed.*, **2014**, 53, 12629-12633.



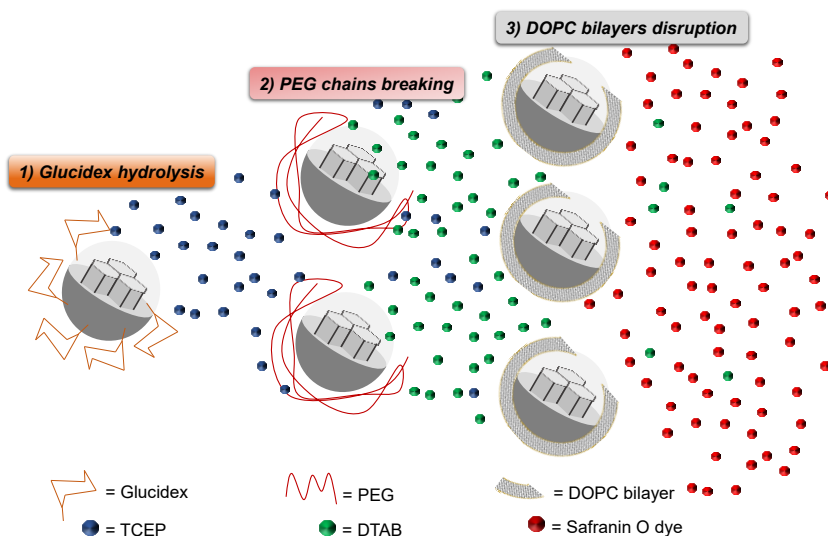


**Figure 18:** Figurative illustration of the communication event between three sets of nanoparticles. TCEP molecules released from the first particles opens the second particles pores, which DTAB released induced the delivery of the safranin O dye entrapped in the third nanodevice.

The first nanodevice was charged with the reducing agent tris(2-carboxyethyl)phosphine (TCEP) and capped with glucidex (a polysaccharide). The second set of nanoparticles was capped with polyethylene glycol (PEG) chains attached to the surface through a disulphide bond that inhibited the release of cargo dodecyltrimethylammonium bromide (DTAB). Finally, in the third nanodevice, a lipid bilayer (of 1,2-dioleoyl-*sn*-glycero-3-phosphocholine, DOPC) inhibited the release of the encapsulated safranin O dye. In a typical experiment (Figure 18), the presence of pancreatin in an aqueous solution caused the hydrolysis of the polysaccharide that capped the first nanodevice, allowing the delivery of the loaded reducing agent (TCEP). TCEP broke down disulphide bonds in the PEG chain of the second gated system, which resulted in pore opening and DTAB release. Finally, DTAB molecules delivered from the second nanoparticles disrupted the lipid bilayer of the third nanodevice thus allowing the release of safranin O dye, which was monitored by fluorescence spectroscopy. Individual optimization process was undertaken for each one of the presented systems and, in all cases, “zero release” was observed until the

appropriate stimulus was present in the aqueous solution. In further experiments, the presented sequence of activation was confirmed as well as the need of an intact intermediate communication chain. This proof of concept opened up a broad range of applications in drug delivery, sensing, catalysis and in biomimetic chemistry.

In order to provide an overview of the extensive development carried out in this field, Table 4 summarizes some of the most important stimuli used and the mechanism that modulates cargo release.

**Table 4:** Examples of external stimulus and mechanism that control gates open/close state.

Stimulus	Mechanism	Ref.
<i>Light</i>	✓ Dimerization/Isomerization	87
	✓ Photocleavage of covalently anchored stalks	88
	✓ Photo-thermal destabilization of the capping entity	89
	✓ ROS photogenerated able to disrupt chemical bonds	90
<i>Magnetic fields</i>	✓ Conformation/structural changes induced by thermic variations	91
<i>Temperature</i>	✓ Temperature responsive polymers	92
	✓ Grafted DNA melting	93
<i>Ultrasound</i>	✓ Structural disruption by cavitation	94
<i>pH</i>	✓ Conformational changes from rigid to flexible	95
	✓ Disruption of metal complexes and pH-sensitive bonds	96
	✓ Volume change in pH sensitive polymers	97
	✓ Disruption of lipid bilayers and layer-by-layer depositions	98
	✓ Dissolution of inorganic capping structures	99
<i>Molecules</i>	✓ Molecular recognition events	100
<i>Biomolecules</i>	✓ Oligonucleotides chain recognition	101
<i>Enzymes</i>	✓ Hydrolysis and other enzymatic reactions	102
<i>Redox</i>	✓ Reduction of inclusion complexes and redox labile bonds	103

- <sup>86</sup> a) E. Aznar, R. Casasús, B. García-Acosta, M.D. Marcos, R. Martínez-Máñez, F. Sancenón, J. Soto, P. Amorós, *Adv. Mater.*, **2007**, *19*, 2228–2231; b) Q. Xing, N. Li, D. Chen, W. Sha, Y. Jiao, X. Qi, Q. Xu, J. Lu, *J. Mater. Chem. B*, **2014**, *2*, 1182–1189; c) L. Chen, W. Wang, B. Su, Y. Wen, C. Li, Y. Zhou, M. Li, X. Shi, H. Du, Y. Song, L. Jiang, *ACS Nano*, **2014**, *8*, 744–751.
- <sup>87</sup> a) T.M. Guardado-Alvarez, L.S. Devi, J.M. Vabre, T.A. Pecorelli, B.J. Schwartz, J.O. Durand, O. Mongin, M. Blanchard-Desce, J.I. Zink, *Nanoscale*, **2014**, *6*, 4652–4658; b) Y. Yang, B. Velmurugan, X. Liu, B. Xing, *Small*, **2013**, *9*, 2937–2944.
- <sup>88</sup> a) P. Shi, Z. Liu, K. Dong, E. Ju, J. Ren, Y. Du, Z. Li, X. A. Qu, *Adv. Mater.*, **2014**, *26*, 6635–6641; b) P. Shi, E. Ju, J. Ren, X. Qu, *Adv. Funct. Mater.*, **2014**, *24*, 826–834.
- <sup>89</sup> a) S. Yang, N. Li, Z. Liu, W. Sha, D. Chen, Q. Xu, J. Lu, *Nanoscale*, **2014**, *6*, 14903–14910; b) P.M. Dobay, A. Schmidt, E. Mendoza, T. Bein, J. Rädler, *Nano Lett.*, **2013**, *13*, 1047–1052.
- <sup>90</sup> a) A. Baeza, E. Guisasaola, E. Ruiz-Hernandez, M. Vallet-Regí, *Chem. Mater.*, **2012**, *24*, 517–524; b) D.H. Kim, Y. Guo, Z.L. Zhang, D. Procissi, J. Nicolai, R.A. Omary, A.C. Larson, *Adv. Healthcare Mater.*, **2014**, *3*, 714–724.
- <sup>91</sup> a) M.M. Russell, L. Raboin, T.M. Guardado-Alvarez, J.I. Zink, *J. Sol–Gel Sci. Technol.*, **2014**, *70*, 278–285; b) C.L. Wu, X. Wang, L.Z. Zhao, Y.H. Gao, R.J. Ma, Y.L. An, L.Q. Shi, *Langmuir*, **2010**, *26*, 18503–18507.
- <sup>92</sup> a) C. Chen, J. Geng, F. Pu, X. Yang, J. Ren, X. Qu, *Angew. Chem., Int. Ed.*, **2011**, *50*, 882–886; b) Z.Z. Yu, N. Li, P.P. Zheng, W. Pan, B. Tang, *Chem. Commun.*, **2014**, *50*, 3494–3497.
- <sup>93</sup> X. Wang, H. Chen, Y. Zheng, M. Ma, Y. Chen, K. Zhang, D. Zeng, J. Shi, *Biomaterials*, **2013**, *34*, 2057–2068; b) X. Wang, H. Chen, K. Zhang, M. Ma, F. Li, D. Zeng, S. Zheng, Y. Chen, L. Jiang, H. Xu, J. Shi, *Small*, **2014**, *10*, 1403–1411.
- <sup>94</sup> V. Morales, M. Gutiérrez-Salmerón, M. Balabasquer, J. Ortiz-Bustos, A. Chocarro-Calvo, C. García-Jiménez, R.A. García-Muñoz, *Adv. Funct. Mater.*, **2016**, *40*, 7291–7303.
- <sup>95</sup> a) Z. Zou, S. Li, D. He, X. He, K. Wang, L. Li, *J. Mat. Chem. B*, **2017**, *11*, 2126–2132; b) B. Tian, S. Liu, S. Wu, W. Lu, D. Wang, L. Jin, B. Hu, K. Li, Z. Whang, Z. Quan, *Colloids Surf., B*, **2017**, *154*, 287–296.
- <sup>96</sup> a) J.K. Fu, Y.C. Zhu, Y.J. Zhao, *Mater. Chem. B*, **2014**, *2*, 3538–3548; b) C. Smart, P. Prawingwong, S. Amnuaypanich, H.B. Zhang, K. Kajiyoshi, P.J. Reubroycharoen, *Ind. Eng. Chem.*, **2014**, *20*, 2153–2158.
- <sup>97</sup> a) W. Feng, W. Nie, C. He, X. Zhou, L. Chen, K. Qiu, W. Wang, Z. Yin, *ACS Appl. Mater. Interfaces*, **2014**, *6*, 8447–8460; b) J. Zhang, D. Desai, J.M. Rosenholm, *Adv. Funct. Mater.*, **2014**, *24*, 2352–2360.
- <sup>98</sup> a) C. Yang, W. Guo, L. Cui, D. Xiang, K. Cai, H. Lin, F. Qu, *Mater. Sci. Eng. C*, **2014**, *36*, 237–243; b) Q.S. Zheng, Y.L. Hao, P.R. Ye, L.Q. Guo, H.Y. Wu, Q.Q. Guo, J.Z. Jiang, F.F. Fu, G.N. Chen, *J. Mater. Chem. B*, **2013**, *1*, 1644–1648.
- <sup>99</sup> a) E. Aznar, C. Coll, M.D. Marcos, R. Martínez-Máñez, F. Sancenón, J. Soto, P. Amorós, J. Cano, E. Ruiz, *Chem. Eur. J.*, **2009**, *15*, 6877–6888; b) E. Climent, M.D. Marcos, R. Martínez-Máñez, F. Sancenón, J. Soto, K. Rurack, P. Amorós, *Angew. Chem., Int. Ed.*, **2009**, *48*, 8519–8522; c) M. Yu, Z. Gu, T. Ottewell, C. Yu, *J. Mat. Chem.*, **2017**, *18*, 3241–3252.
- <sup>100</sup> E. Climent, R. Martínez-Máñez, F. Sancenón, M.D. Marcos, J. Soto, A. Maquieira, P. Amorós, *Angew. Chem. Int. Ed.*, **2010**, *49*, 7281–7283.
- <sup>101</sup> a) L. Pascual, S. Sayed, M.D. Marcos, R. Martínez-Máñez, F. Sancenón, *Chem. Asian J.*, **2017**, *7*, 775–784; b) A. Llopis-Lorente, B. Lozano-Torres, A. Bernardos, R. Martínez-

Most of the gated materials presented in Table 4 are used in controlled release protocols. Among them, those which used biomolecules as gating units have gained much relevance due to their specificity, selectivity and biocompatibility, and have been extensively used in drug delivery protocols due to their well-known advantages (such as target-release, low side effects, improved effectiveness). Moreover, the use of biomolecule-gated materials in sensing protocols has received increasing interest recently.

### 1.5.1 Sensing applications.

As stated above, during the last years, gated systems for sensing purposes have received increased attention. Analogously to drug delivery devices, the development of gated nanoprobe for sensing are based in the design of a stimuli-responsive hybrid gated material with the ability to release an entrapped signalling unit (a dye, a fluorophore or a redox-active molecule) in the presence of a specific stimuli (in this case a certain molecule or biomolecule).<sup>103</sup> The signal reporter delivered is monitored, commonly, by different spectroscopic or electrochemical procedures.

In order to achieve this goal, gates are designed to adopt two main conformations depending on whether the target is present or not. Preparing a good sensing material requires high specific and sensitive response, and this relies in how easy and strong the coordination or reaction between the target and gate-binding site is. Depending of the chemical nature of the analyte, sensing gated materials can be divided into four main groups: detection of anions, detection of cations, sensing of small neutral molecules and sensing of biomolecules. Table 5 summarizes most relevant sensing mechanisms in these four groups.

---

Máñez, F. Sancenón, *J. Mater. Chem.*, **2017**, *17*, 3069–3083; c) N. Más, A. Agostini, L. Mondragón, A. Bernardos, F. Sancenón, M.D. Marcos, R. Martínez-Máñez, A.M. Costero, S. Gil, M. Merino-Sanjuan, M.; P. Amorós, M. Orzaez, E. Perez-Payá, *Chem. Eur. J.*, **2013**, *19*, 1346–1356.

<sup>102</sup> a) B. Lozano-Torres, L. Pascual, A. Bernardos, M.D. Marcos, J.O. Jeppesen, Y. Salinas, R. Martínez-Máñez, F. Sancenón *Chem. Comm.*, **2017**, 53,25 3559–3562; b) B.Y. Lee, Z. Li, D.L. Clemens, B.J. Dillon, A.A. Hwang, J.I. Zink, M.A. Horwitz, *Small*, **2016**, *12*, 27, 3690–3702.

<sup>103</sup> F. Sancenón, Ll. Pascual, M. Oroval, E. Aznar, R. Martínez-Máñez, *ChemistryOpen*, **2015**, *4*, 418–437.

**Table 5:** Summary of most representative sensing mechanism developed for sensing applications.

Analyte	Mechanism	Ref.
Anions	✓ Gate-triggering anion complex formation	77a
	✓ Selective DNA recognition	104
Cations	✓ Complex formation and interaction with thiol groups	105
	✓ Selective DNA recognition	106
	✓ Displacement	107
Small neutral molecules	✓ Nucleophilic substitution	108
	✓ pH changes	109
	✓ Disulfide bonds reduction	110
	✓ Complex formation	111
	✓ Specific biomolecules recognition	112
Biomolecules	✓ Selective DNA recognition	113

These nanodevices present remarkable advantages that potentiate their use as detection systems. In one side, the recognition step is disconnected from

<sup>104</sup> L. Hou, C. Zhu, X. Wu, G. Chen, D. Tang, *Chem. Commun.*, **2014**, 50, 1441-1443.

<sup>105</sup> E. Climent, M.D. Marcos, R. Martínez-Máñez, F. Sancenón, J. Soto, K. Rurack, P. Amorós, *Angew. Chem. Int. Ed.*, **2009**, 48, 8519-8522.

<sup>106</sup> L. Fu, J. Zhuang, W. Lai, X. Que, M. Lu, D. Tang, *J. Mater. Chem. B*, **2013**, 1, 6123-6128.

<sup>107</sup> M. Chen, C. Huang, C. He, W. Zhu, Y. Xu, Y. Lu, *Chem. Commun.*, **2012**, 48, 9522-9524.

<sup>108</sup> P. Díez, A. Sánchez, M. Gamella, P. Martínez-Ruiz, E. Aznar, C. de La Torre, J.R. Murguía, R. Martínez-Máñez, R. Villalonga, M.J. Pingarrón, *J. Am. Chem. Soc.*, **2014**, 136, 9116-9123.

<sup>109</sup> R. Villalonga, P. Díez, A. Sánchez, E. Aznar, R. Martínez-Máñez, J. M. Pingarrón, *Chem. Eur. J.*, **2013**, 19, 1017-1021.

<sup>110</sup> S. El Sayed, C. Giménez, E. Aznar, R. Martínez-Máñez, F. Sancenón, M. Licchelli, *Org. Biomol. Chem.*, **2015**, 13, 1017-1021.

<sup>111</sup> Y. Salinas, A. Agostini, E. Pérez-Esteve, R. Martínez-Máñez, F. Sancenón, M.D. Marcos, J. Soto, A.M. Costero, S. Gil, M. Parra, P. Amorós, *J. Mater. Chem. A*, **2013**, 1, 3561-3564.

<sup>112</sup> E. Climent, R. Martínez-Máñez, A. Maquieira, F. Sancenón, M.D. Marcos, E.M. Brun, J. Soto, P. Amorós, *ChemistryOpen*, **2012**, 1, 251-259.

<sup>113</sup> M. Oroval, E. Climent, C. Coll, R. Eritja, A. Aviñó, M.D. Marcos, F. Sancenón, R. Martínez-Máñez, P. Amorós, *Chem. Commun.*, **2013**, 49, 5480-5482.

the signalling event, which makes the last independent of the host-guest interaction.<sup>114</sup> In addition, an important signal amplification event is usually observed without any chemical or biological concentration or amplification step. This amplification is related with the fact that upon the presence of relative few analyte molecules, gates open and therefore a large number of reporter molecules are delivered.<sup>115</sup>

Besides, both approaches are highly flexible given the possible selection of different porous supports, diverse guest-selective binding sites (molecular gates) and a wide range of signalling reporters, predominantly dyes/fluorophores. In the next sections, several examples of sensing nanodevices will be discussed for a better understanding of the research objectives of this thesis.

» Sensing of anions:

One of the first gated systems for sensing applications was developed by Martínez-Máñez research group in 2007 for the detection of long-chain carboxylates in an “on-off” response system.<sup>116</sup> For the preparation of this nanodevice, MCM-41 silica particles were loaded with Ru(bpy)<sub>3</sub><sup>2+</sup> dye (Rubpy) and the external surface of the support was functionalized with imidazolium binding sites. When solid was suspended in aqueous solution, pores were opened and Rubpy was released from the support whereas in the presence of long chain carboxylates delivery of the entrapped dye was highly inhibited. Carboxylates interacted electrostatically with the positively charged imidazolium binding units forming a highly hydrophobic layer around pore entrances which inhibited dye delivery to the solution (Figure 20). Carboxylate-imidazolium interaction was very specific because evaluation of the response of the system in the presence of other anions and cations (such as chloride,

---

<sup>114</sup> a) L. E. Santos-Figueroa, M. E. Moragues, E. Climent, A. Agostini, R. Martínez-Máñez, F. Sancenón, *Chem. Soc. Rev.*, **2013**, *42*, 3489–3613; b) M. E. Moragues, R. Martínez-Máñez, F. Sancenón, *Chem. Soc. Rev.*, **2011**, *40*, 2593–2643; c) Y. Salinas, R. Martínez-Máñez, M. D. Marcos, F. Sancenón, A. M. Costero, M. Parra, S. Gil, *Chem. Soc. Rev.*, **2012**, *41*, 1261–1296.

<sup>115</sup> M. Hecht, E. Climent, M. Biyical, F. Sancenón, R. Martínez-Máñez, K. Rurack, *Coord. Chem. Rev.* **2013**, *257*, 2589–2606.

<sup>116</sup> C. Coll, R. Casasús, E. Aznar, M.D. Marcos, R. Martínez-Máñez, F. Sancenón, J. Soto, P. Amorós, *Chem. Commun.*, **2007**, 1957-1959.

bromide, carbonate, nitrate, sulphate, phosphate, sodium, potassium and calcium) revealed a negligible dye release inhibition. Otherwise, coordination with carboxylates with small or medium alkyl chains ( $\text{CH}_3(\text{CH}_2)_n\text{COO}^-$ ,  $n < 8$ ) was evaluated and no inhibition of dye delivery was observed. These carboxylates interacted with the imidazolium groups but the monolayer formed around pore outlets was not hydrophobic enough to inhibit dye release.

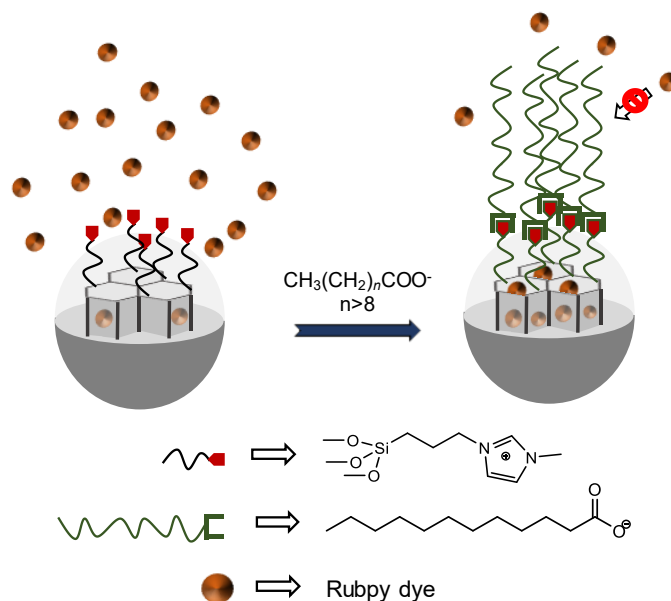


**Figure 20:** MSNs for the detection of long chain carboxylates through cargo release inhibition.

Concerned by the possibility that carboxylates directly attached to the silica surface, MSNs previously loaded with Rubpy dye but not functionalized with imidazolium salts were prepared. Dye delivery of this nanodevice was the same in the absence and in the presence of carboxylates indicating that grafted imidazolium salts are the responsible of the observed selectivity. Finally, the system's response to the presence of different concentrations of dodecanoate and octanoate was evaluated. When dodecanoate concentration rises to mM level dye release became completely inhibited, in contrast, octanoate up to higher concentrations did not cause any inhibition because its insufficient length.

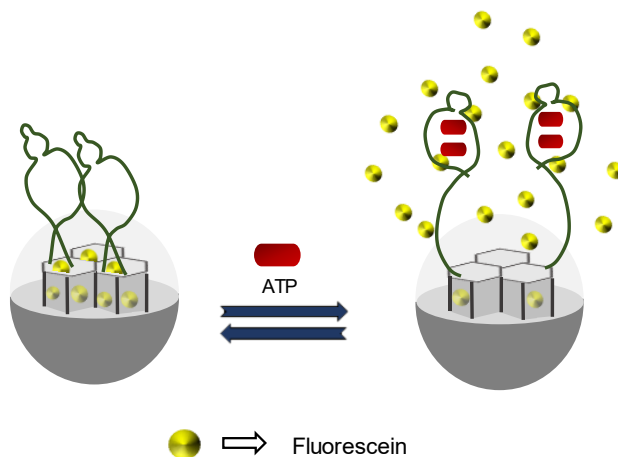


**Figure 21:** Schematic illustration of aptamer-based switchable nanovalves for the selective recognition of ATP nucleotide.

Another example of a hybrid material for anion detection was reported by Schäfer et al. in 2011. In this case, MCM-41 type nanoparticles previously loaded with fluorescein were functionalized with an aptamer sequence specifically designed for the detection of adenosine triphosphate (ATP).<sup>117</sup> Aptamers are nucleic acids chains with bio-recognition properties that are easily anchored to the silica surface. This specific aptamer adopt two different structural conformations depending on whether target is present or not, which modulate cargo transport from the inner of the nanoparticle. In the absence of ATP, aptamer hairpin duplex conformation blocked pore entrances and prevented guest molecules release. However, in the presence of ATP, aptamer coordinated with the oligonucleotide yielding a complex with less steric hindrance that allowed dye diffusion from the inner of the pores to the solution (Figure 21). This conformational change was reversible and was examined by repeatedly adding and removing ATP. The prepared nanodevice presented a marked selectivity because negligible cargo release was observed in the presence of other nucleotides. Besides, system dependence to guest concentration was proved evaluating the nanodevice response to different concentrations of ATP, which resulted in linear dependence that evolved to

<sup>117</sup> V.C. Özalp, T. Schäfer, *Chem. Eur. J.*, **2011**, *17*, 9893-9896.



saturation curve at high ATP concentrations. Finally, specificity was successfully proven by the preparation of a set of MSNs capped with a similar (but not the same) nucleic acid sequence. These new nanoparticles were unable to respond to the presence of ATP.

» Sensing of cations:

Capped mesoporous materials designed for the detection of small cations are scarce. One of the first examples of gated nanodevices, in which cargo release was triggered by  $K^+$  cations, was reported in 2011 by Jung and co-workers.<sup>118</sup> At this respect, MSNs were loaded with the well-known chemopreventive agent curcumin (diferuloylmethane), and then, a 18-crown-6 derivative was covalently attached onto the external surface of the support. In the presence of  $Cs^{2+}$ , a sandwich-type complex with 2:1 stoichiometry between this cation and the grafted crown ether was formed with an affinity constant of ca.  $1.25 \times 10^{-4} \text{ M}^{-1}$ . The generated bulky complex capped thoroughly pores entrances avoiding unspecific release of curcumin. However, in the presence of  $K^+$  and due to a higher affinity constant for the grafted macrocycle ( $5.20 \times 10^{-4} \text{ M}^{-1}$ ), ion exchange with  $Cs^{2+}$  cations was produced. Since 18-crown-6 derivative complex with  $K^+$  presents a 1:1 stoichiometry, ion exchange induced a conformational variation that resulted in pores opening and thus, in curcumin diffusion to the solution (Figure 22). Finally, the releasing capacity of the prepared material was evaluated studying its response to different  $K^+$  concentrations. With the addition of 1.0 equivalent, 45% of the entrapped curcumin was released in approximately 170 minutes, while in the presence of 3 equivalents of  $K^+$ , 100 % of the load was delivered in the first 90 minutes.

---

<sup>118</sup> Y.L. Choi, J. Jaworski, M.L. Seo, S.J. Lee, J.H. Jung, *J. Mater. Chem.*, **2011**, *21*, 7882-7885.

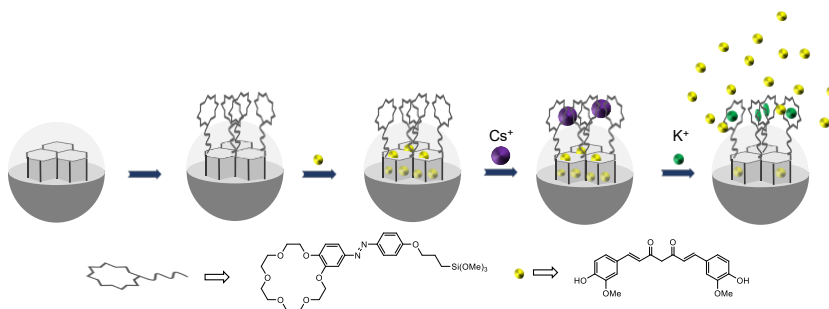


**Figure 22:** MSNs functionalized with a 18-crown-6 derivative able to release an entrapped cargo (curcumin) in the presence of K<sup>+</sup> cation.

Later in 2014, an example of DNA gated material for cation detection was reported by Willner and co-workers.<sup>119</sup> At this respect, MSNs were functionalized with two different catalytic nucleic acids (DNAzymes) pH-programmed and dependent of Mg<sup>2+</sup> and UO<sub>2</sub><sup>2+</sup> cations respectively. For this purpose, MSNs were functionalized with aminopropyl moieties that were reacted with *N*-( $\epsilon$ -maleimidocaproyloxy) sulfosuccinimide ester (sulfo-EMCS) to yield surface active maleimide groups. Then, thiolated ribonucleobase-containing nucleic acid sequences, were linked to maleimide groups. The resulting nanoparticles were loaded with methylene blue (MB<sup>+</sup>) for Mg<sup>2+</sup> detection, and thionine (Th<sup>+</sup>) for UO<sub>2</sub><sup>2+</sup> sensing. Finally, pores were successfully capped by hybridization of specific Mg<sup>2+</sup> and UO<sub>2</sub><sup>2+</sup> dependent DNAzyme sequences (Figure 23), showing almost zero release in the absence of target cations (Mg<sup>2+</sup> and UO<sub>2</sub><sup>2+</sup>) or in the presence of other divalent cations. DNAzymes employed showed pH dependence. Mg<sup>2+</sup> dependent DNAzyme showed optimal catalytic activity at pH 7.2, while in the case of UO<sub>2</sub><sup>2+</sup> optimal conditions were achieved at pH 5.2. At pH 6, both showed 50% of activity, and no catalytic activity at all was observed at pH 5.2 for Mg<sup>2+</sup>-DNAzyme or pH 7.2 for UO<sub>2</sub><sup>2+</sup>-DNAzyme.

<sup>119</sup> Z. Zhang, F. Wang, D. Balogh, I. Willner, *J. Mater. Chem. B*, **2014**, *2*, 4449-4455.

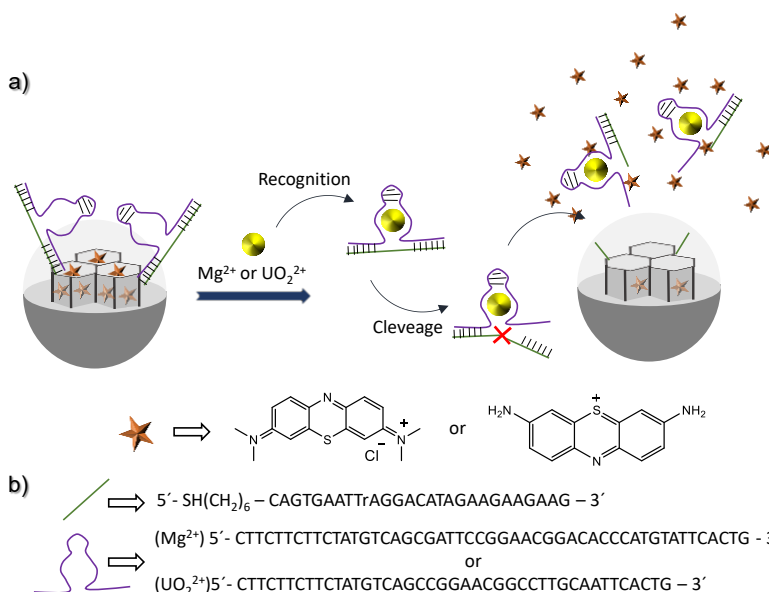


**Figure 23:** a) Schematic representation of the DNAzyme entities opening mechanism in the presence of cations  $Mg^{2+}$  or  $UO_2^{2+}$ . b) Nucleic acid sequences employed in the designed nanodevices.

In the presence of  $Mg^{2+}$  (and analogously  $UO_2^{2+}$ ) and at the DNAzyme optimal pH solution, the metal catalysed the scission of ribonucleotide phosphodiester bond in the predesigned cleavage site by a transesterification reaction, which resulted in DNAzyme-metal complex displacement from surface and release of the entrapped cargo (Figure 23). Diffused MB<sup>+</sup> (or Th<sup>+</sup>) fluorescence emission intensity was monitored ( $\lambda_{em} = 690$  nm for MB<sup>+</sup> and  $\lambda_{em} = 623$  nm for Th<sup>+</sup>), being enhanced when increasing metal concentrations in the solution. Taking into account the availability of  $Mg^{2+}$  ions in cellular environments and the observed catalytic activity of  $UO_2^{2+}$  DNAzymes in acidic media present in cancer cells, this research group was able to not only confirm the potential use of these nanodevices as drug carriers, but also to show a new cation detection strategy and demonstrate their ability to implement DNA sequences for sensing specific cations that can be critical in industrial or alimentary processes.

» Sensing of small neutral molecules:

Nanodevices sophistication improved along the years. J.M. Pingarrón and co-workers designed in 2012 a system for the detection of urea in which gating mechanism and effector molecule were placed in the same nanodevice.<sup>120</sup> For this purpose “Janus nanoparticles”, a combination of MCM-41 type MSNs and Au nanoparticles, were topo-selectively modified with selected ligands to provide different functionalization onto each of the two different phases. In particular, part of MSNs was capped with a pH-responsive gate, while Au surface was functionalized with the enzyme urease. In order to construct the final nanodevice, first, MSNs were adsorbed in a water-paraffin wax emulsion, which left exposed half of the surface that reacted with (3-mercaptopropyl) trimethoxysilane to bond Au nanoparticles via thiol-Au bonds. Paraffin was then completely dissolved in  $\text{CHCl}_3$ . Next, synthesized Janus nanoparticles were loaded with Rubpy fluorescent dye and silica part was selectively functionalized with 3-(2-aminoethylamino) propyltrimethoxysilane (pH-responsive molecular gate). Finally, thiol modified urease enzyme was anchored specifically to Au surface. Buffered suspensions (pH 5.0) of the nanodevice showed negligible Rubpy dye delivery because at acidic pH the nitrogen atoms of the polyamine are protonated and these molecules adopted rigid conformation blocking pore entrances. However, in the presence of urea, urease enzyme catalysed its decomposition into  $\text{CO}_2$  and  $\text{NH}_3$ . Generated ammonia induced a pH increase with subsequent amine deprotonation, pore opening and Rubpy dye delivery.

A further step in the evolution of gated materials for sensing applications was reported in 2013 by Martínez-Máñez and collaborators for the detection of explosive ingredient triacetone triperoxide (TATP) through a simple test-strip assay.<sup>121</sup> Sulforhodamine B fluorescent indicator was loaded into the MSNs scaffolds, which were subsequently functionalized with a previously derivatized hapten that act as linker. Finally, TATP-selective polyclonal antibody was anchored and pores were successfully closed by the steric hindrance provided by the bulky structure of antibody (Figure 25a).

---

<sup>120</sup> R. Villalonga, P. Díez, A. Sánchez, E. Aznar, R. Martínez-Máñez, J.M. Pingarrón, *Chem. Eur. J.*, **2013**, *19*, 7889-7894.

<sup>121</sup> E. Climent, D. Gröninger, M. Hecht, M.A. Walter, R. Martínez-Máñez, M.G. Weller, F. Sancenón, P. Amorós, K. Rurack, *Chem. Eur. J.*, **2013**, *19*, 4117-4122.

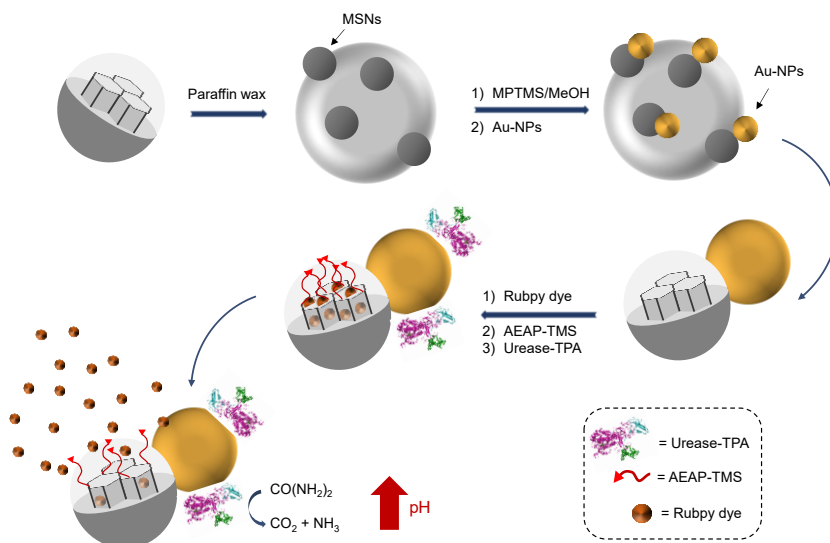


**Figure 24:** Synthesis of Janus Au-MSN nanoparticles for the urea controlled release of Rubpy dye.

Test-strips were prepared with the nanoparticles. Prior to the test, gated nanoparticles were deposited at one end (interaction) of the high-flow nitrocellulose strip. If sample did not contain TATP, system kept closed and no signal was detected. In contrast, when target TATP was present in the sample, competition between analyte and grafted hapten for the binding site of capping antibodies induced gate displacement, pore opening and dye delivery. Because of the flow conditions, released dye moved to the detection site where was monitored by a fluorescence flow assay reader at 625 nm ( $\lambda_{\text{exc}} = 520 \text{ nm}$ ). Dye delivery and TATP correlation was demonstrated evaluating the response of the developed assay in the presence of different target concentration. Limit of detection (LOD) was established in 15 ppb of TATP by using the developed test-strip assay, and according to the results, with an amplification effect of 70 dye molecules per each antibody displaced.

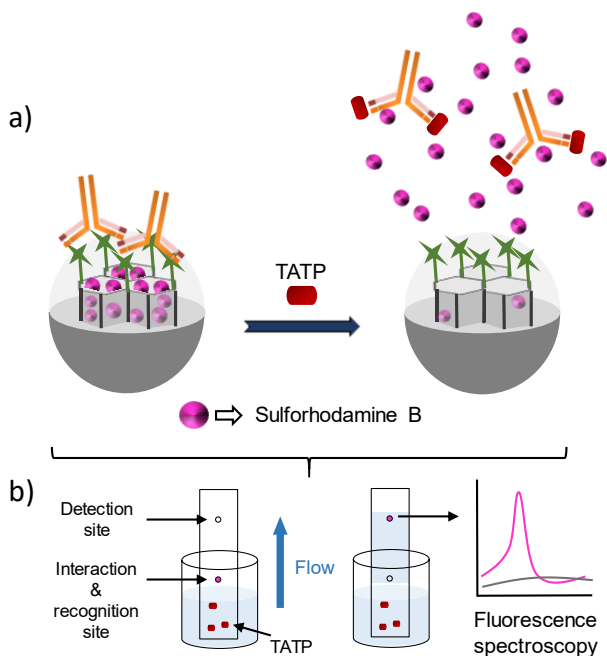


**Figure 25:** a) Uncapping process of antibody-gated nanoparticles in the presence of TATP explosive. b) Schematic representation of the developed test-strip lateral-flow assay for TATP detection.

Furthermore, sensor selectivity in the presence of other common explosives (trinitrotoluene (TNT), hexogen (RDX), nitropenta (PETN), octogen (HMX) and hexamethylene triperoxide diamine (HMTD)), synthetic precursors of TATP (hydrogen peroxide, acetone and 7-oxaotanoic acid), cyclic peroxides (tributanone triperoxide (but-TP), tri-3-pentanone triperoxide (3-pent-TP), tri-2-pentanone triperoxide (2-pent-TP) and diacetone diperoxide (DADP)) and structurally related crown ethers (18C6 and 12C4) was tested. TATP selectivity was certified by the negligible dye release observed in the presence of these other explosives tested. Finally, optimized assay was evaluated in realistic conditions such as tap water, influent and effluent water from sewage treatment plants, showing good sensing capabilities in all of them.

## » Sensing of biomolecules:

In recent years, the detection of biomolecules using gated nanodevices has emerged as a powerful tool and as an alternative for traditional analytical methods. One example of these recently developed bioprobes is the nanomaterial reported by Martínez-Mañez research group for the detection of miRNA-145 as a diagnostic and prognostic tool.<sup>122</sup> For the preparation of the sensing material, MCM-41 type MSNs were loaded with the fluorophore rhodamine B and subsequently functionalized with (3-aminopropyl) triethoxysilane, which conferred a positively charged layer because of protonation of aminopropyl moieties at neutral pH. Finally, five different oligonucleotide sequences (O1-O5) were electrostatically grafted to the surface to prepare five different gated materials (S2-S6). In the presence of miRNA-145 they adopted particular conformations (duplex, antiparallel triplex and parallel triplex) that conditioned sensitivity and specificity properties.

In a typical experiment, gated nanomaterials were suspended in hybridization buffer with and without miRNA-145. In its absence, pore keep closed and negligible rhodamine B release was observed, while in its presence, displacement of capping sequences induced dye delivery and increased fluorescence emission intensity (Figure 26). S3-S4 provided higher sensitivity due to the combination of two factors: more efficient blocking of MSNs pores and more rapid formation of triplex. Nanoprobe sensitivity was established evaluating its response at different miRNA-145 concentrations, resulting in proportional delivery of encapsulated dye and achieving LODs as low as 0.3 pM for the best cases (antiparallel triplex). Moreover, system demonstrated high specificity in the presence of other possible interferents such as miRNA-Let7A and miRNA-141, only being activated by the target miRNA-145. Finally, assays in human serum samples were successfully carried out. Despite higher background, concentrations as low as 5 nM were detected, some orders of magnitude below traditional techniques such as surface plasmon resonance (SPR), Northern blotting and microarrays. The above presented results showed

---

<sup>122</sup> A. Ribes, S. Santiago-Felipe, A. Aviñó, V. Candela-Noguera, R. Eritja, F. Sancenón, R. Martínez-Mañez, *Sens. Actuators B-Chem.*, **2018**, 277, 598-603.

the potential exhibited by the developed system to become a routine clinical tool.

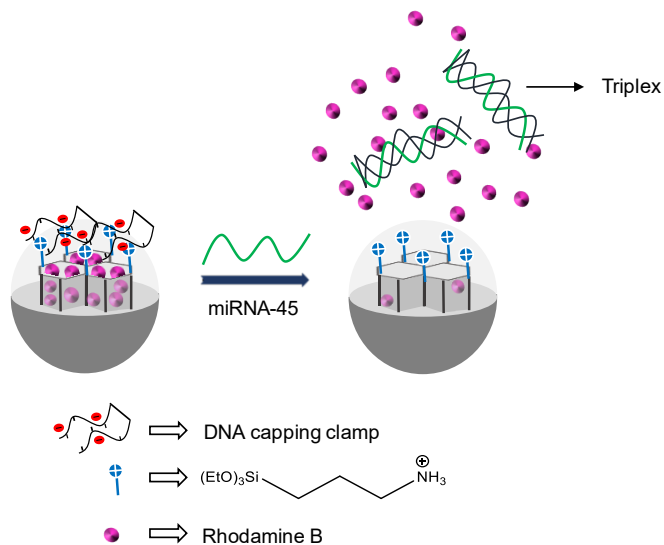


**Figure 26:** Schematic illustration of oligonucleotide gated material for the on-command delivery of cargo rhodamine B in the presence of miRNA-145.

In 2019, Martínez-Máñez and co-workers reported the synthesis and development of a new nanodevice for the detection of fungi *Candida albicans* and thus, the diagnosis of candidiasis, nowadays considered one of the most common invasive fungal diseases that affects to developed countries. For this purpose, NAA loaded with the fluorescent dye rhodamine B and capped with specific oligonucleotides sequences designed for the recognition of *C. albicans* genomic DNA were prepared.<sup>123</sup> NAA films were submerged in a rhodamine B solution for loading and subsequent functionalization with (3-isocyanatepropyl) triethoxysilane linker. Then,  $\text{NH}_2$ -terminated short sequence O1 were attached to the surface through urea bond formation. Finally, pores were capped with oligonucleotide sequence O2, which include a sequence that corresponds to the coding region of the integrin-like alpha Int1p protein (alpha INT1) from *C. albicans*. Almost “zero release” was observed in control hybridization buffer

<sup>123</sup> A. Ribes, E. Aznar, S. Santiago-Felipe, E. Xifré-Perez, M.A. Tormo-Mas, J. Pemán, L.F. Marsal, R. Martínez-Máñez, *ACS Sens.*, **2019**, 4, 1291-1298.



solution in the absence of *C. albicans* genomic DNA due to the presence of O2 sequence blocking the pores of the NAA support. However, in the presence of the target *C. albicans* genomic DNA, preferential hybridization between both, stimulus and capping sequences triggered uncapping and cargo delivery (Figure 27). The specific response of the developed system in the presence of other different genomic DNAs from *C. glabrata*, *C. parapsilopsis*, *S. epidermidis*, *S. aureus*, *K. pneumoniae* and *P. aeruginosa* at the same concentrations were tested, being none of them capable of induce pore opening.

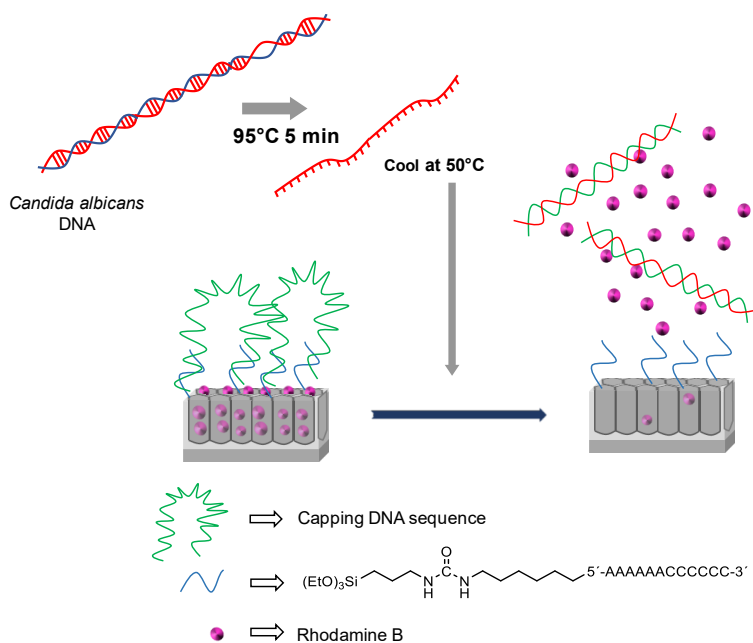


**Figure 27:** Representation of the oligonucleotide gated material, based on NAA as inorganic support, for the specific detection of fungi *Candida albicans*.

In a further step, the proper working of the system was tested in hybridization buffer solutions inoculated with *C. albicans*. When *C. albicans* was present, supernatant fractions showed clear fluorescence emission enhancement that confirmed fungi recognition and cargo delivery without any cell lysis pre-treatment of the yeast culture. A limit of detection as low as  $8 \text{ CFU} \cdot \text{mL}^{-1}$  was established, with an amplification phenomenon of 80,000 reporter

molecules delivered per each DNA strand. The system was validated in typical sterile fluids such as cerebrospinal fluid, plasma, peritoneal fluid and blood cultures, being able to detect *C. albicans* at 10 CFU· mL<sup>-1</sup>. Finally, 18 different blood culture samples from candidiasis patients of Hospital Universitari i Politècnic La Fe (Valencia) were analysed. Results were validated by the reference mycological method, revealing high accuracy for *C. albicans* diagnosis in highly competitive real samples and in shorter times than reference methodologies (30 minutes in front of 2-6 days).

### 1.5.2 Pathogens: Problems & Perspectives.

Attending to its biological definition, a pathogen is anything that can produce a disease, however, it is normally applied for the description of infectious agents. Like other organisms, pathogens *leitmotiv* consists on live and reproduce, in this particular case, at the expense of the host organism, our body. Indeed, these organisms evolve continuously to get the most out of the host biological system, either it is immunocompromised, injured or neither. The most dangerous pathogens are able to (1) colonize the host, (2) nourish from it, (3) avoid, inhibit or adapt to possible immune responses, (4) replicate and finally (5) spread to a new host; all this through reactions and biochemical mechanisms that in some cases have not yet been described and complicate the survival of the infected patient.<sup>124</sup>

Agents that produce these infectious processes can be divided in 6 groups that causes different diseases due to the biochemical mechanism showed by each one (Figure 28): (a) viruses, (b) bacteria, (c) fungi, (d) protozoa, (e) helminths (worms) and (f) prions. In one hand, viral mechanisms rely on virus ability to subvert host cell machinery to produce their proteins and replicate their genome. Bacteria, the ones that contain specific virulence genes and causes diseases, make host cell promotes replication and spread. Fungi and protozoa, on the other hand, base their survival into the host cell on their ability to move to more evolved forms as the infectious process progresses, which complicates the response of the immune system and prions, infectious agents that contain

---

<sup>124</sup> B. Alberts, A. Johnson, J. Lewis, *Molecular Biology of the Cell. Introduction to pathogens*, 4<sup>th</sup> Edition. New York: Garland Science, **2002**.

no nucleic acid, catalyse protein misfolding in the host cell to share their amino acid sequence and convert “normal” proteins into new prions.<sup>125</sup>

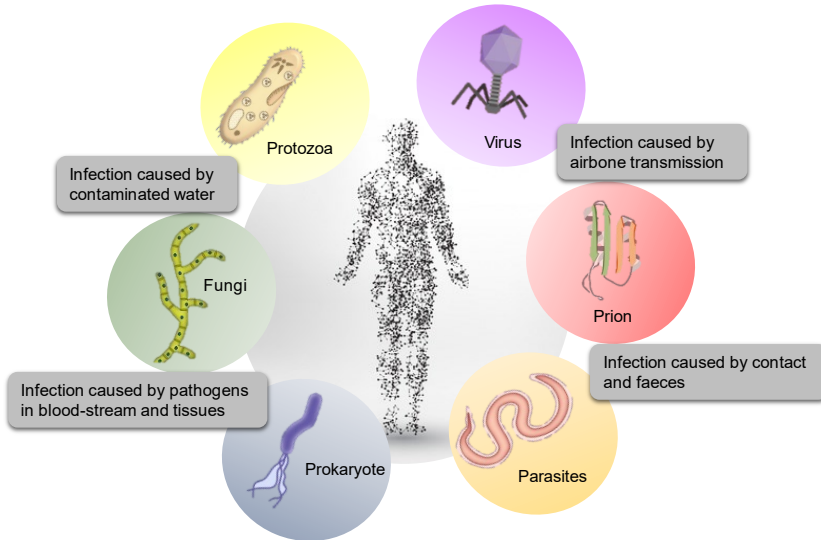


**Figure 28:** Illustrative scheme of reported pathogen types and interaction with host organism.

Annually, infectious diseases caused by pathogens results in numerous hospital admissions, and in some cases, deaths all around the world. In addition, wrong or late diagnosis difficult treatment selection and efficiency which turns out in complications for patients and significant increase of healthcare cost. Every year, Europe register 25,000 deaths with a cost of approximately 1.5 billion € per year, while in US, only pneumonia causes 500,000 hospitalizations and 9.7 billion \$ expenditure in the same period.<sup>126</sup> This led World Health Organization (WHO) to claim for the development of accurate therapies and diagnostic methods that facilitates and prevents contagion and pathogen proliferation.<sup>127</sup>

<sup>125</sup> U.S. Department of Health & Human Services. Centers for Disease Control and Prevention, National Center for Emerging and Zoonotic Infectious Diseases (NCEZID), Division of High-Consequence: <https://www.cdc.gov/prions/index.html>

<sup>126</sup> a) J.F. Guest, A. Morris, *Eur. Respir. J.*, **1997**, 10, 1530-1534; b) B.J. Marston, J.F. Plouffe, T.M. File et al., *Arch. Intern. Med.*, **1997**, 157, 1709-1718.

<sup>127</sup> World Health Organization, *Mortality and global health estimates*, **2013**.

During recent decade, development of detection techniques for rapid and early diagnostic have become a high interest research topic. Nowadays, standardised methodologies such as microscope exploration, culture techniques and polymerase chain reaction (PCR) amplification are long-time consuming (at least 48-72 hours), expensive (100-150 €/test) and require highly prepared personnel and equipment. All these are translated in a deficient health control and favour exponential contagion of infectious diseases when pathogens spread out.

Nanotechnology raising knowledge is providing innovative solutions to overcome drawbacks presented by traditional technologies, and the previous exposed synergic combination of molecular recognition chemistry with nanostructured materials are one of the most exploited. The need for outstanding sensing features (such as high sensitivity and selectivity, robustness, high speed and low cost) have forced the development of systems for the detection of pathogens, for example, the previously discussed gated materials for the detection of miRNA-145 and *C. albicans* fungi, both capped by an oligonucleotide sequence.

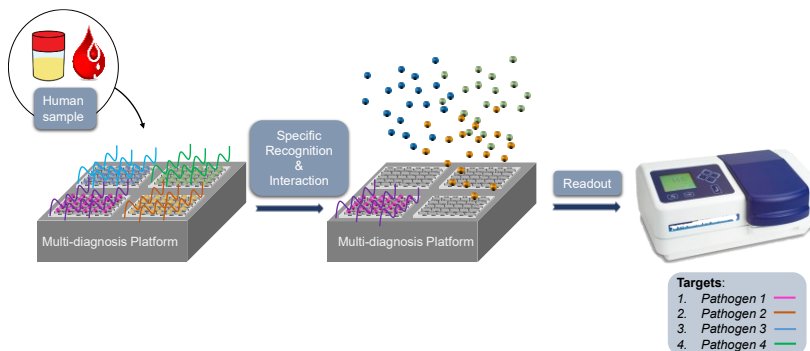


**Figure 29:** Envisioned probes for simultaneous detection of multiple pathogens.

Among the advantages of oligonucleotide capped materials for pathogen detection, versatility is one of the most important for its implementation as a clinical product. *A priori*, if we change capping oligonucleotide sequence designed for *C. albicans* detection by another one designed for the specific recognition of other pathogens, we should be able to develop probes capable

to detect these specific targets. If we can combine some of them in a single test platform (Figure 29), we would provide a unique rapid screening test for clinical purposes that would make the difference in patient's treatments and health system budget.

To sum up, short-term future pathogen detection might be developed by multianalyte gate-like diagnostic systems with amplification signal capabilities that will compete with conventional detection methodologies.

### 1.5.3 Food control. Bringing security to consumer.

Food industry and food supply companies are one of the most relevant and powerful economic sector around the world. Indeed, competent authorities have established every year food industry turnover in approximately 1192 billion €, making it the largest manufacturing sector in EU, as well as leading EU employment with 4.72 million people working in the 294000 companies distributed around the whole continent.<sup>128</sup>

Globalized food supply chains and their intention to provide cheaper food products have contributed to subsistence of food fraud among years. As a consequence, European Commission created in 2013 the EU Food Fraud Network to led EU Member States (and other European countries adhered) fight against companies that prioritize economic gain over the law, the environment and the health of fellow citizens. At the same time, the European Food Safety Authority contributes with their security food policy looking out for protecting human, animal and vegetal health in each one of the steps that encompasses food production and consumption. They work assuring citizens a more secure and nutritive feed, without neglecting the employees work conditions or animals and plants care.<sup>129</sup>

Some of the most recent and relevant cases of fraud and food contamination are the olive oil commercialized in United Kingdom as "Virgen Extra" quality (being 30 % refined oil), the false fresh 51 tuna tones (chemically

---

<sup>128</sup> EU Food and Drink industry. Data & Trends 2019: [https://www.fooddrinkurope.eu/uploads/publications\\_documents/FoodDrinkEurope\\_-\\_Data\\_Trends\\_2019.pdf](https://www.fooddrinkurope.eu/uploads/publications_documents/FoodDrinkEurope_-_Data_Trends_2019.pdf)

<sup>129</sup> European Food Safety Agency (EFSA) - <http://www.efsa.europa.eu/>

altered to change aspect) seized by police,<sup>130</sup> and the commercialization of meat products affected by *Listeria monocytogenes* in southern Spain, which has affected more than 200 people and has even reached Germany.<sup>131</sup>

However, these energetic controls over agro-food exploitations and food processing companies results in products price increase that make business less competitive. In some cases, and in order to reduce the cost of the production and gain a greater profit margin, fabricators decide to skip current regulations. In other cases, an accidental error triggers an irregularity that can become vital for the health of the population and the environment. Both require rapid, competitive and efficient analytical tools that allow to detect and correct the anomalies that every day are noticed.

In food chains, hazards can come from several ways, from production to storage, and may include all kinds of chemical and biological elements.<sup>132</sup> Nowadays official methods comprise enzyme-linked immunosorbent assays (ELISAs), as quantitative technique, and Western blotting and polymerase chain reactions (PCRs), as qualitative. These are thoroughly developed analytical methodologies with high sensibility and sensitivity, however, they present also some important inconvenience. For instance, high degree trained personnel should undertake analysis, machinery is complex and expensive, time needed is normally up to 12 hours and they cannot be used as a point of care tool, all these making them highly cost effective.

Again nanotechnology might play an important role to solve these problems through the previously described implementation of molecular gates and molecular recognition events over nanostructured materials. Hybrid organic-inorganic gated materials offers solution to each one of the demanded qualities: high sensitivity and specificity, low cost, scalable production, ability to be moved and analyse samples *in situ*, etc.

---

<sup>130</sup> The EU Food Fraud Network and the System for Administrative Assistance - Food Fraud Annual Report **2018**.

<sup>131</sup> Ministerio de Sanidad, Consumo y Bienestar Social Agencia Española de Consumo, Seguridad alimentaria y Nutrición: [www.aecosan.msssi.gob.es/AECOSAN/web/noticias\\_y\\_actualizaciones/noticias/2019/Brote\\_Listeria\\_Carne.htm](http://www.aecosan.msssi.gob.es/AECOSAN/web/noticias_y_actualizaciones/noticias/2019/Brote_Listeria_Carne.htm)

<sup>132</sup> S.-H. Song, Z.-F. Gao, X. Guo, G.H. Chen, *Food Anal. Methods*, **2019**, *12*, 966-990.

On the other hand, food allergens deserve special mention, since they affect 8 % children and 3-4 % adult population in EE.UU. With the inexistence of current treatments or vaccines to avoid hypersensitive response to specific food hazards,<sup>133</sup> the only possibility is just radically remove them from diet. Even taking all precautions, patients may be exposed to adulterated products, undeclared substances and cross-contaminations.<sup>134</sup> In addition, globalization, cross-contamination and bad practices increases worldwide hypersensitivities to food allergens every year.<sup>135</sup> Thus, the need of effective devices for food allergens detections are required.

Some food allergies such as celiac disease are type 1 hypersensitivity and induce an immunogenic response that may be detected by immunosensors (ELISAs for example), but there are other antigens that are not immunogenic and require other techniques for its detection. In this point, aptamers rises as a potential solution.

Aptamers are single stranded DNA (ssDNA) or RNA synthesized artificially through SELEX (Systematic evolution of ligands by exponential enrichment) process (Figure 30a) and folded into a 3D structure that binds specifically to specific targets (Figure 30b),<sup>136</sup> that have been applied for the detection of several pesticide residues,<sup>137</sup> pathogenic organisms,<sup>138</sup> biotoxins,<sup>139</sup> allergens<sup>140</sup> and organic pollutants.<sup>141</sup> Apart from high sensitivity, specificity and non-biologically production (as a difference with antibodies), they also show high chemical stability and versatility, insensitiveness to pH changes, and high

---

<sup>133</sup> S. Neethirajan, X. Weng, A. Tah, J.O. Cordero, K.V. Ragavan, *Sens. Biosensing Res.*, **2018**, *18*, 13-30.

<sup>134</sup> T. Cucu, L. Jacxsens, B. De Meulenaer, *J. Agric. Food Chem.*, **2013**, *61*, 5624-5633.

<sup>135</sup> M.A. Ciardiello, M. Tamburrini, M. Liso, R. Crescenzo, C. Rafeiani, A. Mari, *Food Res. Int.*, **2013**, *54*, 1033-1041.

<sup>136</sup> R.D. Jenison, S.C. Gill, A. Pardi, B. Polisky, *Science*, **1994**, *263*, 1425-1429.

<sup>137</sup> R. Bala, S. Dhingra, M. Kumar, K. Bansal, S. Mittal, *Chem. Eng. J.*, **2017**, *311*, 111-116.

<sup>138</sup> Z.H. Yang, X.F. Ding, Q. Guo, Y. Wang, Z.W. Lu, H.C. Ou, Z.F. Luo, X.H. Lou, *Sens. Actuators B-Chem.*, **2017**, *253*, 1129-1136.

<sup>139</sup> H.S. Kim, Y.J. Kim, J.W. Chon, D.H. Kim, J.H. Yim, H. Kim, K.H. Seo, *Sens. Actuators. B-Chem.*, **2017**, *239*, 94-99.

<sup>140</sup> R.K. Mishra, A. Hayat, G.K. Mishra, G. Catanante, V. Sharma, J.L. Marty, *Talanta*, **2017**, *165*, 436-441.

<sup>141</sup> R.J. Cheng, S.Y. Liu, H.J. Shi, G.H. Zhao, *J. Hazard. Mater.*, **2018**, *341*, 373-380.

affinity to targets that ranges from proteins, nucleic acids, cells and even molecular compounds.

In combination with appropriate nanomaterials, resultant nanodevices may quickly replace the complex and tedious current analytical techniques for the detection of food allergens.

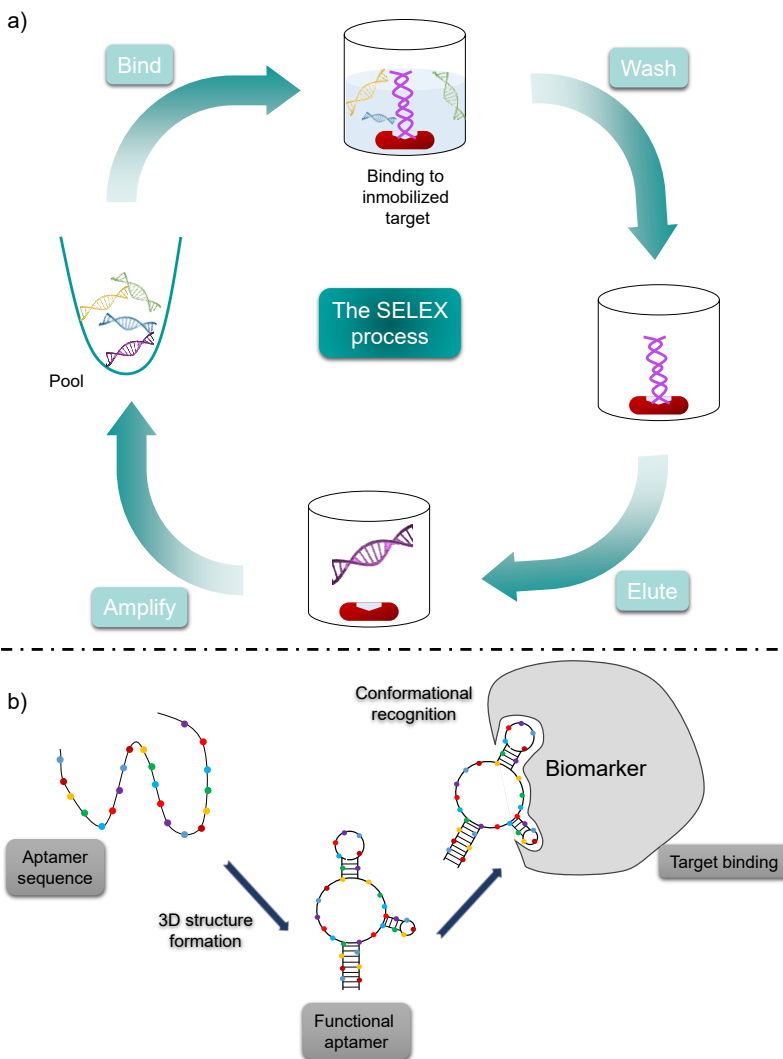
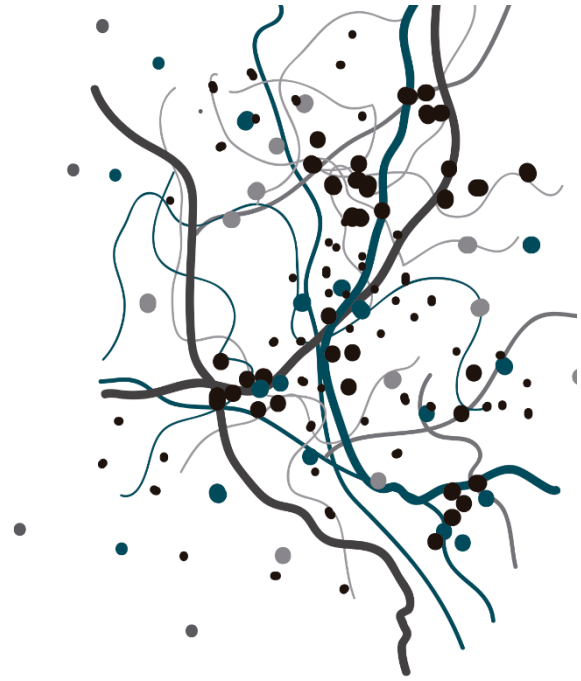


**Figure 30:** a) Illustrative explanation of aptamer SELEX preparation. b) Schematic representation of aptamer-target binding mechanism.





# 2

## Objectives



Attending all above introduced terms and concepts, in this thesis new sensing systems based in gated materials will be developed. Five different gated systems supported on NAA will be reported for the detection of different pathogens and food allergens.

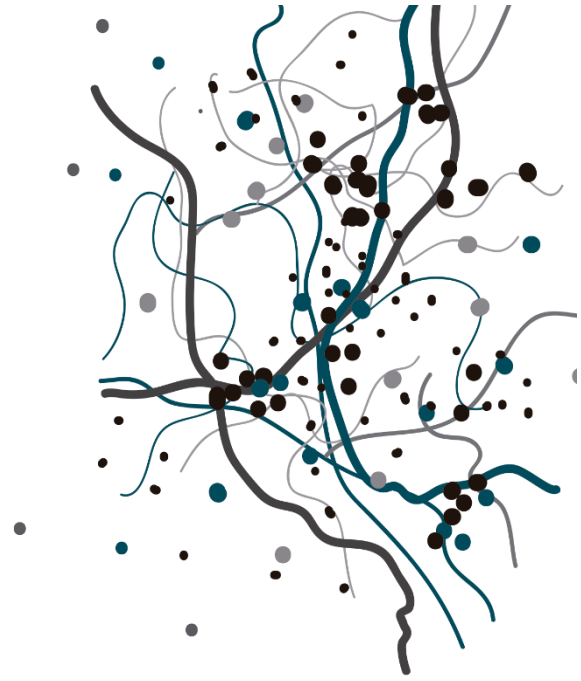
The general objective of this PhD thesis is to **design, synthesize and optimise new sensing gated nanodevices based on nanoporous anodic alumina (NAA) films** for the detection of selected targets.

This general objective can be divided in 5 different goals:

- » To develop a new system based in DNA-capped NAA films for the detection of *Mycoplasma fermentans* genomic DNA.
- » To design, synthesize and evaluate aptamer-capped NAA films for the sensitive and selective detection of *Staphylococcus aureus* bacteria in the early stages of infection.
- » To develop a new system for the detection of *Pneumocystis jirovecii* fungi as diagnosis tool and based on a DNA-gated NAA scaffold.
- » To design and optimise aptamer-gated NAA films for the detection of gluten in food extracts as a new procedure for an accurate identification of this potential allergen in consumable products.

The following chapters discuss in detail the synthesis of the different gated materials prepared in order to detect different analytes, which nature range from whole cells or proteins, to specific DNA sequences. Characterisation of these materials and studies of the release of the entrapped dye in the presence of the corresponding analyte are also described.





# 3

*A Mycoplasma* Genomic DNA  
Probe Using Gated  
Nanoporous Anodic Alumina



# A *Mycoplasma* Genomic DNA Probe using Gated Nanoporous Anodic Alumina

Luís Pla,<sup>[a, b, c]</sup> Elisabet Xifré-Pérez,<sup>[d]</sup> Àngela Ribes,<sup>[a, b, c]</sup> Elena Aznar,<sup>[a, c]</sup> M. Dolores Marcos,<sup>[a, b, c]</sup> Lluís F. Marsal,<sup>\*[d]</sup> Ramón Martínez-Máñez,<sup>\*[a, b, c]</sup> and Félix Sancenón<sup>\*[a, b, c]</sup>

<sup>a</sup> *Departamento de Química Universidad Politécnica de Valencia; Camino de Vera s/n, 46022 Valencia (Spain); E-mail: rmaez@qim.upv.es*

<sup>b</sup> *Instituto Interuniversitario de Investigación de Reconocimiento Molecular y Desarrollo Tecnológico; Universitat Politècnica de València, Universitat de València, Camino de Vera s/n, 46022 Valencia, Spain; E-mail: rmaez@qim.upv.es*

<sup>c</sup> *CIBER de Bioingeniería, Biomateriales y Nanomedicina (CIBER-BBN).*

<sup>d</sup> *Departamento de Ingeniería Electrónica, Eléctrica y Automática Universidad Rovira i Virgili; Avda. Païssos Catalans 26, 43007 Tarragona (Spain); E-mail: lluis.marsal@urv.cat*

**ChemPlusChem 2017, 82, 337 – 341**





### 3.1 Abstract

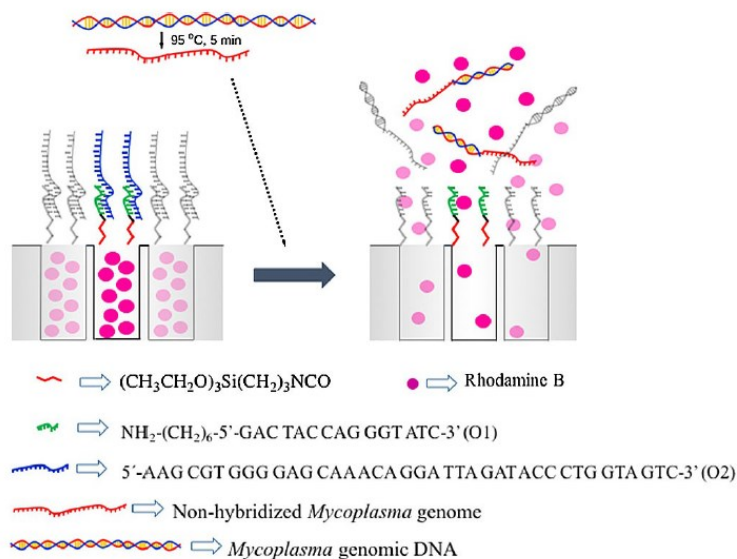
A nanoporous anodic alumina (NAA)-based sensor system for the detection of *Mycoplasma* was developed through the implementation of “molecular gates” selective to the presence of this bacterium. The capped support showed a negligible cargo release, while presence of *Mycoplasma* genomic DNA resulted in the release of rhodamine B fluorescent dye. This sensor system presents a limit of detection of 20 genomic DNA copies·mL<sup>-1</sup> and was applied to the detection of *Mycoplasma* bacteria in competitive environments, such as culture cell media.

### 3.2 Introduction

*Mycoplasma* is a small bacterium (diameter 0.2 μm) without cell wall, immune to common antibiotic, capable of passing through bacterial filters and of great importance because of its common presence in cell cultures in clinical, research and biopharmaceutical industry.<sup>[1]</sup> Besides, *Mycoplasma* is also related with the development of important pathologies such as pneumonia, rheumatoid arthritis, cancer and non-gonococcal urogenital diseases, among others.<sup>[2–6]</sup> Historically, polymerase chain reaction (PCR) methods and culture-based approaches have been used extensively for *Mycoplasma* detection. However, even though these methods are very sensitive, they have several drawbacks such as high cost, the need of trained personnel, and a relatively long time before results are obtained.<sup>7</sup> As an alternative, the design of new sensing systems for *Mycoplasma* detection that overcome the cited drawbacks are of importance and have been recently described. Some of these methods use gold nanoparticles<sup>[8]</sup> or multi-walled carbon nanotubes<sup>[9,10]</sup> decorated with antibodies. Other methods are based on immunoassays coupled with Fe<sub>3</sub>O<sub>4</sub> magnetic nanoparticles<sup>[11]</sup> or use Ag nanorods as biosensing platform for surface enhanced Raman spectroscopy analysis.<sup>[12]</sup>

From another point of view, our research group and others have recently proposed the use of mesoporous organic–inorganic gated supports as suitable materials for the development of new recognition and sensing protocols. In a typical design, a mesoporous silica support is loaded with a dye/fluorophore

and the external surface of the material is functionalized with selected capping molecules able to recognize selectively a certain target analyte. These materials remain capped, until the presence of the analyte induces a displacement of the cap resulting in pore opening and delivery of the entrapped reporter. Based on that simple concept, capped mesoporous silica materials for the selective detection of certain cations, anions, and biomolecules have been described.<sup>[13–15]</sup> Moreover, in this context, we have recently reported the design of gated materials for the detection of genomic DNA from bacteria,<sup>[16,17]</sup> although studies in this field are still rare. In our examples, the capped materials were prepared using mesoporous silica nanoparticles as inorganic support. However, silica nanoparticles presented certain drawbacks such as difficult handling and can be harmful if skin deposited or breathed. In addition, an intrinsic difficulty exists in forming desired uniform suspensions that may hamper development of a highly reproducible sensing systems.



**Scheme 1:** Schematic representation of **S3** material capped with a double strand DNA. Delivery of the entrapped dye (rhodamine B) is selectively achieved in the presence of *Mycoplasma* genomic DNA.

In this context, we were interested in explore the possible use of other porous scaffolds to design gated materials for sensing applications and thus we

selected nanoporous anodic alumina (NAA). NAA is a competitive support in nanotechnology that has been used for many different applications.<sup>[18–21]</sup> Preparation of NAA is easy and scalable by using well-known techniques.<sup>[22,23]</sup> Moreover, NAA is stable, biocompatible, and does not degrade in aqueous solutions, all of which may contribute to the development of robust reproducible devices.<sup>[21,24]</sup> Finally, it was also considered that NAA can be calcined and reused, which may prolong the support's lifespan.

Taking into account the above-mentioned factors, we report herein a new hybrid gated material based on NAA and capped with a double-stranded oligonucleotide sequence for the fluorogenic detection of *Mycoplasma fermentans* genomic DNA. A schematic representation of the gated support is shown in Scheme 1. NAA supports have been applied previously for the preparation of electrochemical DNA sensors.<sup>[25–30]</sup> In these sensors, oligonucleotides sequences were grafted in the inner of the pores of the NAA support and hybridization with certain DNA sequences controlled the access of an electrochemical marker to the electrode surface. In our approach, oligonucleotides are grafted onto the external surface of the alumina support and the presence of certain DNA (i.e. *Mycoplasma fermentans* genomic DNA) control the delivery of dye molecules entrapped in the pores.

### 3.3 Results and discussion

NAA was prepared by following reported procedures.<sup>[22–24]</sup> The pores of the NAA support were loaded with rhodamine B and, afterward, an excess of (3-isocyanatopropyl)triethoxysilane was added to functionalize the external surface with isocyanatopropyl moieties (solid **S1**). Then, oligonucleotide **O1**, functionalized with an aminohexyl moiety at the 5'-end position (i.e. NH<sub>2</sub>-(CH<sub>2</sub>)<sub>6</sub>-5'-GAC TAC CAG GGT ATC-3'), was anchored onto **S1** through the formation of urea bonds yielding solid **S2**. The final material **S3** was prepared by hybridization of oligonucleotide **O2** (5'-AAG CGT GGG GAG CAA ACA GGA TTA GAT ACC CTG GTA GTC-3' which is a highly conserved sequence of the 16S ribosomal subunit in *Mycoplasma* species genome), with sequence **O1** grafted in the external surface of solid **S2** (see the Supporting Information for further details).

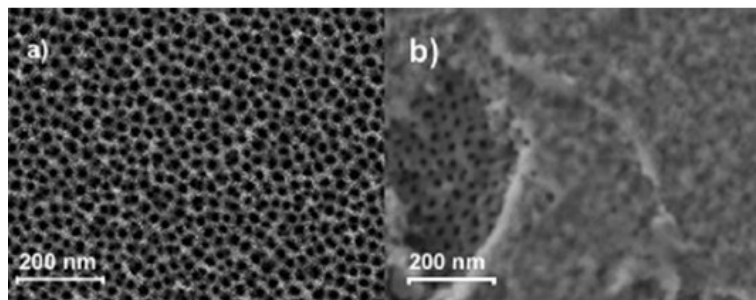


**Figure 1:** Representative FESEM images of NAA scaffold (a) and **S3** (b).

NAA, **S1**, **S2**, and **S3** supports were characterized by using field emission scanning electron microscopy (FESEM). As seen in Figure 1a, the NAA support presented a disordered pore distribution with an average pore diameter of about 8 nm. Upon loading of the pores with rhodamine B, functionalization with isocyanatopropyl moieties, grafting of **O1** oligonucleotide, and subsequent hybridization with **O2** a dense organic layer covering most of the NAA surface was observed (see Figure 1b for the final **S3** support). Besides, the porous framework of the NAA scaffold was preserved after the various loading and functionalization steps as seen in Figure 1b, which that shows a small part in **S3** where the organic layer was absent and the disordered porous network was observed. Furthermore, powder X-ray diffraction studies of the differently prepared supports were carried out to confirm that the support does not present an ordered pore distribution (see the Supporting Information). Moreover, from thermogravimetric analyses, contents of organic matter for the differently prepared supports were determined (see Table 1).

**Table 1:** Organic matter contents ( $\alpha$  in mmol·g<sup>-1</sup>) for the different prepared supports.

Support	$\alpha_{\text{RhB}}$	$\alpha_{\text{Isocyanate}}$	$\alpha_{\text{O1}}$	$\alpha_{\text{O2}}$
<b>S1</b>	0.67	0.01		
<b>S2</b>	0.25	0.01	0.1	
<b>S3</b>	0.24	0.01	0.1	0.1

The response of **S3** was tested in the absence and in the presence of *Mycoplasma fermentans* genomic DNA by measuring the emission of rhodamine B dye at 585 nm ( $\lambda_{\text{ex}}=555$  nm) delivered from the pores of the NAA support. In a typical experiment, two independent **S3** samples were submerged in 1.0 mL of TRIS buffer (pH 7.4). At the same time, a solution of 5000 copies  $\cdot \mu\text{L}^{-1}$  of *Mycoplasma fermentans* quantification standard in water was heated to 90 °C for 5 min (in order to dehybridize the double helix structure) and then cooled on an ice bath for 3 min.

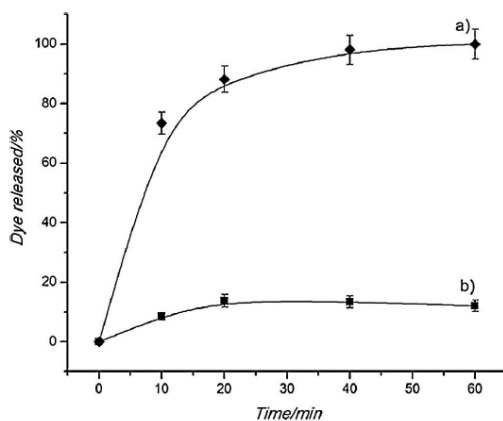


**Figure 2:** Release of rhodamine B from **S3** support in the absence (b) and in the presence (a) of *Mycoplasma fermentans* genomic DNA (100 copies  $\cdot \mu\text{L}^{-1}$ ) in TRIS buffer at pH 7.4.

After cooling, 50  $\mu\text{L}$  of *Mycoplasma fermentans* genomic DNA solution was added to one of the supports whereas 50  $\mu\text{L}$  of water were added to the other. Both solutions were maintained at 25 °C and aliquots were taken at scheduled times. Cargo release was then determined by the emission of the rhodamine B dye in the solution. As shown in Figure 2, in the absence of *Mycoplasma fermentans* genomic DNA a low payload release was found (ca. 15% of the total dye delivered after 60 min) indicating an effective pore closure, whereas in the presence of *Mycoplasma* genomic DNA, a marked delivery of rhodamine B was observed. This release was ascribed to pore opening resulting from the displacement of **O2** from **S3** support in the presence of genomic DNA.

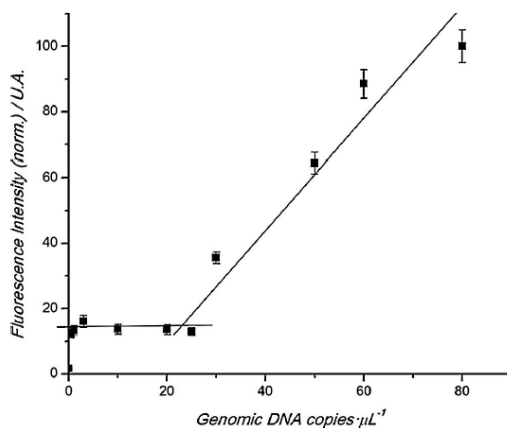


**Figure 3:** Release of rhodamine B in TRIS buffer (pH 7.4) from support **S3** in the presence of different *Mycoplasma fermentans* genomic DNA copies.

In a second step, a study of the response of **S3** to different concentrations of *Mycoplasma* genomic DNA was carried out. Following a similar procedure to that described above, solutions containing different concentrations of *Mycoplasma fermentans* genomic DNA were added to several **S3** supports in 1 mL of TRIS buffer and the rhodamine B released from the support was measured after 60 min. As seen in Figure 3, a clear correlation between the number of copies of *Mycoplasma* genomic DNA added and dye released from **S3** was found. This observation is in agreement with the uncapping protocol shown in Scheme 1 and linked with the displacement of **O2** from **S3** support. A limit of detection (LOD) as low as 20 DNA copies  $\cdot \mu\text{L}^{-1}$  was determined from Figure 3. Furthermore, the LOD we have found is not far from those reported for commercially available PCR *Mycoplasma* detection kits (ca. 10 copies  $\cdot \mu\text{L}^{-1}$ )<sup>[31]</sup> suggesting the potential use of **S3** supports in real applications.

In addition, selectivity in the detection of *Mycoplasma* using **S3** was investigated by carrying out similar delivery experiments in the presence of other genomic DNA. For this purpose, the response of **S3** with *Legionella pneumophila* and *Candida albicans* genomic DNA (1000 copies  $\cdot \mu\text{L}^{-1}$ ) was studied. As seen in Figure 4 there were no significant differences between the blank (cargo release in TRIS buffer) and experiments in the presence of genomic DNA of *Legionella* or *Candida*. There was neither delivery of the

entrapped dye when a mixture of *Legionella pneumophila* and *Candida albicans* (each one at a concentration of  $1000 \text{ copies} \cdot \mu\text{L}^{-1}$ ) was used. As a clear contrast, when *Mycoplasma* genomic DNA was present a clear delivery of rhodamine B was observed. These experiments demonstrated that **S3** is opened selectively in the presence of *Mycoplasma* genomic DNA.

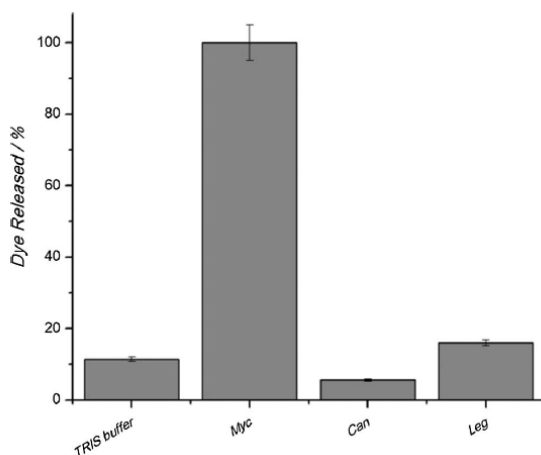


**Figure 4:** Release of rhodamine B from **S3** support in the presence of (from left to right): TRIS buffer, *Mycoplasma fermentans* (Myc), *Candida albicans* (Can), *Legionella pneumophila* (Leg) genomic DNA. All DNA used were in a concentration of  $1000 \text{ copies} \cdot \mu\text{L}^{-1}$ .

Stimulated by these results, we decided to take a step forward and test the possible application of **S3** solid for the qualitative detection of *Mycoplasma* species in real contaminated biological media. For this purpose, we selected MDA-MB-231 breast cancer cell media contaminated and not with *Mycoplasma* (previously confirmed by PCR studies). Two different **S3** supports were submerged in 1 mL of the cell media with and without *Mycoplasma* contamination and the emission intensity of rhodamine B released at 585 nm was measured after 60 min. The obtained results are shown in Figure 5 where a clear difference in payload released from **S3** was observed. When using cell media contaminated with *Mycoplasma* a marked rhodamine B delivery was observed, which was not found in uncontaminated samples, thus strongly

suggesting the potential use of the NAA capped probe for the detection of this bacteria in real environments.

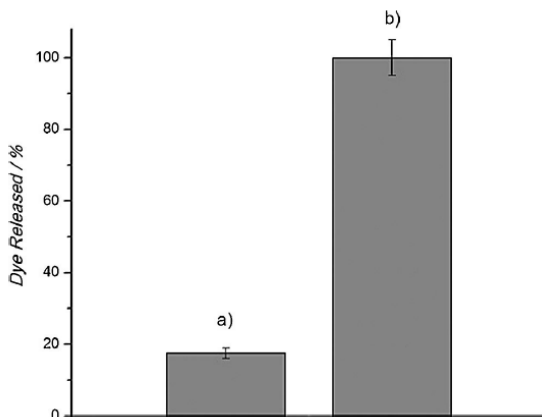


**Figure 5:** Release of rhodamine B from support **S3** submerged in MDA-MB-231 breast cancer cell line extract (a) without and (b) with *Mycoplasma* contamination. The emission of rhodamine B released was measured after 1 h of **S3** immersion into cell media.

Finally, the possible recycling of the NAA support was tested. For this purpose, an already used support was calcined at 550 °C for 5 h to eliminate the organic matter, and then functionalized again following the same process described above and yielded solid **S3-R1**. On the other hand, another already used support **S3** (in which **O2** was displaced and rhodamine B cargo delivered), was again loaded with rhodamine B and then capped with oligonucleotide **O2** to yield **S3-R2**. Both reused supports were able to release rhodamine B in the presence of *Mycoplasma* genomic DNA (see the Supporting Information) thus suggesting the potential for easy reutilization of the NAA support.

### 3.4 Conclusion

In summary, we reported here the use of NAA as inorganic support for the preparation of sensing materials for the sensitive and selective detection of *Mycoplasma fermentans* genomic DNA. Pores of NAA were loaded with rhodamine B and capped with a covalently linked double-stranded DNA



containing a highly conserved sequence of the 16S ribosomal subunit of *Mycoplasma* species genome. In the presence of *Mycoplasma fermentans* genomic DNA a marked delivery of the entrapped dye was observed. A LOD of about 20 DNA copies· $\mu\text{L}^{-1}$  was determined. Besides, genomic DNA of *Legionella pneumophila* and *Candida albicans* were unable to induce pore opening and cargo delivery. Furthermore, the effective use of **S3** for the detection of *Mycoplasma* in contaminated culture media without any complex sample pre-treatment was demonstrated. The probe is very simple to prepare, easy to handle, reusable, does not require trained personnel, and has high potential for the selective and sensitive detection of *Mycoplasma* in real environments.

### 3.5 Acknowledgements

We thank the Spanish Government (projects MAT2015-64139-C4- 1-R, AGL2015-70235-C2-2-R, and TEC2015-71324-R (MINECO/FEDER, UE)), the Generalitat Valenciana (project PROMETEOII/2014/047), the Catalan authority (project AGAUR 2014SGR1344), and ICREA under the 2014 ICREA Academia Award for support. L.P. thanks to PROMETEOII/2014/047 for his contract. We thank the Electron Microscopy Service at the UPV for support.

### Conflict of Interest

The authors declare no conflict of interest.

### Keywords

DNA · gated materials · Mycoplasma detection · nanoporous anodic alumina

### References

- [1] *Basic Cell Culture Protocols in Methods in Molecular Biology*, 4th ed. (Eds. C. D. Helgason, C. L. Miller), Springer Protocols, Humana Press, New York, **2013**.
- [2] L. Matas Andreu, S. Molinos Abós, G. Fernández Rivas, V. González Soler, V. Ausina Ruiz, *Enferm. Infecc. Microbiol. Clin.* **2006**, 24, 19–23.
- [3] V. Ausina, *Infecciones Causadas por Micoplasmas in Medicina Interna*, 15th ed., Elsevier, Madrid, Barcelona, España, **2004**, pp. 2362–2365.

- [4] S. Tsai, D. J. Wear, J. W. Shih, S. C. Lo, *Proc. Natl. Acad. Sci. USA* **1995**, *92*, 10197–10201.
- [5] J. Y. Ning, C. C. Shou, *Chin. J. Cancer* **2004**, *23*, 602–604.
- [6] M. B. Rogers, *Oncotarget* **2011**, *2*, 271–273.
- [7] C. M. Nübling, S. A. Baylis, K.-M. Hanschmann, T. Montag-Lessing, M. Chudy, J. Kreß, U. Ulrych, S. Czurda, R. Rosengarten, *Appl. Environ. Microbiol.* **2015**, *81*, 5694–5702.
- [8] K. Meng, W. Sun, P. Zhao, L. Zhang, D. Cai, Z. Cheng, H. Guo, J. Liu, D. Yang, S. Wang, T. Chai, *Biosens. Bioelectron.* **2014**, *55*, 396–399.
- [9] H. Fayazfar, A. Afshar, M. Dolati, A. Dolati, *Anal. Chim. Acta* **2014**, *836*, 34–44.
- [10] L. Zhang, C. Z. Huang, Y. F. Li, S. J. Xiao, J. P. Xie, *J. Phys. Chem. B* **2008**, *112*, 7120–7122.
- [11] M. Yang, Y. Guan, Y. Yang, T. Xia, W. Xiong, C. A. Guo, *Mater. Lett.* **2014**, *137*, 113–116.
- [12] K. C. Henderson, E. S. Sheppard, O. E. Rivera-Betancourt, J.-Y. Choi, R. A. Dluhy, K. A. Thurman, J. M. Winchell, D. C. Krause, *Analyst* **2014**, *139*, 6426–6434.
- [13] a) Z. Wang, X. Yang, J. Feng, Y. Tang, Y. Jianga, N. He, *Analyst* **2014**, *139*, 6088–6091; b) Li. Pascual, S. El Sayed, R. Martínez-Máñez, A. M. Costero, S. Gil, P. Gaviña, F. Sancenón, *Org. Lett.* **2016**, *18*, 5548–5551; c) R. Bhat, A. Ribes, N. Mas, E. Aznar, F. Sancenón, M. D. Marcos, J. R. Murguía, A. Venkataraman, R. Martínez-Máñez, *Langmuir* **2016**, *32*, 1195–1200; d) S. El Sayed, M. Milani, M. Licchelli, R. Martínez-Máñez, F. Sancenón, *Chem. Eur. J.* **2015**, *21*, 7002–7006; e) M. Oroval, E. Climent, C. Coll, R. Eritja, A. Aviñó, M. D. Marcos, F. Sancenón, R. Martínez-Máñez, P. Amorós, *Chem. Commun.* **2013**, *49*, 5480–5482.
- [14] F. Sancenón, L. Pascual, M. Oroval, E. Aznar, R. Martínez-Máñez, *ChemistryOpen* **2015**, *4*, 418–437.
- [15] E. Aznar, M. Oroval, L. Pascual, J. R. Murguía, R. Martínez-Máñez, F. Sancenón, *Chem. Rev.* **2016**, *116*, 561–718.
- [16] E. Climent, L. Mondragón, R. Martínez-Máñez, F. Sancenón, M. D. Marcos, J. R. Murguía, P. Amorós, K. Rurack, E. Perez-Payá, *Angew. Chem. Int. Ed.* **2013**, *52*, 8938–8942; *Angew. Chem.* **2013**, *125*, 9106–9110.
- [17] L. Pascual, I. Baroja, E. Aznar, F. Sancenón, M. D. Marcos, J. R. Murguía, P. Amorós, K. Rurack, R. Martínez-Máñez, *Chem. Commun.* **2015**, *51*, 1414–1416.

- 
- [18] G. Macias, L. P. Hernández-Eguía, J. Ferre-Borrull, J. Pallares, L. F. Marsal, *ACS Appl. Mater. Interfaces* **2013**, *5*, 8093–8098.
- [19] T. Kumeria, M. M. Rahman, A. Santos, J. Ferré-Borrull, L. F. Marsal, D. Losic, *Anal. Chem.* **2014**, *86*, 1837–1844.
- [20] T. Kumeria, M. M. Rahman, A. Santos, J. Ferre, L. F. Marsal, D. Losic, *ACS Appl. Mater. Interfaces* **2014**, *6*, 12971–12978.
- [21] E. Xifre-Perez, S. Guaita-Esteruelas, M. Baranowska, J. Pallares, L. Masana, L. F. Marsal, *ACS Appl. Mater. Interfaces* **2015**, *7*, 18600–18608.
- [22] L. Vojkuvka, L. F. Marsal, J. Ferré-Borrull, P. Formentin, J. Pallarés, *Superlattices Microstruct.* **2008**, *44*, 577–582.
- [23] A. Santos, P. Formentín, J. Ferré-Borrull, J. Pallarés, L. F. Marsal, *Mater. Lett.* **2012**, *67*, 296–299.
- [24] L. F. Marsal, L. Vojkuvka, P. Formentin, J. Pallarés, J. Ferré-Borrull, *Opt. Mater.* **2009**, *31*, 860–864.
- [25] V. Rai, J. Deng, C.-S. Toh, *Talanta* **2012**, *98*, 112–117.
- [26] A. de la Escosura-Muñiz, A. Mercoçi, *TrAC Trends Anal. Chem.* **2016**, *79*, 134–150.
- [27] A. Santos, T. Kumeria, D. Losic, *TrAC Trends Anal. Chem.* **2013**, *44*, 25–38.
- [28] L. Wang, Q. Liu, Z. Hu, Y. Zhang, C. Wu, M. Yang, P. Wang, *Talanta* **2009**, *78*, 647–652.
- [29] P. Takmakov, I. Vlassiuk, S. Smirnov, *Analyst* **2006**, *131*, 1248–1253.
- [30] S.-J. Li, J. Li, K. Wang, C. Wang, J.-J. Xu, H.-Y. Chen, X.-H. Xia, Q. Huo, *ACS Nano* **2010**, *4*, 6417–6424.
- [31] a) <http://www.lifetechnologies.com>; b) <http://www.sigmaldrich.com>; c) <http://www.lgcstandards-atcc.org>. All websites accessed on 02/01/2017.

## 3.6. Supporting Information: *A Mycoplasma* Genomic DNA Probe using Gated Nanoporous Anodic Alumina.

Luís Pla,<sup>[a, b, c]</sup> Elisabet Xifré-Pérez,<sup>[d]</sup> Àngela Ribes,<sup>[a, b, c]</sup> Elena Aznar,<sup>[a, c]</sup>  
M. Dolores Marcos,<sup>[a, b, c]</sup> Lluís F. Marsal,<sup>\*[d]</sup> Ramón Martínez-Máñez,<sup>\*[a, b, c]</sup> and  
Félix Sancenón<sup>\*[a, b, c]</sup>

cplu\_201600651\_sm\_miscellaneous\_information.pdf

**General techniques:** PXRD measurements were performed on a D8 Advance diffractometer using CuK $\alpha$  radiation (Philips, Amsterdam, The Netherlands). Field Emission Scanning Electron Microscopy (FESEM) analysis was performed with a ZEISS Ultra 55 microscope. Fluorescence spectroscopy was carried out on a Felix 32 Analysis version 1.2 (Build 56) PTI (Photon Technology International) instrument. Thermogravimetric analyses were carried out on a TGA/SDTA 851e balance (Mettler Toledo, Columbus, OH, USA), using an oxidizing atmosphere (air, 80 mL min<sup>-1</sup>) with a heating program: gradient of 393-1273 K at 10 °C min<sup>-1</sup>, followed by an isothermal heating step at 1273 K for 30 min.

**Chemicals:** (3-isocyanatopropyl) triethoxysilane, rhodamine B, tris(hydroxymethyl) aminomethane (TRIS) and hydrochloric acid were purchased from Sigma-Aldrich Química (Madrid, Spain). Oligonucleotides **O1** (NH<sub>2</sub>-(CH<sub>2</sub>)<sub>6</sub>-5'-GAC TAC CAG GGT ATC-3') and **O2** (5'-AAG CGT GGG GAG CAA ACA GGA TTA GAT ACC CTG GTA GTC-3') were purchased from Isogen-Lifesciences (Barcelona, Spain). *Mycoplasma fermentans* genomic DNA was purchased from Labclinics (Barcelona, Spain). All products were used as received.

**Fabrication of nanoporous anodic alumina (NAA) support:** Porous alumina substrates were produced by electrochemical anodization of high purity (99.99%) aluminium sheets. The electrolyte used was sulfuric acid 0.3 M. Before the anodization, the aluminium sheets were electropolished in a mixture of ethanol and perchloric acid 4:1 (v:v) at 20 V for 4 min to reduce their surface roughness. Then the sheets were cleaned with abundant water and ethanol and dried with air to avoid any acid residue. The electropolished aluminium sheets were then anodized in the H<sub>2</sub>SO<sub>4</sub> electrolyte using a two-step anodization process. The first anodization step was performed for 24 h at 10 V. The temperature of the electrolyte was 2 °C. The resulting nanostructure is a layer of porous alumina with disordered pores. This porous alumina layer was dissolved by wet chemical etching in a mixture of phosphoric acid 0.4 M and chromic acid 0.2 M at 70 °C for 3 h, obtaining a pre-patterned aluminium surface. Subsequently, the second anodization step was performed under the same anodization conditions than the first step. The anodization time for this

second step, that determines the thickness of the layer, was adjusted to produce a porous alumina layer with thickness 8  $\mu\text{m}$ .

**Synthesis of support S1:** In a typical synthesis, NAA was immersed in 8 mL of a mixture of rhodamine B (18.6 mg, 0.04 mmol) in  $\text{CH}_3\text{CN}$  (30 mL). The suspension was stirred at room temperature for 24 h. Then an excess of (3-isocyanatopropyl) triethoxysilane (328  $\mu\text{L}$ , 1.32 mmol) was added, and the final mixture was stirred at room temperature for 24 h. The resulting pink support (**S1**) was slightly washed with acetonitrile and dried at 37  $^\circ\text{C}$  for 2 h.

**Synthesis of support S2:** Support **S1** was immersed in 700  $\mu\text{L}$  of a solution of rhodamine B in  $\text{CH}_3\text{CN}$  (1 mM), then 150  $\mu\text{L}$  of oligonucleotide **O1** (at 20  $\mu\text{M}$  concentration) and 3.5  $\mu\text{L}$  of triethylamine were added. Finally, the mixture was stirred 3 h at room temperature.

**Synthesis of support S3:** Support **S2** was immersed in a solution containing 750  $\mu\text{L}$  of hybridization buffer (20 mM TRIS-HCl, 37.5 mM  $\text{MgCl}_2$ , pH 7.5) and 100  $\mu\text{L}$  of **O2** (100  $\mu\text{M}$ ). The mixture was stirred for 2 h at room temperature. The resulting material was thoroughly washed with hybridization buffer (20 mM TRIS-HCl, 37.5 mM  $\text{MgCl}_2$ , pH 7.5) to eliminate the unbounded oligonucleotide.

**Characterization of the prepared supports:** The prepared supports were characterized by PXRD, FESEM and thermogravimetric analysis. The nanostructure of the starting NAA support was assessed by FESEM. Representative images (see Figure S1) showed disordered pores with an average diameter of 8 nm. FESEM images of the **S3** support clearly show the presence of an organic layer that covered most of the pores. The presence of this organic layer evidenced the suitable consecutive loading, functionalization and capping steps, while the visualization of the porous framework in certain areas confirmed the preservation of the nanoporous structure in **S3**.

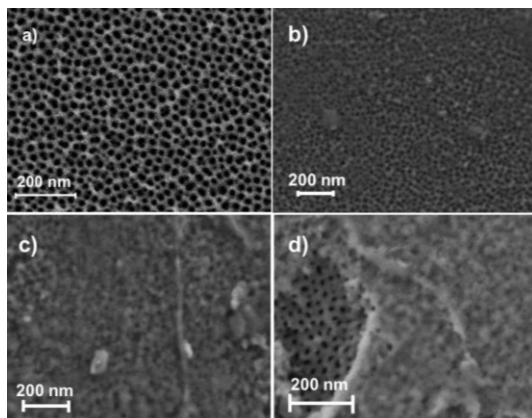


**Figure S1:** Representative FESEM images of a) NAA scaffold, b) **S1**, c) **S2** and d) **S3**.

The disordered structure of NAA support was confirmed by powder X-ray diffraction (see Figure S2), where only a very strong peak at  $2\theta = 38$ , which corresponds to crystalline aluminium, and a weak and broad peak corresponding to amorphous alumina oxide were found. No more peaks were registered, indicating that the support does not present an ordered pore distribution. **S1**, **S2** and **S3** supports show the same powder X-ray diffraction pattern than the initial support.

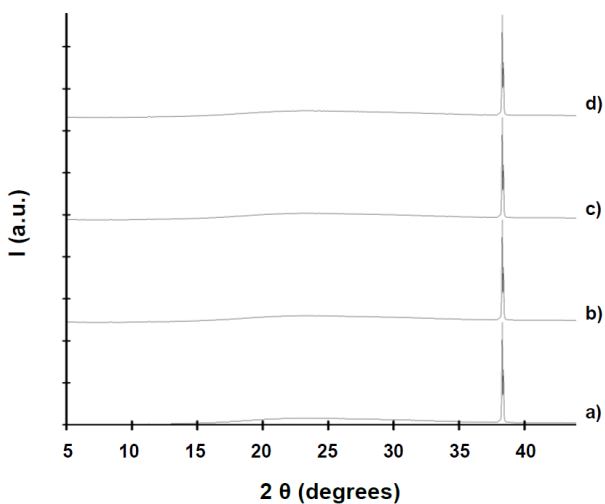


**Figure S2:** PXRD pattern for a) NAA support, b) **S1**, c) **S2** and d) **S3**.

The organic content of the different prepared materials was calculated from thermogravimetric analysis (see Table 1 in the manuscript).

**Release experiments of support S3:** To investigate the gating properties of **S3** two fractions of this material were immersed in 1.6 mL of hybridization buffer (20 mM tris-HCl, 37.5 MgCl<sub>2</sub>, pH 7.5). Then 50  $\mu$ L of a *Mycoplasma* genomic DNA aqueous solution (5000 copies· $\mu$ L<sup>-1</sup>) was added to one of the supports after being subjected to a dehybridation treatment (5 min 90 °C and 3 min 0 °C), while 50  $\mu$ L of water subjected to the same treatment was added to the other support. Both experiments were maintained at 25 °C and, at certain times, fractions were taken. Cargo release to the solution was then measured by the rhodamine B fluorescence at 585 nm ( $\lambda_{exc}$ =555 nm).

**Calcination of S3:** Calcination of support **S3** was performed on a MC/1300 oven (Gallur) using a heating gradient from 25 °C to 550 °C (3 ° per min) followed by an isothermal period at 550 °C for 5 h.

**Reutilization and Reusability:** An already used support **S3** was calcined (in order to remove all the organic matter) according to the above described procedure. Then, the obtained support was loaded with rhodamine B and the external surface functionalized using the same procedure than that employed for the preparation of **S3**. This protocol yielded solid **S3-R1**. On the other hand, another already used **S3** material was reloaded with rhodamine B and then capped with **O2** oligonucleotide yielding **S3-R2** support. Figure S3 shows the release from **S3-R1** and **S3-R2** supports in the absence and in the presence of *Mycoplasma fermentans* genomic DNA. As could be seen, in the absence of *Mycoplasma* genomic DNA a negligible dye release was observed for both supports. However, when *Mycoplasma* genomic DNA was present, a remarkable rhodamine B delivery was found. These results suggested the potential reusability of the NAA supports employed in the preparation of the sensing system.



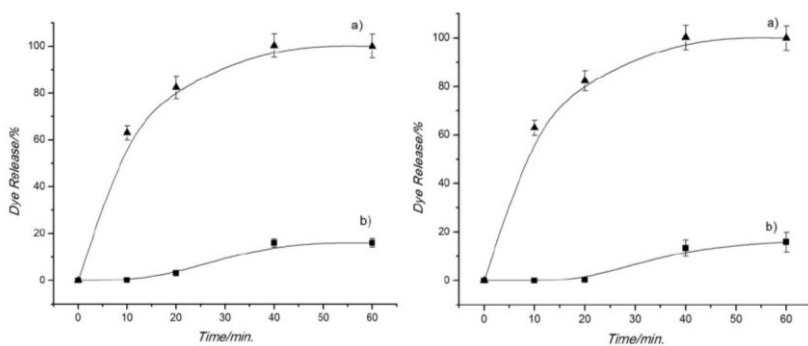
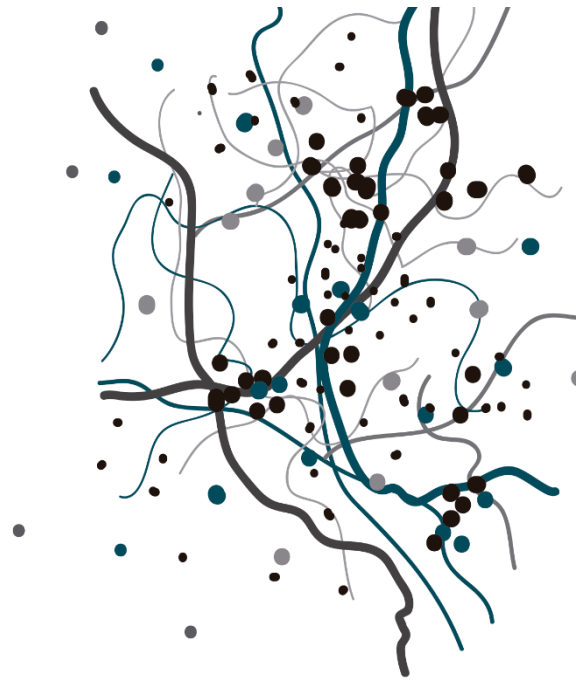


**Figure S3:** Release of rhodamine B from support **S3-R1** (left) and **S3-R2** (right) in the absence (b) and in the presence (a) of *Mycoplasma fermentans* genomic DNA (150 copies· $\mu\text{L}^{-1}$ ) in TRIS buffer at pH 7.4.





# 4

Aptamer-capped Nanoporous  
Anodic Alumina for  
*Staphylococcus Aureus*  
Detection



# Aptamer-Capped Nanoporous Anodic Alumina for *Staphylococcus aureus* Detection

Luis Pla<sup>a,b,c,‡</sup>, Sara Santiago-Felipe<sup>a,b,c,‡</sup>, María Ángeles Tormo-Mas<sup>d\*</sup>, Javier Pemán<sup>d,e</sup>, Félix Sancenón<sup>a,b,c,f</sup>, Elena Aznar<sup>a,b,c,f\*</sup>, and Ramón Martínez-Máñez<sup>a,b,c,f\*</sup>

<sup>a</sup> CIBER de Bioingeniería, Biomateriales y Nanomedicina (CIBER-BBN), Spain

<sup>b</sup> Instituto Interuniversitario de Investigación de Reconocimiento Molecular y Desarrollo Tecnológico; Universitat Politècnica de València, Universitat de València, Camino de Vera s/n, 46022, Valencia, Spain; E-mail: elazgi@upvnet.upv.es

<sup>c</sup> Unidad Mixta de Investigación en Nanomedicina y Sensores; Universitat Politècnica de València, Instituto de Investigación Sanitaria La Fe, Valencia, Spain

<sup>d</sup> Grupo Acreditado de Infección Grave. Instituto de Investigación Sanitaria La Fe, Hospital Universitari i Politècnic La Fe, Avenida Fernando Abril Martorell, 46026, Valencia, Spain..

<sup>e</sup> Servicio de Microbiología Hospital Politècnic i Universitari La Fe. Instituto de Investigación Sanitaria La Fe, Avenida Fernando Abril Martorell, 46026, Valencia, Spain.

<sup>f</sup> Unidad Mixta UPV-CIPF de Investigación en Mecanismos de Enfermedades y Nanomedicina. Universitat Politècnica de València, Centro de Investigación Príncipe Felipe, Valencia, Spain.

‡ These authors contributed equally

\* Corresponding author:

E-mail: elazgi@upvnet.upv.es; tormo\_man@iislafe.es; rmaez@upvnet.upv.es

***Sensors & Actuators: B. Chemical. 2020, 320, 128281***



## 4.1 Abstract

The development of new detection systems for an accurate and rapid identification of pathogens has become an essential challenge in the biomedical field. Herein a highly selective platform based on aptamer-gated nanomaterials for specific *Staphylococcus aureus* detection is presented. In the proposed design, a nanoporous anodic alumina (NAA) scaffold is loaded with the fluorescent indicator rhodamine B, while pores entrances are capped by a DNA aptamer which selectively recognizes *S. aureus* cells in less than 1 hour. When *S. aureus* cells are present, the solid is selectively uncapped, and the dye is released to the medium. This nanodevice allows the detection of bacterial concentrations between 2 and 5 CFU mL<sup>-1</sup> (in buffer and blood, respectively) and it has demonstrated excellent behavior in terms of specificity and robustness. A set of 25 different clinical samples are analyzed using this simple procedure obtaining excellent results, which agree with conventional hospital reference techniques for the identification of *S. aureus*. This new method is sensitive, rapid and low cost, and avoids steps such as polymerase chain amplification reaction, which makes it suitable for use in point-of-care detection systems.

## Keywords

Aptamers, gated materials, *Staphylococcus aureus*, biosensors

## 4.2 Introduction

*Staphylococcus aureus* is a Gram-positive and facultative anaerobic bacterium, and it is considered as one of the most important human pathogens. Although it is not always pathogenic, the existence of *S. aureus* is highly common in the environment and can cause numerous diseases, from mild skin infections to life-threatening complications. Moreover, it is one of the most important causes of nosocomial contagions and it is often the cause of wound infections after surgical interventions [1].

*S. aureus* has been traditionally identified by detection methods that involve culture growing, colony isolation and different serological and biochemical tests.

More recently, several works have focused on the advancement of detection strategies based on the biomolecular recognition of *S. aureus*, including amplification reactions such as polymerase or ligase chain reactions, strand displacement amplification or enzyme-linked immunosorbent assay [2-5]. Although these techniques usually show high sensitivity and selectivity, their complexity, cost and time of analysis, have limited their widespread application for clinical diagnosis.

Biosensor-based technologies have demonstrated an enormous potential for the recognition of toxins, pathogens and other biomolecules in a rapid, sensitive and reproducible way [6, 7]. Different methods using surface plasmon resonance, fluorescence, colorimetric, electrochemical or light scattering signals have been described for *S. aureus* bacterium detection [8, 9]. In most cases, antibodies are used as a recognition element. Antibody-based immunosensors have demonstrated high specificity and have been well-established [10, 11]. However, the use of antibodies could encounter some limitations due to their low stability, high cost and complicated modification and functionalization. In this context, aptamers are other class of high-affinity molecules that have provided excellent results for the recognition of a great variety of analytes in the biotechnological field [12-15]. Aptamers are single-chain nucleic acids (RNA or DNA) that are generally *in vitro* synthesized through the known process of "Systematic Evolution of Ligands by EXponential enrichment" (SELEX). They have shown affinities for their targets similar or higher than that obtained by most of the reported monoclonal antibodies, presenting dissociation constants from the picomolar to low micromolar ranges. Furthermore, aptamers are easy to modify, easily scalable for chemical synthesis of large quantities of product and stable for long term storage [16]. Recently, some sequences of aptamers have been chosen and used for the specific recognition of bacteria including *Bacillus anthracis*, *Escherichia coli*, *Salmonella enterica*, *Mycobacterium tuberculosis* or *Staphylococcus aureus*. Nevertheless, none of these works was capable of identifying the bacteria at low concentrations without a previous DNA amplification reaction [8, 9, 17].

Progress in nanotechnology has significantly increased the number of possibilities for biosensors development. A key issue in this field is the design of new hybrid organic-inorganic materials that combine, in a single entity, the



potential of nanomaterials with the recognition, sensitivity and selectivity capabilities of biomolecules. The anchoring of a variety of supramolecules, biomolecules or organic molecules onto several inorganic scaffolds with diverse chemical nature, size or shape, has allowed the development of a great variety of smart nanodevices as probes that have demonstrated advantages such as rapidity, simplicity and sensitivity [17-20]. In this context, several works have been recently published that combine nanomaterials and the use of aptamers to develop different methods for *S. aureus* detection [9, 21-23]. In these studies, nanodevices are mainly used to pre-concentrate bacteria cells as a previous step to further detection by optical systems. For example, Kurt *et al.* (2016) developed quantum dots functionalized with aptamer and upconverting nanoparticles for the luminescent identification of *S. aureus* reaching a limit of detection of 16 CFU mL<sup>-1</sup> [21]. In another work, few tens of *S. aureus* cells were detected by combining functionalized gold nanoparticles with surface-assisted laser desorption and ionization mass spectrometry [22]. Likewise, Wang *et al.* achieved the recognition of 10 CFU mL<sup>-1</sup> of *S. aureus* using a biosensor based on the magnetically assisted Surface-Enhanced Raman Scattering technology [9]. A simple detection system able to recognize the bacterium and provide a signal in several minutes could facilitate the assay and deliver a highly valuable information in a shorter period of time, which directly affects patients' disease evolution.

Porous materials provided with "molecular gates" have been widely applied in direct detection and diagnosis systems based on stimuli-response methods. In these gated-materials, fluorescent dye rhodamine B is encapsulated into the porous support structure, and the capping mechanism is designed so that the release of the cargo is only induced when the target analyte is present [19, 24, 25]. Following this mechanism, gated systems have been recently developed for the selective detection of cations, anions, neutral molecules and biomolecules [18, 26, 27]. Among supports used in gated sensing protocols, nanoporous anodic alumina (NAA) has arisen as a promising material thanks to its wide variety of applications [28-31]. NAA supports are stable, do not degrade in aqueous solutions and can be reused several times after calcination treatment. NAA supports have demonstrated excellent performances in sensing applications using nucleic acids (DNA, RNA or aptamers) as molecular gate

[32, 33, 34]. Nevertheless, as far as we are aware, no aptamer-capped NAA system dedicated to bacterial optical detection has been reported yet.

Based on what has been mentioned above, a new hybrid gated nanostructured sensor for the fluorogenic identification of *S. aureus* cells is presented. In the proposed system the NAA scaffold is charged with the rhodamine B and capped with an aptamer specific of *S. aureus* cells. The capping aptamer blocks the pores and inhibits the fluorophore release. The recognition mechanism is such that if the analyte is present, the aptamer is selectively displaced, with the subsequent pore opening and cargo delivery. The proposed gated materials are characterized and employed for the recognition of *S. aureus* bacteria in real clinical samples from infected patients, obtaining results in less than an hour.

## 4.3 Materials and methods

### 4.3.1 General techniques

A ZEISS Ultra 55 microscope was employed to perform Field Emission Scanning Electron Microscopy (FSEM) and Energy Dispersive X-ray spectroscopy (EDX) analyses. Measurements of fluorescence spectroscopy were carried out on a Synergy H1 microplate reader (BioTek, Winooski, VT, USA).

### 4.3.2 Chemicals

3-(Triethoxysilyl)propyl isocyanate, rhodamine B, tris(hydroxymethyl)aminomethane (TRIS), triethylamine (TEA), and hydrochloric acid were obtained from Sigma-Aldrich Química (Madrid, Spain). Oligonucleotide (NH<sub>2</sub>-(CH<sub>2</sub>)<sub>6</sub>-5'-AAA AAA CCC CCC-3') (**O1**) and the aptamer (5'-TTT TGG GGG GTC CCT ACG GCG CTA ACC CCC CCA GTC CGT CCT CCC AGC CTC ACA CCG CCA CCG TGC TAC AAC GGG GGG TTT T-3') (**O2**) were purchased from Invitrogen by Thermo Fisher Scientific (Madrid, Spain). NAA scaffolds were purchased from InRedox (CO, USA).

### 4.3.3 Synthesis of S1, S2 and S3

In a conventional synthesis of material **S1**, 8 independent NAA supports of 2 mm of diameter were submerged in a mixture of rhodamine B dye in CH<sub>3</sub>CN

(18.6 mg, 1 mM, 8 mL). To enable the loading of the pores, the solution was agitated for 24 h. Then, the surface of the support was functionalized by the addition of (3-(triethoxysilyl)propyl isocyanate (0.01 mmol, 328  $\mu$ L) and stirring the mixture for 6 h.

For the preparation of **S2**, **S1** was immersed in a mixture of rhodamine B in CH<sub>3</sub>CN (1 mM, 700  $\mu$ L), and then 100  $\mu$ L of the oligonucleotide **O1** (10  $\mu$ M) and 2  $\mu$ L of TEA were dropped. Then, the solution was mixed for 3 h at room temperature.

To prepare **S3**, **S2** was immersed with 90  $\mu$ L of PBS buffer and oligonucleotide **O2** was added (10  $\mu$ L, 100  $\mu$ M). The suspension was agitated for 2 h at 30 °C, and the obtained nanomaterial was washed dropwise with PBS buffer (phosphate-buffered saline, pH 7.5) to eliminate the unattached oligonucleotide.

#### 4.3.4 Bacterial growth

The main bacterial strains employed in this work were *Staphylococcus aureus* (RN4220 strain) [35], *Staphylococcus conhii* (SCN123 strain) [36], *Staphylococcus capitis* (IPA57 strain) [36], *Staphylococcus epidermidis* (RP62A strain) [37], *Staphylococcus carnosus* (TM300 strain) [38], *Staphylococcus saprophyticus* (SCN159 strain) [35], *Staphylococcus chromogenes* (C483 strain) [39], *Staphylococcus xylosus* (C482 strain) [39], *Staphylococcus haemolyticus* (IPA71 strain) [36], *Staphylococcus lugdunensis* (IPA26 strain) [36], *Staphylococcus hominis* (SCN4 strain) [36], *Staphylococcus warneri* (SCN44 strain) [36]. All bacteria were cultured in tryptic soy broth medium (TSB) or agar plates (TSA) and were grown at 37 °C for 24 hours. The bacteria concentration was calculated by determining the optical density at 600 nm, given that OD<sub>600</sub> = 1.0 corresponds to 1.5·10<sup>8</sup> CFU mL<sup>-1</sup>. 100  $\mu$ L were grown in TSA plates to check that the experiments were carried out with the corresponding inoculum concentration.

#### 4.3.5 Assay protocol

Solids' behavior were evaluated by measuring the emitted fluorescence of rhodamine B delivered from the pores in the presence of *S. aureus* cells. In a common experiment, two independent **S3** nanomaterials were submerged in

900  $\mu\text{L}$  of PBS. Then, 100  $\mu\text{L}$  of an *S. aureus* suspension ( $10^3$  CFU  $\text{mL}^{-1}$ ) was inoculated to only one of the supports while 100  $\mu\text{L}$  of buffer was transferred to the other. Both solutions were stirred at 25  $^{\circ}\text{C}$  and aliquots were obtained at scheduled times. Finally, dye released was determined by registering the fluorescence of the indicator in the solution at 575 nm ( $\lambda_{\text{exc}} = 555$  nm).

#### 4.3.6 Real media experiments

The applicability of the method in a more realistic context was tested. For that, 400  $\mu\text{L}$  of different competitive media (serum, pleural, peritoneal, synovial or cerebrospinal fluid) were artificially inoculated with *S. aureus* (100  $\mu\text{L}$ ,  $10^3$  CFU  $\text{mL}^{-1}$ ) and added to independent **S3** supports in a final volume of 1 mL of PBS. Solutions were maintained at 25  $^{\circ}\text{C}$ , and rhodamine B released from the porous was measured at 575 nm ( $\lambda_{\text{exc}} = 555$  nm) after 60 min.

#### 4.3.7 Quantification of the loaded dye

In order to estimate the amount of the Rhodamine B that can be loaded in the pores, two individual **S3** solids were submerged in 1000  $\mu\text{L}$  of PBS. Then, one of them was stirred at 90  $^{\circ}\text{C}$  during 60 min to force the opening of the pores and the maximum cargo release, and the other was maintained in agitation at 25  $^{\circ}\text{C}$  during 60 min as a control. The delivered fluorophore was observed at 575 nm ( $\lambda_{\text{exc}} = 555$  nm), and the experiment was done by triplicate. Quantification of final released dye was undertaken using a calibration curve with different concentrations of rhodamine B.

#### 4.3.8 Amplification assay

In order to calculate the amplification of the signal, two individual **S3** solids were submerged in 900  $\mu\text{L}$  of PBS. Then, 100  $\mu\text{L}$  of an *S. aureus* suspension ( $10^3$  CFU  $\text{mL}^{-1}$ ) was inoculated to one of them and 100  $\mu\text{L}$  of buffer was added to the other. Both solutions were stirred at 25  $^{\circ}\text{C}$  during 60 min and the delivered fluorophore was observed at 575 nm ( $\lambda_{\text{exc}} = 555$  nm). Quantification of finally released dye was undertaken using a calibration curve with different concentrations of rhodamine B, to then directly correlate with the number of CFU  $\text{mL}^{-1}$  that opened the system.

#### 4.3.9 Response vs. concentration experiments

The response of the material to different decreasing concentrations of *S. aureus* was evaluated and compared in both buffer and blood media. For that, 500  $\mu\text{L}$  of 10-fold dilutions of *S. aureus* suspensions ( $10^3 - 0 \text{ CFU mL}^{-1}$ ) were added to seven independent **S3** supports in a final reaction volume of 1 mL of PBS or non-contaminated blood. After 60 min at 25 °C rhodamine B released from the porous was measured at 575 nm ( $\lambda_{\text{exc}} = 555 \text{ nm}$ ).

#### 4.3.10 Selectivity

The selectivity of the nanosensor was determined by performing the same delivery experiments in the presence of other *Staphylococcus* species and different mixtures of them (*S. conhii*, *S. capitis*, *S. epidermidis*, *S. carnosus*, *S. saprophyticus*, *S. chromogenes*, *S. xylosus*, *S. haemolyticus*, *S. lugdunensis*, *S. hominis*, *S. warneri* and a mixture of *S. aureus* and *S. carnosus*, a mixture of *S. aureus*, *S. hominis* and *S. capitis*, and a mixture of *S. conhii* and *S. warneri*). For that, 100  $\mu\text{L}$  of a bacterial suspension of each specie ( $10^3 \text{ CFU mL}^{-1}$ ) were added to fifteen independent **S3** supports in a final reaction volume of 1 mL of PBS. After 60 min at 25 °C rhodamine B released from the pores was measured at 575 nm ( $\lambda_{\text{exc}} = 555 \text{ nm}$ ).

#### 4.3.11 Validation in Clinical Real Samples

Probe performance was evaluated in real clinical samples from patients. Twenty-five blood culture samples were examined using the automated BacT/ALERT VIRTUOTM system (bioMérieux, Madrid, Spain). Positive bottles were subcultured in chocolate agar plates (bioMérieux) for 24 hours, and definitive identification of *S. aureus* isolates was carried out by MALDI-TOF Mass Spectrometry (VITEK MS, bioMérieux). In parallel, for each sample, 500  $\mu\text{L}$  of blood culture from infected and non-infected patients was added to independent **S3** supports in a final reaction volume of 1 mL of PBS and the rhodamine B delivered from the support was measured after 30 min at 25 °C.

#### 4.3.12 Ethical Committee

The present study was approved by the Ethics Committee of Hospital Universitari i Politècnic La Fe (2017/0370).

## 4.4 RESULTS AND DISCUSSION

### 4.4.1 Development and characterization of the sensing system

The developed sensing system consists of a nanoporous NAA scaffold in which the pores were loaded with the fluorophore rhodamine B. The outer surface was functionalized with the organic linker 3-(triethoxysilyl)propyl isocyanate to allow the covalently anchoring of the capping DNA molecules by the formation of urea bonds with the short oligonucleotide  $\text{NH}_2\text{-(CH}_2\text{)}_6\text{-5'}$ -AAA AAA CCC CCC-3' (**O1**), which is designed to recognize and hybridize with the sequence 3'-TTT TGG GGG G-5'. The oligonucleotide 5'-TTT TGG GGG GTC CCT ACG GCG CTA ACC CCC CCA GTC CGT CCT CCC AGC CTC ACA CCG CCA CCG TGC TAC AAC GGG GGG TTT T-3' (**O2**), which contains the specific sequence to recognize *S. aureus* cells (i.e. 5'-TCC CTA CGG CGC TAA CCCCC CAG TCC GTC CTC CCA GCC TCA CAC CGC CAC CGT GCT ACA AC-3'), was employed to block the pores by hybridization with **O1**, obtaining the final sensing gated nanomaterial **S3** (Figure 1).

In the absence of target analyte, the dsDNA **O1-O2** anchored to the external surface of the inorganic scaffold was expected to be bulky enough to block pores and to inhibit dye delivery. On the contrary, due to the higher affinity of the aptamer for *S. aureus* cells than for **O1**, it was expected that in the presence of the target bacteria, the aptamer would selectively be displaced from the surface resulting in *S. aureus*-aptamer binding, pore opening and dye release.

The starting NAA scaffold and the obtained **S1**, **S2** and **S3** supports were characterized by FESEM and EDX analysis. The NAA support (InRedox®) consisted on anodic aluminum oxide film grown on a 0.1 mm thick aluminum layer with a pore density of  $9 \cdot 10^{11} \text{ cm}^{-2}$ . Pores entrance present a funnel-like shape which gradually switches from a larger size (20-30 nm) at the top of the funnel to a 5 nm size at the end. Transition from one size to another extends to a profundity of approximately 3 times the pore diameter, and below this depth, the pore structure becomes uniform along 10  $\mu\text{m}$ . With this pore morphology, the maximum amount of cargo that is possible to load and release was estimated to be 4 ng of Rhodamine B per  $\mu\text{g}$  of NAA.

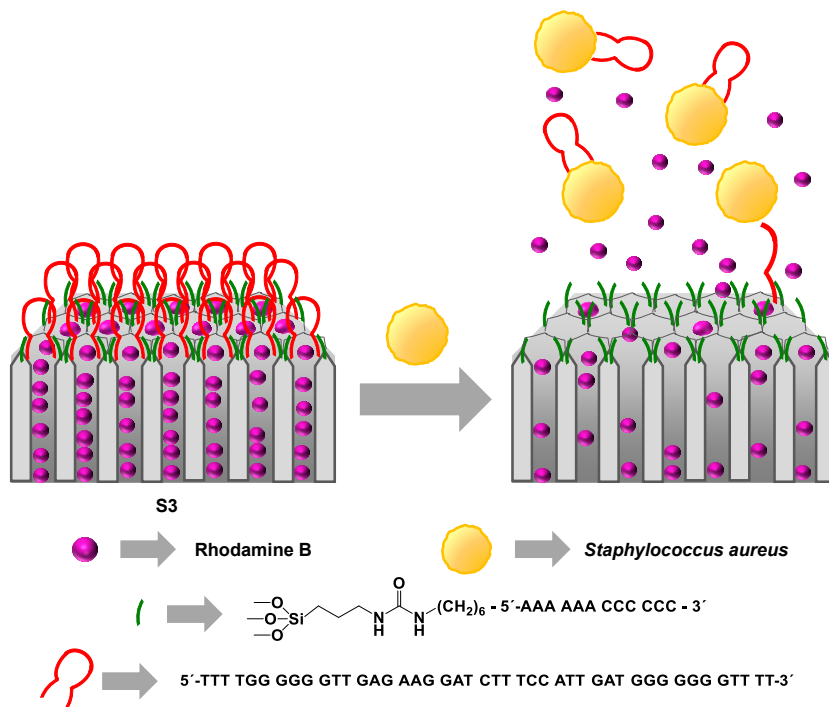


**Figure 1.** Scheme of the capped NAA material **S3** selective performance in the presence of *S. aureus* cells. In the lack of *S. aureus*, pores are blocked while in the presence of bacteria, the cell interacts with the aptamer allowing oligonucleotide displacement and delivery of the entrapped dye.

The FESEM images of the starting NAA confirmed the described structure. Representative images of solid **S2** showed the same porous structure as the parent material. FESEM images of material **S3** revealed the existence of an organic covering on the top of the pores. In contrast, the visualization of the porous configuration in specific areas confirmed the preservation of the nanoporous structure in **S3** (Figure 2). Organic content in **S1**, **S2** and **S3** was analyzed by energy-dispersive X-ray spectroscopy (Table 1). As expected, high carbon content (C/Al 1.424) was found in solid **S1**, due to the high loading capacity of NAA material. Solid **S2** showed a decrease of carbon content due to the experimental conditions for **O1** attachment, which do not prevent a partial cargo release (C/Al 0.624). Finally, solid **S3** presented a slight increase in organic matter content (C/Al 0.704) that can be associated with an effective

capping of the support with the oligonucleotide **O2**. Likewise, the presence of nitrogen and phosphorous atoms from the capping oligonucleotide in the final material was confirmed.

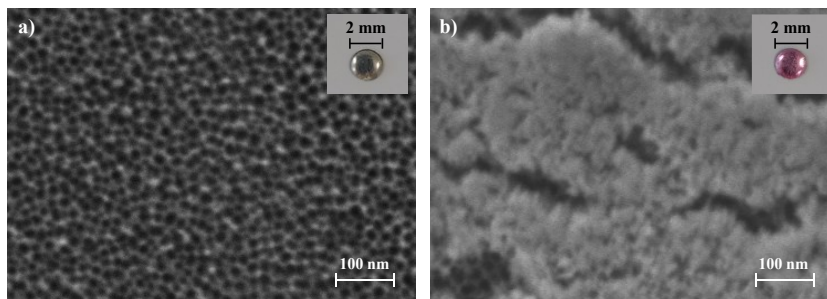


**Figure 2.** FESEM images of NAA support (a) and solid **S3** (b). Insets: Digital photographs of the corresponding solids

**Table 1.** Atomic elements relation in the different prepared solids.

	C/AI	N/AI	P/AI
<b>S1</b>	1.424 ± 0.030	-	-
<b>S2</b>	0.624 ± 0.008	ND	ND
<b>S3</b>	0.704 ± 0.021	0.044 ± 0.004	0.012 ± 0.003

#### 4.4.2 Delivery kinetics

The *S. aureus* recognition through solid **S3** mechanism is founded on the opening of the gated nanomaterial in the presence of the bacteria that leads to selective rhodamine B delivery. The response of **S3** to *S. aureus* was studied employing a bacterial suspension of  $10^3$  CFU mL<sup>-1</sup>. To conduct this experiment, two separated gated **S3** supports were immersed in PBS buffer (pH 7.5). Then, 100 μL of the bacterial suspension was transferred to one of the materials (final *S. aureus* concentration of  $10^2$  CFU mL<sup>-1</sup>), and 100 μL of PBS was added to the other. To calculate the delivered dye in the aqueous phase, the fluorescence of the aliquots taken at predetermined times was measured. As depicted in Figure 3, in the absence of the bacteria, little rhodamine B emission was recorded, which is suggestive of notable pore closure by the dsDNA **O1-O2** anchored to



the surface of the scaffold (curve a). On the contrary, when *S. aureus* cells were present, a remarkable dye diffusion to the aqueous solution was registered (Figure 3, curve b). The observed enhancement in fluorescence emission was attributed to the migration of capping aptamers from **S3** support to the solution as a result of a specific interaction with the bacteria cell. It is worth mentioning that in previous works the binding capacity of the aptamer for *S. aureus* cells, measured as dissociation constant, was 35 nM [23], which is indicative of a high aptamer-bacteria affinity and it is in accordance with our results.

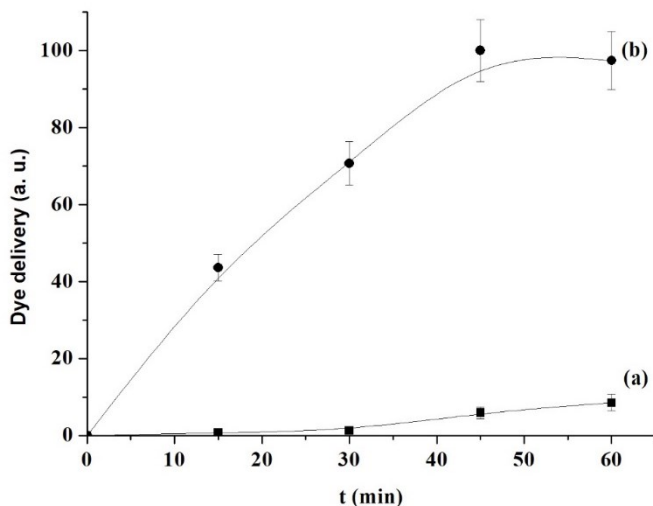


**Figure 3.** Rhodamine B delivery from the pores of material **S3** in PBS buffer (pH 7.5) at different periods of time. Curve (a) indicates dye release in the lack of *S. aureus* cells and curve (b) represents cargo delivery in the presence of target *S. aureus* at a concentration of  $10^2$  CFU mL<sup>-1</sup>.

#### 4.4.3 Analytical performance: sensitivity, specificity and robustness studies

The sensitivity of the method was determined by submitting the support to different concentrations of *S. aureus* and studying the response generated. For that, 6 independent **S3** supports were immersed in PBS, and 100  $\mu$ L of 10-fold bacterial suspension dilutions were added to each material, reaching a range of final concentrations between  $10^3$  and  $10^{-5}$  CFU mL<sup>-1</sup>. After 60 min, the total sum of rhodamine B diffused to the aqueous phase was measured. Results

showed that delivered dye was directly related to *S. aureus* concentration, upholding the sensing protocol detailed above (Figure 4A). A limit of detection (LOD) of 2 CFU mL<sup>-1</sup> was calculated based on the intersection point of the two slopes of the represented curve. This LOD value is equivalent to those obtained by most aptamer-based nanosystems described in the literature for *S. aureus* detection [8, 9, 17, 22, 23]. Providing similar sensitivity, the presented nanosensor is also simpler and faster (ca. 60 min). Moreover, in the proposed system, amplification takes place in the signalling step and not in the recognition event, which is a substantial improvement in the progress of sensing systems technology. Specifically, in gated materials, the recognition mechanism is separated from the signalling event, having an independent stoichiometric relation. This implies that the aptamer-bacteria recognition involves the liberation of a large amount of reporter molecules. In the presented system, it was found that 10 CFU mL<sup>-1</sup> of *S. aureus* was capable of release an average of  $5 \cdot 10^{12}$  molecules of rhodamine B, which means a signal amplification of  $10^{11}$  reporter molecules per recognized bacteria. This signal amplification depends both on the geometry of the pores, which will determine the amount of cargo loaded, and on the affinity of the probe for the target, which will determine the efficiency of opening the pores. In line with this, published works have estimated that a single *S. aureus* cell can bind from 900 to 1200 aptamer molecules, which may contribute to that high signal amplification [23].

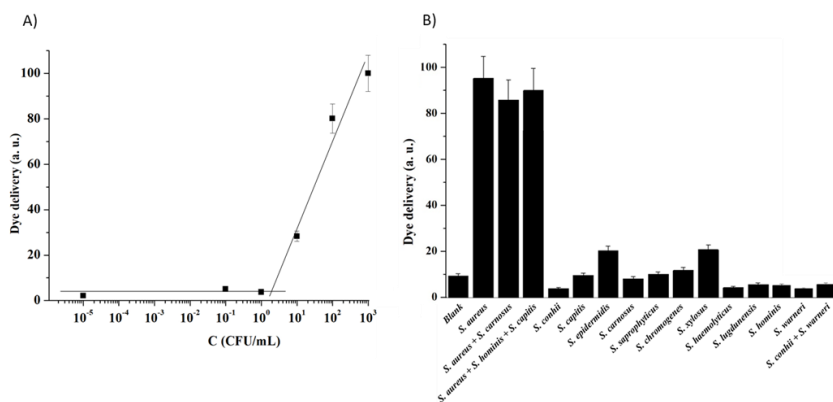


**Figure 4.** Dye release from solid S3 (A) in the presence of decreasing amounts of *S. aureus*; (B) in the presence of 10<sup>2</sup> CFU mL<sup>-1</sup> of *S. aureus*, a mixture of *S. aureus* + *S. carnosus*, a mixture of *S. aureus* + *S. hominis* + *S. capitis*, *S. conchii*,

*S. capitis*, *S. epidermidis*, *S. carnosus*, *S. saprophyticus*, *S. chromogenes*, *S. xylosus*, *S. haemolyticus*, *S. lugdunensis*, *S. hominis*, *S. warneri* and a mixture of *S. conhii* + *S. warneri*. Assays were carried out at 60 min in PBS buffer at pH 7.5.

Additionally, the specificity of the nanomaterials was assessed by testing the response of **S3** to other *Staphylococcus* species (*S. conhii*, *S. capitis*, *S. epidermidis*, *S. carnosus*, *S. saprophyticus*, *S. chromogenes*, *S. xylosus*, *S. haemolyticus*, *S. lugdunensis*, *S. hominis* and *S. warneri*) and mixtures of some of them (*S. aureus* + *S. carnosus*, *S. aureus* + *S. hominis* + *S. capitis* and *S. conhii* + *S. warneri*) (Table 2). For that, the dye delivered from 15 independent **S3** supports was monitored in the presence of  $10^2$  CFU mL<sup>-1</sup> of each bacterium. As it is depicted in Figure 4B, *S. aureus* was the only microorganism capable of producing a remarkable dye release. It should be noted that the selective aptamer-cell recognition, and therefore the measured fluorescence, was not affected by the presence of other microorganisms in the media, indicating the absence of interference. On the other hand, all the other *Staphylococcus* species induced fewer pore uncapping and less cargo delivery, which demonstrates the capacity of the system to selectively discriminate between *S. aureus* and other *Staphylococcus* species.

In addition, to evaluate the robustness of the system, the behavior of **S3** to the presence of 100  $\mu$ L of  $10^3$  CFU mL<sup>-1</sup> of *S. aureus* was evaluated in different clinical relevant media (serum, pleural, peritoneal, synovial and cerebrospinal fluid). As it is depicted in Figure 5, the presence of *S. aureus* cells produced a selective displacement of the aptamer, pore uncapping and dye delivery in all tested media. Moreover, although a slightly higher residual release was observed in competitive media than in buffer (20% vs 5%), the measured fluorescence in the presence of bacteria cells was comparable to that achieved in PBS buffer (ca. 60-80%). Likewise, the possibility to directly detect *S. aureus* using the gated material **S3** was investigated. Taking into account the usual bloodstream *S. aureus* concentration ( $1 \cdot 10^3$  CFU mL<sup>-1</sup>), aliquots of fresh blood were inoculated with different amounts of *S. aureus* (0,  $2 \cdot 10^{-6}$ ,  $2 \cdot 10^{-3}$ ,  $2 \cdot 10^{-1}$ , 20,  $2 \cdot 10^2$  and  $2 \cdot 10^3$  CFU mL<sup>-1</sup>, respectively) to emulate *S. aureus* contaminated blood. Then, 500  $\mu$ L of each sample was added to an Eppendorf tube containing the **S3** support and 500  $\mu$ L of PBS buffer. After 60 min at 25 °C rhodamine B

released from pores was registered at 575 nm ( $\lambda_{exc} = 555$  nm). As depicted in Figure 5B, released rhodamine B was proportional to the analyte concentration and, based on the intersection point of the two slopes of the curve, a LOD of 5 CFU mL<sup>-1</sup> was calculated. This LOD is in the same order of magnitude as that obtained in buffer media, demonstrating its high potential of the probe for clinical applications without the need of previous culture, sample treatment or amplification steps. Moreover, preliminary studies carried out to assess the stability of aptamer-gated nanomaterials have demonstrated that this type of nanosensors can be stored up to 12 weeks without any changes in their sensing performance [27].

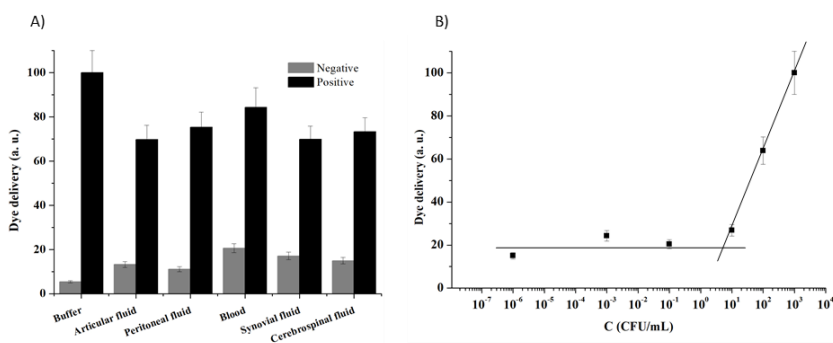


**Figure 5.** Delivery of rhodamine B from material **S3** (A) in diverse clinical media with 10<sup>2</sup> CFU mL<sup>-1</sup> of *S. aureus*, and (B) in the presence of decreasing concentrations of *S. aureus* cells in blood. Assays took place at 60 min in PBS buffer at pH 7.5.

#### 4.4.4 *S. aureus* detection in clinical samples

The detection of *S. aureus* cells directly in clinical samples is crucial for the successful application of the probe in the real medical practice. Hence, the applicability of the sensing materials to detect *S. aureus* from infected samples was studied. The current reference method for *S. aureus* detection in most hospitals is based on specimen culture attached to subsequent identification techniques. In the first step, the clinical sample is cultured using automated culture equipment until bottles are detected as positive (10<sup>6</sup>-10<sup>8</sup> CFU mL<sup>-1</sup>), which takes around 12 h. Then, a gram stain is performed with a sub-sample from the bottle to confirm the presence of microorganisms and to determine its

morphotype. Subsequently, a sample from the positive bottle is subcultured in chocolate agar, and after 24 h more, *S. aureus* colonies are identified by MALDI-TOF MS. The total time until *S. aureus* identification could range between 36 h to several days [40-44].

In the present work, 25 clinical blood samples from Hospital Universitari i Politècnic La Fe from *S. aureus* infected and noninfected patients were analyzed. These samples were managed by the standard procedure that is automated blood culture, subsequent subculture and *S. aureus* identification by MALDI-TOF Mass Spectrometry. In parallel, the same 25 samples were assessed by triplicate by using the gated material **S3**. For that, 25 individual **S3** supports were immersed in 500  $\mu\text{L}$  PBS, and 500  $\mu\text{L}$  of blood culture was added to each one. As in previous experiments, released rhodamine B was measured by fluorescence after 30 min. Results showed a total coincidence between the current reference methods for *S. aureus* in hospitals and our procedure using **S3** in the 25 analyzed samples. In the course of the study, one sample was negative for *S. aureus* but positive for *S. lugdunensis* (Table 2). Based on these results, our system is demonstrating a sensitivity of 100% and positive and negative predictive values of 100%. The high competitiveness of the gated materials compared to the conventional reference methods is remarkable, providing high accuracy, easiness to use, rapidity and lower cost. In addition, a final confirmation experiment was performed. All **S3** evaluation studies, prior clinical validation, were performed using *S. aureus* RN4220 strain. However, in the clinical context, other *S. aureus* strains can be found in *S. aureus* infected samples. To confirm that the method was able of detect *S. aureus* in blood samples at a lower concentration than in blood culture (avoiding bacterial growth), the same 25 samples of the study were grown in TSB media and diluted to a concentration of  $10^3$  CFU  $\text{mL}^{-1}$ . Then, **S3** supports were immersed in a solution of PBS-blood (50% v/v) and then 100  $\mu\text{L}$  of the bacterial dilution was added to each one (final concentration of  $10^2$  CFU  $\text{mL}^{-1}$ ). Results showed a positive rhodamine B release for all the *S. aureus*-containing samples independently of the strain, demonstrating the ability of the developed system to recognize a variety of different *S. aureus* strains at a lower concentration than in blood culture.

**Table 2.** Results from blood samples analyzed using the gated material **S3** and the reference blood culture technique.

# Sample	Reference method (blood culture) <sup>a</sup>	S3 <sup>b</sup>
1	+	+
2	+	+
3	+	+
4	+	+
5	+	+
6	+	+
7	+	+
8	+	+
9	+	+
10	+	+
11	+	+
12	+	+
13	+	+
14	+	+
15	+	+
16	+	+
17	+	+
18	+	+
19	- <sup>c</sup>	-
20	-	-
21	-	-
22	-	-
23	-	-
24	-	-
25	-	-

<sup>a</sup>) Positive (+) means that any *S. aureus* colony was isolated from blood samples.

<sup>b</sup>) Positive (+) means that the fluorescence intensity at 575 nm ( $\lambda_{exc} = 555$  nm) was equal or higher than 3-fold the standard deviation of three negative controls.

<sup>c</sup>) Negative for *S. aureus* but positive for *S. lugdunensis*.

## 4.5 Conclusion

Herein, we demonstrate that nanoporous materials and a suitable aptamer can be combined to obtain a sensitive, robust and competitive fluorogenic sensor for *S. aureus* detection in clinical blood samples. The probe consists of

an NAA scaffold previously charged with the fluorescent dye rhodamine B and blocked with a selective aptamer for *S. aureus*. The presence of the bacteria results in the migration of capping aptamer, pore opening and release of the fluorophore. The probe shows a limit of detection of 2 CFU mL<sup>-1</sup> in PBS buffer and 5 CFU mL<sup>-1</sup> in blood media, which are equivalent to other *S. aureus* state-of-the-art reported detection systems. Moreover, the probe demonstrates a high selectivity to *S. aureus* and does not respond to the presence of other *Staphylococcus* species. Using this simple method, the probe is applied to the identification of *S. aureus* in clinical samples with very good results in terms of sensitivity and predictive values. The proposed method is simple, fast, and portable, and it can be easily modified by using different reporters and capping sequences. It also may inspire the development of new simple tests that offer a great potential for point-of-care pathogen testing.

## 4.6 Acknowledgements

This study was supported by the Spanish Government (projects RTI2018-100910-B-C41 and SAF2017-82251-R (MCUI/AEI/FEDER, UE)), the Generalitat Valenciana (project PROMETEO/2018/024), the Universitat Politècnica de València–Instituto de Investigación Sanitaria La Fe (B02-MIRSA project), CIBER-BBN (NANOPATH and valorization project CANDI-EYE) and co-financed by the EU through the Valencian Community ERDF PO 2014-2020. S.S. thanks the Instituto de Salud Carlos III and the European Social Fund for the financial support “Sara Borrell” (CD16/000237). L.P. thanks to Ministerio de Economía, Industria y Competitividad for his FPI grant. The authors are grateful for the professional English language editing to Mr. Arash Javadinejad, English Instructor and publication Editor at the Instituto de Investigación Sanitaria La Fe, Valencia, Spain.

### Declaration of competing interest

The authors declare that they have no known competing financial interests or personal relationships that could have appeared to influence the work reported in this paper.

### **CRedit authorship contribution statement**

Luis Pla: Investigation; Methodology; Writing - original draft, Sara Santiago-Felipe: Investigation; Methodology; Writing - original draft, María Ángeles Tormo-Más: Investigation; Funding acquisition, Writing - review & editing , Javier Pemán: Investigation; Writing - review & editing, Félix Sancenón: Investigation; Supervision, Elena Aznar: Conceptualization; Funding acquisition, Writing - review & editing, Ramón Martínez-Máñez: Conceptualization, Funding acquisition, Writing - review & editing

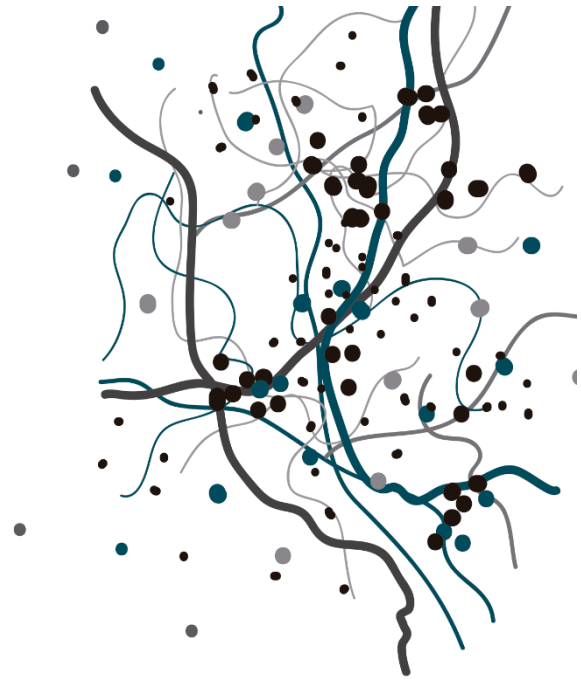
### **References**

- [1] Lai, H. Z., Wang, S. G., Wu, C. Y., Chen, Y. C., 2015. *Anal Chem.* 87, 2114-2120.
- [2] Cheng, J. C., Huang, C. L., Lin, C. C., Chen, C. C., Chang, Y. C., Chang, S. S., Tseng, C. P., 2006. *Clin. Chem.* 52, 1997-2004.
- [3] Moore, D. F., Curry, J. I., 1998. *J. Clin. Microbiol.* 36, 1028-1031.
- [4] Edman, C. F., Mehta, P., Press, R., Spargo, C. A., Walker, G. T., Nerenberg, M., 2000. *J. Invest. Med.* 48, 93-101.
- [5] Chang, T. C., Huang, S. H., 1994. *J. Food Protect.* 57, 184-189.
- [6] Vigneshvar, S., Sudhakumari, C. C., Senthilkumaran, B., Prakash, H., 2016 *Front. Bioeng. Biotechnol.* 4, 11-20.
- [7] Girigoswami, K., Akhtar, N., 2019. *Int. J. Nano. Dimens.* 10, 1-17.
- [8] Abbaspour, A., Norouz-Sarvestani, F., Noori, A., Soltani, N., 2015. *Biosens. Bioelectron.* 68, 149-155.
- [9] Wang, J., Wu, X., Wang, C., Shao, N., Dong, P., Xiao, R., Wang, S., 2015. *ACS Appl. Mater. Interfaces* 7, 20919-20929.
- [10] Felix, F.S., Angnes, L., 2018. *Biosens. Bioelectron.* 102, 470-478.
- [11] Lippa, P. B., Sokoll, L. J., Chan, D. W., 2001. *Clin Chim Acta* 314, 1-26.
- [12] Lim, Y. C., Kouzani, A. Z., Duan, W., 2010. *J. Biomed. Nanotech.* 6, 93-105.
- [13] Feng, C., Dai, S., Wang, L., 2014. *Biosens. Bioelectron.* 59, 64-74.
- [14] O'Sullivan, C. K., 2002. *Anal. Bioanal. Chem.* 72, 44-48.



- [15] Leca-Bouvier, B., Blum, L. J., 2005. *Anal. Lett.* 38, 1491-1517.
- [16] Kim, Y. S., Gu, M. B., 2013. *Biosensors Based on Aptamers and Enzymes*, Springer, Berlin, Heidelberg.
- [17] Aznar, E., Oroval, M., Pascual, L., Murguía, J. R., Martínez-Máñez, R., Sancenón, F., 2016. *Chem. Rev.* 116, 561-718.
- [18] Sancenón, F., Pascual, L., Oroval, M., Aznar, E., Martínez-Máñez, R., 2015. *ChemistryOpen* 4, 418-437.
- [19] Zelada-Guillén, G. A., Sebastián-Avila, J. L., Blondeau, P., Riu, J., Rius, F. X., 2012. *Biosens. Bioelectron.* 31, 226-232.
- [20] Castillo, R. R., Baeza, A., Vallet-Regí, M., 2017. *Biomater. Sci.* 5, 353-377.
- [21] Kurt, H., Yüce, M., Hussain, B., Budak, H., 2016. *Biosens. Bioelectron.* 81, 280-286.
- [22] Lai, H. Z., Wang, S. G., Wu, C. Y., Chen, Y. C., 2015. *Anal. Chem.* 87, 2114-2120.
- [23] Chang, Y. C., Yang, C. Y., Sun, R. L., Cheng, Y. F., Kao, W. C., Yang, P. C., 2013. *Sci. Rep.* 3, 1863-1870.
- [24] Borsa, B. A., Tuna, B. G., Hernandez, F. J., Hernandez, L. I., Bayramoglu, G., Arica, M. Y., Ozalp, V. C., 2016. *Biosens. Bioelectron.* 86, 27-32.
- [25] Otri, I., El Sayed, S., Medaglia, S., Martínez-Máñez, R., Aznar, E., Sancenón, F., 2019. *Chem. Eur. J.* 25, 3770-3774.
- [26] Pascual, L., Baroja, I., Aznar, E., Sancenón, F., Marcos, M. D., Murguía, J.R., Amorós, P., Rurack, K., Martínez-Máñez, R., 2015. *Chem. Commun.*, 51, 1414-1416.
- [27] Ribes, À., Santiago-Felipe, S., Bernardos, A., Marcos, M.D., Pardo, T., Sancenón, F., Martínez-Máñez, R., Aznar, E., 2017. *ChemistryOpen* 6, 653-659.
- [28] Chen, Y., Santos, A., Wang, Y., Kumeria, T., Li, J., Wang, C., Losic, D., 2015. *ACS Appl. Mater. Interfaces* 7, 19816-19824.
- [29] Losic, D., Santos, A., 2015. *Nanoporous Alumina: Fabrication, Structure, Properties and Applications*, Springer Series in Materials Science, Springer International Publishing Switzerland.

- [30] De la Escosura-Muniz, A., Merkoci, A., 2012. *Acs Nano* 6, 7556-7583.
- [31] Baranowska, M., Slota, A. J., Eravuchira, P. J., Macias, G., Xifré-Pérez, E., Pallares, J., Ferré-Borrull, J., Marsal, L. F., 2014. *Colloids Surf., B.* 122, 375-383.
- [32] Ribes, A., Xifré-Pérez, E., Aznar, E., Sancenón, F., Pardo, T., Marsal, L. F., Martínez-Máñez, R., 2016. *Sci. Rep.* 6, 38649.
- [33] Pla, L., Xifré-Pérez, E., Ribes, A., Aznar, E., Marcos, M. D., Marsal, L. F., Martínez-Máñez, R., Sancenón, F., 2017. *ChemPlusChem* 82, 337-341.
- [34] Ribes, À., Aznar, E., Santiago-Felipe, S., Xifré-Pérez, E., Tormo-Mas, M. A., Pemán, J., Marsal, L. F., Martínez-Máñez, R., 2019. *ACS Sensors* 5, 1291-1298.
- [35] Kreiswirth, B. N., Löfdahl, S., Betley, M. J., O'reilly, M., Schlievert, P. M., Bergdoll, M. S., Novick, R. P., 1983. *Nature*, 305, 709-712.
- [36] Laboratory collection of diverse species of *Staphylococcus* obtained under the approval of the Ethic Committee of Hospital Universitario y Politécnico La Fe (2017/0523) for project SAF2017-82251-R.
- [37] Christensen, G. D., Simpson, W. A., Bisno, A. L., Beachey, E. H., 1982. *Infect Immun.* 37, 318-326.
- [38] Wagner, E., Doskar, J., Götz, F., 1998. *Microbiology* 144, 509-517.
- [39] Tormo, M. A., Knecht, E., Götz, F., Lasa, I., Penades, J. R., 2005. *Microbiology* 151, 2465-2475.
- [40] Oliveira, K., Procop, G. W., Wilson, D., Coull, J., Stender, H., 2002. *J. Clin. Microbiol.*, 40, 247-251.
- [41] Song, Z., Liu, X., Zhu, M., Tan, Y., Wu, K., 2017. *Mol. Vis.* 23, 407-415.
- [42] Marlowe, E. M., Bankowski, M. J., 2011. *J. Clin. Microbiol.* 49, S53-S59.
- [43] Huang, S. H., Chang, T. C., 2004. *Clin. Chem.* 50, 1673-1674.
- [44] Burghardt, E. L., Flenker, K. S., Clark, K. C., Miguel, J., Ince, D., Winokur, P., McNamara, J. O., 2016. *PLoS one* 11, e0157234.



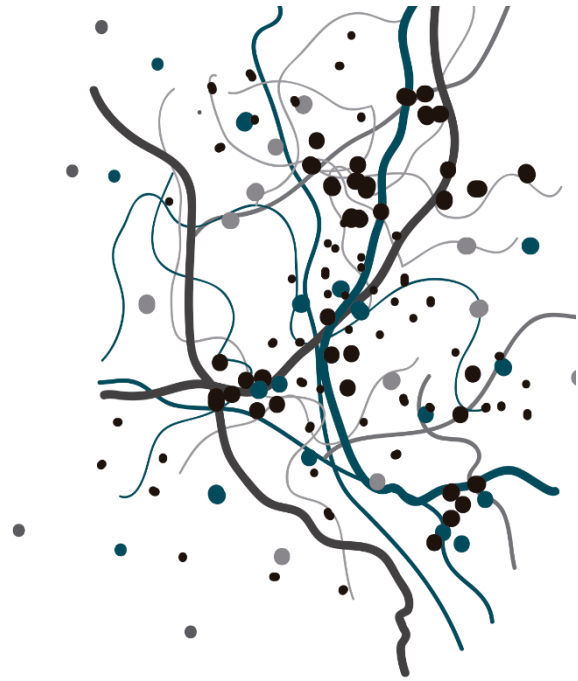
# 5

Design of  
Oligonucleotide-capped  
Nanoporous Anodic Alumina  
Biosensor for the  
Rapid Detection of  
*Candida Auris* Infection



PATENT  
PROTECTION  
IN PROGRESS





# 6

Triplex Hybridization-based  
Nanosystem for the  
Rapid Screening of  
*Pneumocystis Pneumonia*  
in Clinical Samples





# Triplex Hybridization-based Nanosystem for the Rapid Screening of *Pneumocystis Pneumonia* in Clinical Samples

Luis Pla<sup>1,2,3</sup>, Anna Aviñó<sup>3,4</sup>, Ramón Eritja<sup>3,4</sup>, Alba Ruiz-Gaitán<sup>5</sup>, Javier Pemán<sup>5</sup>, Vicente Friaza<sup>6</sup>, Enrique J. Calderón<sup>6,7</sup>, Elena Aznar<sup>\*1,2,3,8</sup>, Ramón Martínez-Máñez<sup>\*1,2,3,8</sup> and Sara Santiago-Felipe<sup>1,2,3</sup>

<sup>1</sup> Instituto Interuniversitario de Investigación de Reconocimiento Molecular y Desarrollo Tecnológico, Universitat Politècnica de València, Universitat de València, Camino de Vera s/n, 46022, Valencia, Spain.

<sup>2</sup> Unidad Mixta de Investigación en Nanomedicina y Sensores. Universitat Politècnica de València, Instituto de Investigación Sanitaria La Fe, Valencia, Spain.

<sup>3</sup> CIBER de Bioingeniería, Biomateriales y Nanomedicina (CIBER-BBN).

<sup>4</sup> Institute for Advanced Chemistry of Catalonia (IQAC), CSIC, Jordi Girona 18-26, 08034, Barcelona, Spain.

<sup>5</sup> Grupo Acreditado de Infección Grave. Instituto de Investigación Sanitaria La Fe and Hospital Universitari i Politècnic La Fe, Avenida Fernando Abril Martorell, 46026, Valencia, Spain.

<sup>6</sup> Instituto de Biomedicina de Sevilla, Hospital Universitario Virgen del Rocío/Consejo Superior de Investigaciones Científicas/Universidad de Sevilla.

<sup>7</sup> Centro de Investigación Biomédica en Red de Epidemiología y Salud Pública (CIBERESP).

<sup>8</sup> Unidad Mixta UPV-CIPF de Investigación en Mecanismos de Enfermedades y Nanomedicina. Universitat Politècnica de València, Centro de Investigación Príncipe Felipe, Valencia, Spain.

\* Correspondence: Elena Aznar - [elazqi@upvnet.upv.es](mailto:elazqi@upvnet.upv.es)

R. Martínez-Máñez: [rmaez@qim.upv.es](mailto:rmaez@qim.upv.es)

***Journal of Fungi. 2020, 6, 292***



## 6.1 Abstract

*Pneumocystis pneumonia* (PcP) is a disease produced by the opportunistic infection of the fungus *Pneumocystis jirovecii*. As delayed or unsuitable treatments increase the risk of mortality, the development of rapid and accurate diagnostic tools for PcP are of great importance. Unfortunately, current standard methods present severe limitations and are far from adequate. In this work, a time-competitive, sensitive and selective biosensor based on DNA-gated nanomaterials for the identification of *P. jirovecii* is presented. The biosensor consists of a nanoporous anodic alumina (NAA) scaffold which pores are filled with a dye reporter and capped with specific DNA oligonucleotides. In the presence of *P. jirovecii* genomic DNA, the gated biosensor is unlocked, and the cargo is delivered to the solution where it is monitored through fluorescence spectroscopy. The use of capping oligonucleotides able to form duplex or triplex with *P. jirovecii* DNA is studied. The final diagnostic tool shows a limit of detection (LOD) of 1 nM for *P. jirovecii* genomic DNA and does not require previous amplification steps. The method was applied to identify DNA from *P. jirovecii* in unmodified bronchoalveolar lavage, nasopharyngeal aspirates and sputum samples in 60 minutes. This is a promising alternative method for the routinely diagnosis of *Pneumocystis pneumonia*.

**Keywords:** nanoporous anodic alumina, *Pneumocystis jirovecii*, molecular gates, oligonucleotidesdied.

## KEYWORDS

Nanoporous anodic alumina, DNA, molecular gates, *Pneumocystis jirovecii*, biosensor, triplex

## 6.2 Introduction

*Pneumocystis jirovecii* is an opportunistic fungus that can cause asymptomatic or mild infection in healthy people and fulminating pneumonia in immunocompromised individuals [1]. *Pneumocystis* spp. can affect many species of mammals (rodent, horses and primates) and presents strong specificity for host species. The fungus was identified as a human pathogen in

the 1940s when it was detected in the lungs of children affected with interstitial pneumonia of plasmatic cells [2]. Usually, in humans, the pathogen is disseminated from person to person producing asymptomatic or subclinical infection, however, when it is transmitted to an immunocompromised host, a severe pneumonia can take place (*Pneumocystis* pneumonia, PcP) [3]. In the 1980s, the high incidence of acquired immunodeficiency syndrome (AIDS) led to a markedly interest in PcP due to the high incidence in those patients. Nowadays, the widespread use of immunosuppressive treatments such as corticosteroid therapies, chemotherapies or biological therapies, has increased the incidence of *P. jirovecii* infections. In addition, recent studies have provided evidence of transplacental transmission in humans and established a relation between *P. jirovecii* colonization in preterm infants and neonatal Respiratory Distress Syndrome risk [4–5].

In the last decade, several published works have allowed a high progress in the knowledge of the *Pneumocystis* pathobiology, however, morbidity and mortality due to PcP still remains high, especially in developing countries. One of the main challenges in the diagnosis of PcP is the absence of a specific clinical manifestation, which difficult diagnosis and makes it stand on non-specific symptoms [6]. Therefore, a proper diagnosis of *Pneumocystis* pneumonia involves correct recognition of the fungus. Unfortunately, the current standard methods for *P. jirovecii* detection are far from adequate and, further aggravated by the impossibility to keep continuous fungus *ex vivo* axenic culture [7].

Classical methodologies for the identification of *P. jirovecii* comprise microscopic observation of stained biological samples that reveal the characteristic morphology of *Pneumocystis* cystic and/or trophic forms. These techniques provide sensitivity and specificity values between 60-75% and 80-90%, respectively, however, they remain time-consuming and require high experienced staff and specific equipment [8–10]. Some alternatives for PcP diagnosis involve the detection of blood biomarkers that indicate the host-pathogen interaction, including (bio)molecules such as (1,3)- $\beta$ -d-glucan (BG), lactate dehydrogenase (LDH), Krebs von den Lungen-6 antigen (KL-6) and adenosylmethionine (SAM) [10]. Nonetheless, despite their good sensitivity (70-95%), the detected metabolites are not strictly specific to *P. jirovecii*

infection, which significantly reduces the specificity values (50-70%) [10]. On the other hand, serological methods detect the antibodies produced by the patient as consequence of the presence of the fungus, but despite their greater selectivity, they are expensive, require long-time procedures and there is still a need to better characterize the immune response to obtain better standardized protocols [9,11,12].

Among molecular techniques, PCR assays have revealed to be highly efficient, allowing even the early detection of the fungus in samples from patients that were confirmed negative by microscopic examination [8]. During the last 15 years, numerous PCR techniques for the detection of genomic DNA from *P. jirovecii* have been reported, obtaining sensitivity and specificity values close to 90-100%. The most remarkable studies employ both conventional PCR and its variants nested-PCR, and real time PCR, and they are applied to recognize target gene such as the mitochondrial large subunit RNA (mtLSUrRNA), the internally transcribed spacer (ITS) or 18S or 5S ribosomal RNA (18S rRNA or 5S rRNA) [8]. However, despite its great potential, it must be bearing in mind that PCR is not exempt from limitations such us high susceptibility to polymerase inhibitors or cross contamination [13].

In the last decades, new diagnostic platforms based upon nanotechnology have become a reality thanks to their ability to provide sensitive, accurate and rapid results. For instance, nanotechnology has burst into *Pneumocystis* diagnosis by developing serological biosensors that uses gold nanoparticles (AuNPs) to detect anti-*P. jirovecii* antibodies by a colorimetric assay in a lateral flow immunoassay [14,15]. Nevertheless, the development of nanosensors for PcP detection is still an incipient area. However, this is a stimulating field of research and recent advances have demonstrated that the design of new hybrid organic-inorganic systems in a single entity can benefit from both, the potential of nanomaterials and the recognition, selectivity and sensitivity properties of biomolecules. On that regard, several hybrid systems have been extensively applied in sensing and drug delivery applications [16–23].

Among the great variety of nanomaterials available, nanoporous anodic alumina (NAA) has been widely used because of its biocompatibility, high surface area, high loading capacity and easy modification of the surface.

Moreover, NAA supports can be easily prepared by cost-competitive and well-known production techniques [24]. NAA have additionally been used to develop capped stimuli-responsive systems, in which the mesoporous support is loaded with a cargo and capped with a biomolecule, so that only target molecules are able to induce cargo release. In NAA, oligonucleotides as capping systems have recently been demonstrated to be excellent candidates to detect and quantify a range of molecules and biomolecules [24-25]. Some of these tools rely on the use of DNA as caps and base their recognition mechanism on duplex hybridization interactions (DNA-DNA or DNA-RNA) between the probe and the target. Nevertheless, innovative triple-helix hybridization formats based on Hoogsteen and reverse-Hoogsteen base pairs to the Watson-Crick duplex are also interesting approaches that have demonstrated increased recognition efficiency.

Triplex formation is observed at certain polypurine-polypyrimidine sequences that are widely found in the human genome, particularly at promoter regions [26-29]. Several published studies have described the triplex-stabilizing features of 8-aminopurines and the use of parallel and antiparallel tail-clamps to improve the efficacy of triplex recognition with complementary RNA and DNA targets [30, 31]. On that regard, this triplex hybridization has been effectively applied to develop biosensors. For example, Carrascosa *et al.* and Aviñó *et al.* developed a sensitive and label-free method for the detection of an mRNA from *Listeria* and miRNA-145 by the formation of triplex hybridization structures in SPR biosensors [32]. More recently, Wei *et al.* have reported a method that combines the formation of triplex DNA structures with further amplification reactions for the sensitive detection of microRNAs [33] and some of us have developed an oligonucleotide-gated mesoporous support for the identification of miRNA-145 based on the formation of triple-helix structure, allowing a sensitivity as low as 2.5 pM and accurate qualitative determination in human serum samples [34].

Based on the above, we report herein two probes for the specific identification of *Pneumocystis jirovecii* using gated nanomaterials. The diagnostic tool is based in NAA, whose pores are loaded with the fluorophore rhodamine B and blocked with different oligonucleotide probes (single or hairpin strands) able to form duplex or triplex structures with the target gene of

mtLSUrRNA of *P. jirovecii* DNA. Best analytical performances are obtained for the triplex hybridization with a LOD of 1 nM in less than one hour without previous DNA amplification. Likewise, this method detects *P. jirovecii* DNA in unmodified sputum, nasopharyngeal aspirates (NPA) and bronchoalveolar lavage (BAL) samples, showing its great potential in point-of-care applications.

## 6.3 Experimental section

### 6.3.1 General techniques

A ZEISS Ultra 55 microscope was employed to perform Field Emission Scanning Electron Microscopy (FSEM) and Energy Dispersive X-ray spectroscopy (EDX) analyses. Fluorescence spectroscopy measurements were carried out on a Synergy H1 microplate reader (BioTek, Winooski, VT, USA).

### 6.3.2 Chemicals

Tris(hydroxymethyl)aminomethane (TRIS), hydrochloric acid, (3-aminopropyl)triethoxysilane (APTES) and rhodamine B, were obtained from Sigma-Aldrich Quimica (Madrid, Spain). NAA scaffolds were purchased from InRedox (CO, USA).

### 6.3.3 Synthesis of oligonucleotides

In this study it was used the gene encoding the mitochondrial large-subunit of *Pneumocystis jirovecii* (mt LSU rRNA). Design of oligonucleotides and in silico analysis is described in the Electronic Supplementary Information (Scheme 1, ESI). Table 1 shows the sequences of the oligonucleotides employed in this study. The synthesis took place by the well-defined phosphoramidite solid phase protocol [36]. For that, oligonucleotides were assembled on controlled pore glass (CPG) scaffolds by consecutive incorporation of the suitable phosphoramidites employing an automated Applied Biosystems 394 DNA synthesizer (CA, USA). Then, the scaffolds were treated overnight with concentrated ammonia at 55 °C. Finally, synthesized oligonucleotides were purified by Glen-Pack™ DNA cartridges (Glen Research, USA) and mass spectrometry was used to analyze them (Table S1, ESI).

**Table 1.** Sequences of the used oligonucleotides.

	<b>Oligonucleotide</b>	<b>Sequence (5'-3')</b>
<b>O1</b>	Duplex antiparallel	5'-GAAGGGAAACAGCCCAG-3'
<b>O2</b>	Clamp antiparallel	5'-GACAAAGGGAAAAG-TTTT- GAAAGGGAAACAGCCCAG-3'
<b>O3</b>	Control clamp antiparallel	5'-AGAGCAGAAAGGA-TTTT- GAAAGGGAAACAGCCCAG-3'
<b>O4</b>	Target complementary	5'-CTGGGCTGTTTCCCTTTC-5'

### 6.3.4 Synthesis of nanomaterials **S0**, **S1 (clamp)**, **S2 (duplex)** and **S3 (control)**

For the synthesis of **S0**, 10 individual NAA scaffolds (2 mm of diameter each one) were submerged in a solution of rhodamine B in CH<sub>3</sub>CN (1 mM, 8 mL). The mixture was stirred at room temperature for 24 h. Then the functionalization of the surface with aminopropyl moieties was carried out by adding 40  $\mu$ L per individual NAA scaffold of (3-aminopropyl)triethoxysilane (1.25  $\mu$ M) and stirring the mixture at room temperature for 6 h. For the synthesis of the sensing probes **S1**, **S2** and **S3**, different pieces of solid **S0** were capped by adding to each support 10  $\mu$ L of the corresponding oligonucleotide (**O1**, **O2** or **O3**, respectively) (100  $\mu$ M) in a final volume of 250  $\mu$ L of hybridization buffer (20 mM Tris-HCl, 37.5 mM MgCl<sub>2</sub>, pH 7.5). The mixtures were shaken for 60 min at 37 °C. The capped materials were rinsed with hybridization buffer to remove the unbounded oligonucleotide.

### 6.3.5 Release kinetics

The response of the gated materials was determined by measuring the fluorescence of the dye released from the pores to the solution in the presence of the target complementary DNA. In a common experiment, two independent supports of each material **S1**, **S2** and **S3** were immersed in 900  $\mu$ L of hybridization buffer. Then, 100  $\mu$ L of the complementary DNA (10  $\mu$ M) was added to one of the supports while 100  $\mu$ L of hybridization buffer was added to the other. Both solutions were stirred at 37 °C and aliquots were taken at scheduled times. Finally, dye delivery was determined by registering the fluorescence of the rhodamine B in the solution at 575 nm ( $\lambda_{exc}$  = 555 nm).



### 6.3.6 Real Media Experiments

The response of **S2** was assessed in a more realistic context. For that, 500  $\mu\text{L}$  of sputum, bronchoalveolar lavage (BAL) and nasopharyngeal aspirate (NPA) samples were artificially inoculated with 100  $\mu\text{L}$  of DNA from *P. jirovecii* (10  $\mu\text{M}$ ) and added to two independent **S2** supports in a final volume of 1 mL in hybridization buffer. Solutions were maintained at 37 °C and rhodamine B released from the pores was measured at 575 nm ( $\lambda_{\text{exc}} = 555$  nm) after 60 min.

### 6.3.7 Response to different target concentrations

The response of the material **S2** to different concentrations of the target DNA was assessed. For that, six independent supports were submerged separately in 900  $\mu\text{L}$  of hybridization buffer and 100  $\mu\text{L}$  of 10-fold diluted target solutions were added to each one, reaching final concentrations from  $10^{-5}$  to 1  $\mu\text{M}$ . After 60 min at 37 °C, the released rhodamine B from the porous was measured at 575 nm ( $\lambda_{\text{exc}} 555$  nm).

### 6.3.8 Selectivity to possible interferents

The selectivity of the method was determined for **S2** by carrying out cargo delivery experiments in the presence of 100  $\mu\text{L}$  of DNA (10 ng/ $\mu\text{L}$ ) from other microorganisms (*Aspergillus spp.*, *Candida albicans*, *Candida tropicalis*, *Candida auris*, *Schizosaccharomyces pompe* and two samples of *Taphrina deformans*) in a final reaction volume of 1 mL of hybridization buffer. In the same experiment, 100  $\mu\text{L}$  of complementary DNA from *P. jirovecci* at 10 ng/ $\mu\text{L}$  was used as a positive control and 100  $\mu\text{L}$  of hybridization buffer as a negative control. Mixtures were maintained in agitation for 60 min at 37 °C and the delivered rhodamine B was determined by measuring the fluorescence in the solution ( $\lambda_{\text{exc}}=555$  nm,  $\lambda_{\text{em}} = 585$  nm).

### 6.3.9 Validation of the method in clinical real samples

In order to determine the clinical applicability of the gated nanosensor, the performance of **S2** was evaluated in a more realistic media. First, the system was used to analyze 8 sputa and 4 bronchoalveolar lavages (BAL) from infected and non-infected patients from the Hospital Universitario i Politècnic La Fe. In another experiment, 21 nasopharyngeal aspirates (NPA) from colonized and non-colonized newborn infants from the Hospital Universitario Virgen del Rocío

were analyzed using **S2** nanomaterials. For both assays, 250  $\mu\text{L}$  of each sample were added to individual **S2** solids in a final volume of 400  $\mu\text{L}$  of hybridization buffer. After 60 minutes at 37  $^{\circ}\text{C}$ , dye released from the pores to the solution was measured by fluorescence spectroscopy at 575 nm ( $\lambda_{\text{exc}}$  555 nm).

## 6.4 Results and discussion

### 6.4.1 Synthesis and characterization of the biosensors

NAA scaffolds were selected as inorganic supports to develop the capped nanomaterials. First, pores were filled with the dye rhodamine B which has demonstrated excellent properties for the preparation of optical gated nanosensors applied to the detection of different analytes.<sup>18,27</sup> In a second step, the outer surface of the NAA support was functionalized with the linker (3-aminopropyl)triethoxysilane, yielding **S0**. At a neutral pH, aminopropyl moieties are partially protonated (and therefore positively charged) being able to electrostatically interact with negatively charged oligonucleotides. Based on this, the interaction of oligonucleotides **O1**, **O2** or **O3** with the amino-functionalised **S0**, yielded the gated sensing solids **S1**, **S2** and **S3**. **O1** consists of a single strand oligonucleotide that hybridizes with the DNA sequence forming a duplex structure, **O2** is a clamp that forms a triplex hybridization structure, whereas **O3** is also a clamp but results in a duplex conformation.

The recognition and detection mechanism of the loaded and capped **S1**, **S2** and **S3** materials takes place as follows. In the absence of target analyte, the oligonucleotides **O1**, **O2** or **O3**, electrostatically attached to the external surface of the inorganic scaffold, were expected to be bulky enough to block pores and to inhibit dye delivery. On the contrary, due to the higher affinity of the oligonucleotide probes for the target than for the aminopropyl moieties, it was expected that in the presence of the analyte, the capping oligonucleotides were selectively displaced from the surface resulting in DNA target-probe hybridization, pore opening and dye diffusion from the pores to the aqueous solution. Finally, the used solids were calcined to remove organic matter, allowing supports to be used again (Fig. 1).

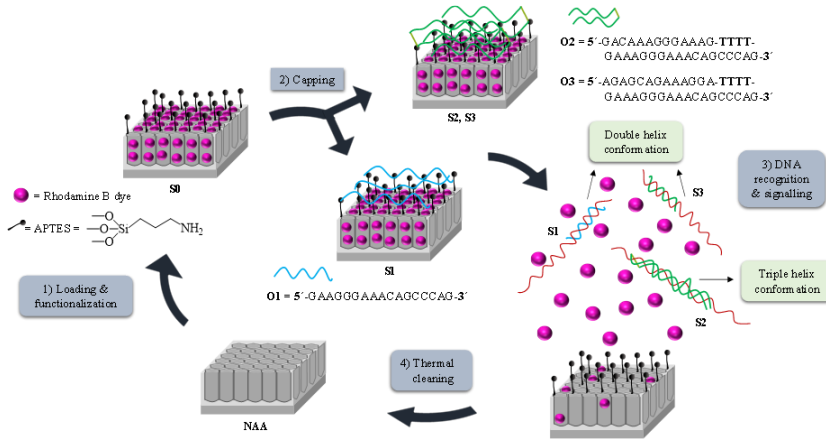


**Figure 1.** Representation of the preparation and sensing process: 1) Loading and functionalization of the NAA support; 2) Capping with the oligonucleotides **O1**, **O2** or **O3**, to obtain solids **S1**, **S2** and **S3**, respectively; 3) Release of the cargo in the presence of *P. jirovecii* genomic DNA by forming (A) duplex structures when using solids **S1** or **S3** or (B) triplex hybridization structures when using **S2** and 4) Calcination prior to the reutilization of the scaffold.

The starting NAA supports were commercially obtained from InRedox® (CO, USA). The supports are anodic aluminum oxide (AAO) films grown on a 0.1 mm thick aluminum layer with a pore density of  $9 \cdot 10^{11} \text{ cm}^{-2}$ . Pore entrance has a funnel-like form which gradually decreases from a larger size (20–30 nm) at the top of the funnel to a 5 nm size at the end. Pores have a profundity of ca. 10  $\mu\text{m}$ . The starting NAA scaffold and **S1**, **S2** and **S3** were characterized following standard techniques such as FESEM and EDX analysis. FESEM images of the starting NAA scaffolds confirmed the expected non-ordered porous structure, whereas typical images of **S1**, **S2** and **S3** showed the presence of an organic layer attributed to the capping oligonucleotides (Fig. 2). Furthermore, in **S1**, **S2** and **S3**, the porous structure of the NAA scaffolds can still be seen in some places where the surface was not completely covered, demonstrating that the loading, functionalization and capping steps did not modify the NAA structure. This behavior agrees with that observed in previous studies carried out with the same or similar materials [35,36,37].

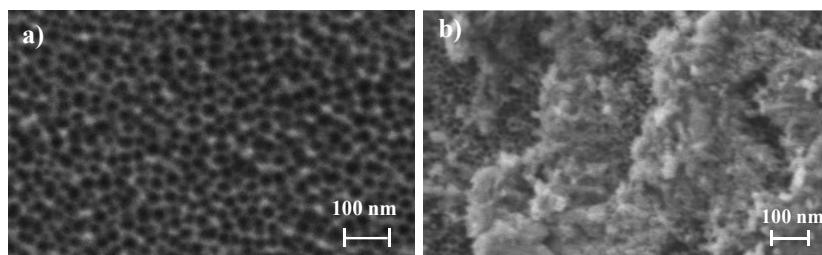


**Figure 2.** Representation of the preparation and sensing process: **a)** Loading and functionalization of the NAA support; **b)** Capping with the oligonucleotides.

The organic content of the different prepared materials (**S0**, **S1**, **S2** and **S3**) was studied by energy dispersive X-ray spectroscopy (EDX) (Table 2). After dye loading and surface functionalization with aminopropyl moieties, solid **S0** shows a high C/AI content, which was reduced in **S1**, **S2** and **S3** due to the partial rhodamine B release that takes place during the gating process. Moreover, the existence of nitrogen in all final solids is indicative of the presence of aminopropyl groups and oligonucleotides. The occurrence of the latter is also confirmed by the presence of phosphorous atoms.

**Table 2.** Atomic elements ratio in the different prepared solids by EDX studies.

	C/AI	N/AI	P/AI
<b>S0</b>	1.52	0.38	-
<b>S1</b>	0.76	0.40	0.01
<b>S2</b>	0.58	0.53	0.02
<b>S3</b>	0.74	0.42	0.02

#### 6.4.2 Delivery kinetics

In a first step, the response of the nanoprobe **S1**, **S2** and **S3** to the presence of the target sequence **O4** was studied. In a typical experiment, two individual solids of each material **S1-S3** were submerged in hybridization buffer. Then, 100  $\mu\text{L}$  of the complementary oligonucleotide sequence (**O4**, 1  $\text{ng } \mu\text{L}^{-1}$ ) were transferred to one of the supports while 100  $\mu\text{L}$  of buffer were added to the other. Mixtures were stirred at 37  $^{\circ}\text{C}$  and at predetermined times (i.e. 15, 30, 45 and 60 min) the fluorescence of the solution was measured to quantify the amount of the dye delivered from the pores to the aqueous phase. As an

example, Fig. 3 shows the delivery profile for solid **S2**. When the target sequence **O4** was present, a remarkable dye delivery from the pores to the solution was observed as a result of the oligonucleotide-DNA hybridization to form a DNA triplex structure (curve b), pore opening and dye release. The maximum dye diffusion from the pores to the solution was reached at 60 min and that was considered the 100% of dye delivery. On the contrary, in the lack of the **O4** sequence, a very low dye is released, what indicates tight pore blockage by the probes electrostatically attached to the scaffold surface (curve a).

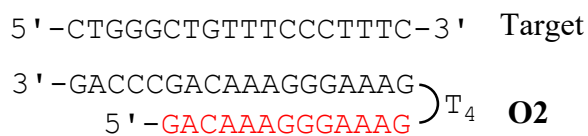
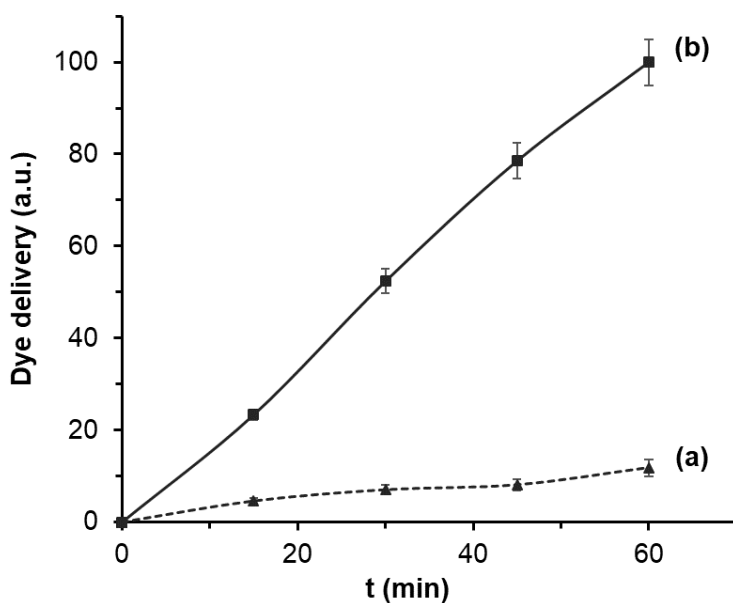


**Figure 3.** Rhodamine B delivery from **S2** (a) in the absence and (b) in the presence of 1 nM of complementary **O4** target sequence in a solution of hybridization buffer (20 mM Tris-HCl, 37.5 mM MgCl<sub>2</sub>, pH 7.5).

Similar delivery profiles were observed for solids **S1** and **S3**, also indicating adequate performance for these solids in the stages of DNA recognition and

dye release (Fig. S1, ESI). In terms of blockage ability, all three developed systems were able to keep the pore entrances closed regardless the capping oligonucleotide was a clamp (**S2** and **S3**) or a single strand, obtaining in all cases a very low residual dye delivery (lower than 20 %) in the absence of **O4** target sequence.

All three nanodevices were also able to deliver the cargo in the presence of target sequence **O4**. However, differences in terms of the amount of dye delivered were observed when comparing the formation of triplex (**S2**) and duplex hybridization (**S1** and **S3**) structures. The obtained results showed that nanomaterial **S2** provided a faster response and the highest cargo release, reaching a first order constant rate of the release kinetics of 1.70 and an amount of ca. 2.8 ng of delivered Rhodamine B. On the other hand, for **S1** and **S3** materials, the uncapping mechanism and subsequent dye release was slower (constant rates of 1.16 and 1.14, respectively), and the amount of dye delivered at 60 min was lower (by ca. 20%). This is tentatively attributed to a more stable, favorable and rapid formation of the triplex structure than those obtained by the duplex conformations (**S1** and **S3**). These results agree with others found in the literature in which the efficiency and stability of triplex hybridization structures were higher than those obtained by duplex conformations [33, 34] Therefore, further studies were carried out using **S2** as sensing material.

#### **6.4.3 Analytical performance: sensitivity and specificity studies**

New diagnostic tools should be evaluated in term of limit of detection (LOD) and specificity. The LOD in **S2** was determined via the study of the response of the gated material to the presence of different amounts of target sequence **O4**. Based on the proposed sensing mechanism, the higher the concentration of the target DNA, the greater the number of capping oligonucleotides that will be displaced from the surface, and therefore more pores will be uncapped, and greater amount of dye will be delivered. Results showed that the amount of dye delivered was directly proportional to the target DNA concentration, which agrees with the uncapping protocol detailed above. A LOD of  $1 \pm 0.1$  nM was calculated based on the intersection point of the two slopes of the represented curve (Figure 4A). This LOD value is in the range of other reported protocols for the detection of *P. jirovecii* genomic DNA. Thus, for instance, several works

based on the diagnosis of PcP by real time PCR reported LODs of 50-200 copies/ $\mu\text{L}$ , which corresponds to a DNA concentration range from ca. 250 pM to 1 nM. However, our system is faster, simpler, and requires no especial equipment or trained personnel [38–42].

The specificity of the system was evaluated by assessing the response of **S2** to the presence of genomic DNA from other fungi considered as possible interferents, such as *Aspergillus spp.*, *Candida albicans*, *Candida tropicalis*, *Candida auris*, *Schizosaccharomyces pompe*, *Taphrina deformans sample CR20* and *Taphrina deformans sample CR34*. For that, the amount of dye delivered from the pores of seven independent **S2** supports was measured in the presence of 100  $\mu\text{L}$  of DNA at 10 ng/ $\mu\text{L}$  of each possible interferent. Also, 100  $\mu\text{L}$  of DNA from target **O4** at 10 ng/ $\mu\text{L}$  and 100  $\mu\text{L}$  of hybridization buffer were added to **S2** as positive and negative control, respectively. As it is shown in Figure 4B, target sequence **O4**, present in *P. jirovecii* genomic DNA, is the only capable of induce a notable pore opening and rhodamine B release, whereas all the other fungi induced less response and lower dye release. That results confirmed the high selectivity of the system, even in the presence of DNA from *S. pompe* and *T. deformans*, which are included in the same subphylum as Pneumocystis genus [43].

In a step forward, the robustness of the system was determined by evaluating the behavior of **S2** to the presence of the target sequence **O4** (0.1 ng/ $\mu\text{L}$ ) in different respiratory fluids such as sputum, bronchoalveolar lavage (BAL) and nasopharyngeal aspirate (NPA) (Figure S2, ESI). In all media, the presence of **O4** produced a selective displacement of the oligonucleotide in **S2**, pore uncapping and dye delivery, whereas in the absence of target, a poor dye release was observed. A lower signal intensity was found in the sputum than in the BAL, NPA and buffer media (60% vs. 100%), probably due to the higher complexity of the sputum samples. Nevertheless, the amount of dye delivered in all cases and the differences with respect to control samples (not having target **O4** sequence) is significant, allowing an accurate fungi DNA detection in all the samples (Figure S2, ESI). These results show that the proposed method may be a promising alternative to classical procedures for the detection of DNA from *P. jirovecii* in realistic environments.

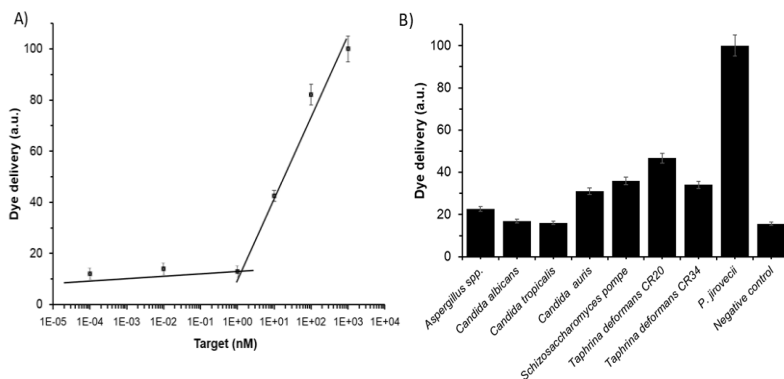


**Figure 4.** Release of rhodamine B from solid **S2** (A) in the presence of different concentrations of **O4** and (B) in the presence of 1 ng/ $\mu$ L of genomic DNA from *Aspergillus spp.*, *Candida albicans*, *Candida tropicalis*, *Candida auris*, *S. pompe*, *T. deformans*, *P. jirovecii* and 100  $\mu$ L of hybridization buffer as a negative control. Assays were performed at 60 min in hybridization buffer at pH 7.5.

In addition, it is worth mentioning that previous studies have demonstrated the possible re-use of these type of gated nanomaterials [25, 36]. In this respect, used NAA supports were calcined to remove organic matter and reused up to 3 times for the detection of **O4** obtaining similar results.

#### 6.4.4 *Pneumocystis jirovecii* detection in clinical samples

Once the method was analytically studied, a clinical validation is required to determine the real utility of the sensing material **S2** as a tool for the diagnosis of PcP produced by the infection of *P. jirovecii* as a possible alternative to existing conventional methods. The gold standard procedure used in most hospitals to diagnose PcP uses extraction of the genomic DNA from the fungus and its subsequent amplification by PCR techniques.

In the present study, 12 respiratory samples consisting of sputum and BAL samples from infected and non-infected patients from Hospital Universitari i Politècnic La Fe, were analyzed using **S2** material and the hospital reference method (i.e. PCR). For that, samples were isolated from patients with respiratory symptoms as part of routine diagnosis treatment. All samples were



analyzed by PCR for the detection of *P. jirovecii* genomic DNA. Extraction of DNA from the samples was carried out by the QIAamp DNA Blood and Tissue kit and PCR reactions were performed using the VIASURE *Pneumocystis jirovecii* Real Time PCR Detection Kit. Following this procedure, ten samples were confirmed as positive and two resulted negative. In parallel, the same samples (i.e. unmodified sputum or BAL samples) were tested using **S2**. For that, 12 individual **S2** supports were immersed in 150 µL of hybridization buffer, then 250 µL of each raw sample were directly added (without any previous treatment) and the fluorescence in the solution, due to rhodamine delivery, was measured after 60 min. Results were considered positives when the fluorescence intensity was higher than the average fluorescence of the negative controls plus three times their standard deviation. As shown in Table 2 (samples 1 to 12), the results show a total coincidence between both methods, obtaining a sensitivity and a specificity of the 100%, and therefore, positive and negative predictive values of 100%, demonstrating an excellent analytical and clinical results when using **S2** as diagnostic tool.

On the other hand, **S2** was employed to evaluate 21 NPA samples from newborn infants with and without primary *Pneumocystis* infection from Hospital Universitario Virgen del Rocío. First, all samples were analyzed by Nested-PCR of the *Pneumocystis* mtLSU rRNA gene as describe elsewhere [6]. Briefly, DNA from *P. jirovecii* was extracted using a QIAamp DNA Mini Kit with proteinase K digestion at 56°C. In the first round of amplification, the external primers pAZ102-E and pAZ102-H were used. This yielded a 346-base pair (bp) fragment. The second round utilized the internal primers pAZ102-X and pAZ102-Y and yielded a 260-bp product. Both rounds of PCR comprised 35 amplification cycles. Specific amplification was corroborated by melting curve analysis (T<sub>m</sub>: 76-77 °C) and amplicons were analyzed by electrophoresis on a 1.5% agarose gel containing ethidium bromide. Following this procedure, 11 samples were confirmed as positive and 10 resulted negative.

Nested-PCR positive samples were quantified by qPCR. Real-time quantitative PCR was performed in a CFX96 real time system (BIO-RAD) using AceQ qPCR SYBR® Green Master Mix (Vazyme) in a final volume of 10 µl containing 0.2 mM of primers pAZ102-X and pAZ102-Y and 2 µl of DNA sample. Serial dilutions of the target sequence cloned in the pGEM-T Easy Vector

(Promega) were used to generate standard curves. After quantification, all the samples showed less than  $10^2$  copies/ $\mu$ l, which is equivalent to less than 25.000 copies per mL of NPA. That concentration confirms the *P. jirovecii* colonization condition and agrees with normal concentrations found in NPA samples from newborns with primary *Pneumocystis* infection [44].

**Table 3.** Detection of *P. jirovecii* in clinical samples by the reference method (PCR) and S2 material. Each sample was analyzed by triplicate.

Sample <sup>a</sup>	Biological fluid	Reference method (PCR) <sup>b</sup>		S2 <sup>c</sup>
		Ct	Result	Result
1	Sputum	28	Infected	+
2	Sputum	27.5	Infected	+
3	BAL	36.6	Infected	+
4	Sputum	28.5	Infected	+
5	BAL	38.8	Infected	+
6	BAL	19	Infected	+
7	Sputum	26.8	Infected	+
8	Sputum	30.28	Infected	+
9	Sputum	35.3	Infected	+
10	Sputum	34.9	Infected	+
11	BAL	> 40	Non-Infected	-
12	Sputum	> 40	Non-Infected	-
13	NPA	-	Non- Infected	-
14	NPA	-	Non- Infected	-
15	NPA	-	Non- Infected	-
16	NPA	33.6	Infected	+
17	NPA	37.2	Infected	+
18	NPA	34.9	Infected	+
19	NPA	28.8	Infected	+
20	NPA	-	Non- Infected	-
21	NPA	33.4	Infected	+
22	NPA	-	Non- Infected	-
23	NPA	-	Non- Infected	-
24	NPA	-	Non- Infected	-
25	NPA	-	Non- Infected	+
26	NPA	-	Non- Infected	+
27	NPA	-	Non- Infected	-
28	NPA	34.9	Infected	-

29	NPA	39.4	Infected	-
30	NPA	34.4	Infected	+
31	NPA	34.6	Infected	+
32	NPA	33.4	Infected	+
33	NPA	35.5	Infected	-

a) Samples 1 to 12 were from patients of Hospital Universitari i Politècnic La Fe and samples 13 to 33 were from newborn infant patients of Hospital Universitario Virgen del Rocío.

b) Samples were considered positives (+) when two different aliquots of each patient were positive by specific PCR for *P. jirovecii*

c) Samples were considered positives (+) when the fluorescence signal at 585 nm ( $\lambda_{exc}$  = 555 nm) was higher than the average fluorescence of the negative controls plus three times the standard deviation.

In parallel, the same samples (i.e. unmodified NPA samples) were analyzed using **S2**. For that, 21 individual **S2** supports were submerged in 150  $\mu$ L of hybridization buffer and 250  $\mu$ L of each raw sample were directly added (without any previous treatment). Finally, the fluorescence of the solution was measured after 60 min and results were considered positives when the fluorescence intensity was higher than the average fluorescence of the negative controls plus three times their standard deviation. As it is depicted in Table 3 (samples 13 to 33), results showed the coincidence between two methods in 16 samples and a total of 5 incongruent values that corresponded to 2 false positives and 3 false negatives, gave a sensitivity of 70%, a specificity of 78%, and positive and negative predictive values of 78% and 70%, respectively. The incongruences observed between the results obtained by PCR and **S2** materials might be due several causes such as sample handling, DNA degradation or the very low concentration of pathogen present in NPA samples (calculated as less than 25.000 copies per mL of NPA). Nevertheless, it is noteworthy the high competitiveness of the gated biosensor as rapid diagnostic tool compared to the standard reference procedures, additionally providing easiness to use and lower cost, and avoiding sample treatments such as DNA extraction steps or amplification reactions [45].

## 6.5 Conclusions

Early diagnosis of PcP is decisive for a suitable treatment and for a better prognosis. On that regard, rapid and accurate diagnostic tools are important for an early identification of the pathogen and to reduce the risk of mortality associated. However, standard diagnosis of PcP in remote or less developed countries or in resource-limited settings is difficult as usually it is necessary the use of costly well-equipped laboratories and trained personnel. In this scenario, the design of low-cost easy-to-use diagnostic systems and point-of-care devices from readily accessible bio-fluids constitute a potential solution. In this study, a new method for the detection of *Pneumocystis jirovecii* genomic DNA by using gated nanomaterials is proposed. In the developed tool, the pores of a NAA scaffold are loaded with a dye and gated with oligonucleotides that selectively recognizes a sequence of the genomic DNA from the fungi. The sensing mechanism relies in the recognition between the gating oligonucleotides and the *P. jirovecii* genomic DNA that induces a displacement of the capping oligonucleotide, pore uncapping and cargo delivery. In addition, the use of different gating oligonucleotides in the form of single strands or clamps to obtain duplex or triple-helix hybridization structures is also studied. From the three evaluated nanomaterials (**S1**, **S2** and **S3**), the solid **S2** provides the highest rhodamine B release and the faster response, probably due to more efficient formation of a triplex with respect to duplex conformations (**S1** and **S3**). **S2** showed a LOD 1 nM in hybridization buffer, which is equivalent to other state-of-the-art reported detection systems. Moreover, the probe presented a high selectivity to *P. jirovecii*, since no response was observed in the presence of DNA from other microorganisms. Finally, the gated material **S2** is tested in unmodified sputum and bronchoalveolar lavages samples from infected and non-infected patients to diagnose PcP, obtaining a sensitivity and a selectivity of 100%. In the same way, **S2** is used to analyze nasopharyngeal aspirate samples from infants to detect primary infected individuals with a sensitivity and a selectivity of 70% and 78%, respectively. In both cases, **S2** detects *P. jirovecii* in 60 minutes without any sample treatment or the use of amplification reactions. This diagnostic tool has great potential for the further development of point-of-care devices for the simple and accurate detection of *P. jirovecii* from

different biofluids avoiding PCR and using a small amount of sample, which could represent a high gain in the fight against PcP.

## 6.6 Acknowledgements

L.P. thanks UPV for her predoctoral fellowship. S.S. thanks the Instituto de Salud Carlos III and the European Social Fund for the financial support “Sara Borrell” (CD16/000237). The authors also thank the Electron Microscopy Service at the UPV and ICTS NANBIOSIS oligonucleotide synthesis platform (U29) for support. The authors would like to thank Dr. Jordi Luque Font, from the IRTA Institute of Agrifood Research and Technology-Cabrils, and Dr. Josep Armengol from the Instituto Agroforestal Mediterráneo-Universitat Politècnica de València for the supply of *T. deformans* samples. The fungal culture of *S. pompe* was supplied by Piet W.J. de Groot from the Regional Center for Biomedical Research, Castilla-La Mancha Science & Technology Park, University of Castilla–La Mancha.

### Funding

This research was funded by the Spanish Government, (projects RTI2018-100910-B-C41 (MCUI/AEI/FEDER, UE) and CTQ2017-84415-R), the Generalitat Valenciana (project PROMETEO/2018/024) and CIBER-BBN (project NANOPATH).

### Supporting Information

The following are available online at [www.mdpi.com/xxx/s1](http://www.mdpi.com/xxx/s1), Scheme S1: Scheme of the duplexes formed by oligonucleotides O1 and O3 with the target, and the triplex formed by oligonucleotide O2 and the target sequence, Table S1: Mass spectrometry analysis of the oligonucleotides, Figure S1: Amount of rhodamine B released from the pores of solids **S1** (A) and **S3** (B) when 1 nM of DNA from *P. jirovecii* was (a) absent and (b) present in a solution of hybridization buffer (20 mM Tris-HCl, 37.5 mM MgCl<sub>2</sub>, pH 7.5), Figure S2: Delivery of rhodamine B from material **S2** in buffer, sputum, BAL and NPA fluids in the presence of complementary DNA from *P. jirovecii* (1 nM).

## AUTHOR INFORMATION

### Corresponding Author

\* Elena Aznar; ORCID NUM.: 0000-0003-0361-3876; Email: [elazgi@upvnet.upv.es](mailto:elazgi@upvnet.upv.es);

\* Ramón Martínez-Máñez; ORCID NUM.: 0000-0001-5873-9674; Email: [rmaez@gim.upv.es](mailto:rmaez@gim.upv.es);

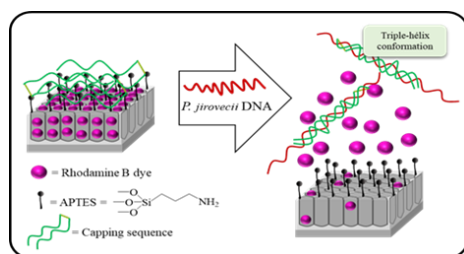
### Author Contributions

L.P.: Investigation, Methodology; Writing - original draft; A.A.: Investigation, resources, Writing - review & editing; R.E.: Investigation, resources, Writing - review & editing, A.R-G.: Resources, Writing - review & editing; J.P.: Resources, Writing - review & editing; V.F.: Resources, Writing - review & editing; E.J-C.: Resources, Writing - review & editing; E.A.: Investigation; Funding acquisition; Ramón Martínez-Máñez: Conceptualization, Funding acquisition, Writing - review & editing; And S.S-F.: Investigation Supervision, Methodology; Writing - original draft, Writing-review and editing. All authors have read and agreed to the published version of the manuscript.

### Notes

The authors declare no competing financial interest.

### Table of Contents



## References

- [1]. Fauchier, T., Hasseine, L., Gari-Toussaint, M., Casanova, V., Marty, P.M. and Pomares, C. Detection of *Pneumocystis jirovecii* by quantitative PCR to differentiate colonization and pneumonia in immunocompromised HIV-positive and HIV-negative patients, *J. Clin. Microbiol.*, **2016**, *54*, 1487–1495.

- 
- [2]. Van de Meer, G. and Brug, S.L. Infection À pneumocystis Chez L'homme et Chez Les Animax. *Annales de la Société Belge de Médecine Tropicale*, 1942, 22, 301–308.
- [3]. Skalski, J.H., Kottom, T.J. and Limper, A.H. Pathobiology of *Pneumocystis pneumonia*: life cycle, cell wall and cell signal transduction. *FEMS Yeast Res.*, 2015, 15, 6.
- [4]. Dellière, S., Gits-Muselli, M., Bretagne S. and Alanio, A. Outbreak-causing fungi: *Pneumocystis jirovecii*. *Mycopathologia*, 2019, 1-18.
- [5]. Montes-Cano, M.A., Chabe, M., Fontillon-Alberdi, M., De La Horra, C., Respaldiza, N., Medrano, F.J., Varela, J.M., Dei-Cas, E. and Calderón, E.J. Vertical transmission of *Pneumocystis jirovecii* in humans. *Emerg. Infect. Dis.*, 2009, 15, 125–127.
- [6]. Jarboui, M.A., Sellami, A., Sellami, H., Cheikhrouhou, F., Makni, F., Ben Arab, N., Ben Jemaa M. and Ayadi, A. Molecular diagnosis of *Pneumocystis jirovecii* pneumonia in immunocompromised patients. *Mycoses*, 2010, 53, 329–333.
- [7]. Durand-Joly, I., Chabé, M., Soula, F., Delhaes, L., Camus D. and Dei-Cas, E. Molecular diagnosis of *Pneumocystis pneumonia*. *FEMS Immunol. Med. Mic.*, 2005, 45, 405-410.
- [8]. Song, Y., Ren, Y., Wang X. and Li, R. The biosynthesis pathway of Swainsonine, a new anticancer drug from three endophytic fungi. *Med. Mycol.*, 2016, 57, 111-116.
- [9]. Tomás, A.L. and Matos, O. *Pneumocystis jirovecii* pneumonia: Current advances in laboratory diagnosis, *OBM Genetics*, 2018, 2, 49.
- [10]. Urabe, N., Sakamoto, S., Sano, G., Ito, A., Sekiguchi, R. and Homma, S. Serial change in serum biomarkers during treatment of Non-HIV *Pneumocystis pneumonia*. *J. Infect. Chemother.*, 2019, 25, 936–942.
- [11]. Esteves, F., Calé, S.S., Badura, R., de Boer, M.G., Maltez, F., Calderón, E.J., van der Reijden, T.J. Márquez-Martín, E., Antunes, F. and Matos, O. Diagnosis of *Pneumocystis pneumonia*: evaluation of four serologic biomarkers. *Clin. Microbiol. Infect.*, 2015, 21, 379.e1-379.e10.
- [12]. Tomás, A.L., Cardoso, F., Esteves, F. and Matos, O. Serological diagnosis of pneumocystosis: production of a synthetic recombinant antigen for immunodetection of *Pneumocystis jirovecii*, *Sci. Rep.*, 2016, 6, 36287-36295.
- [13]. Arvanitis, M., Anagnostou, T., Fuchs, B.B., Caliendo, A.M. and Mylonakis, E. Molecular and nonmolecular diagnostic methods for invasive fungal infections, *Clin. Microbiol. Rev.*, 2014, 27, 490–526.
- [14]. Tomás, A.L., Cardoso, F., Pinto, M., de Almeida, M.P., de Sousa, B. and Pereira, E. 28th European Congress of Clinical Microbiology and Infectious Diseases, 2018, Madrid, Spain.

- [15]. Tomás, A.L., de Almeida, M.P., Cardoso, F., Pinto, M., Pereira, E., Franco, R. and Matos, O. Development of a gold nanoparticle-based lateral-flow immunoassay for pneumocystis pneumonia serological diagnosis at point-of-care, *Front. Microbiol.*, **2019**, *10*, 2917.
- [16]. García-Fernandez, A., Aznar, E., Martínez-Máñez, R. and Sancenón, F., New Advances in In Vivo Applications of Gated Mesoporous Silica as Drug Delivery Nanocarriers, *Small*, **2020**, *16*, 1902242.
- [17]. Aznar, E., Coll, C., Marcos, M.D., Martínez-Máñez, R., Sancenón, F., Soto, J., Amorós, P., Cano, J. and Ruiz, E. Controlled delivery systems using antibody-capped mesoporous nanocontainers, *Chem. Eur. J.*, **2009**, *15*, 6877-6888.
- [18]. Sancenón, F., Pascual, L., Oroval, M., Aznar, E. and Martínez-Máñez, R. Gated silica mesoporous materials in sensing applications, *ChemistryOpen*, **2015**, *4*, 418–437.
- [19]. Mondragón, L., Mas, N., Ferragud, V., De La Torre, C., Agostini, A., Martínez-Máñez, R., Sancenón, F., Amorós, P., Pérez-Payá, E. and Orzáez, M. Enzyme-responsive intracellular-controlled release using silica mesoporous nanoparticles capped with  $\epsilon$ -poly-L-lysine, *Chem.- A Eur. J.*, **2014**, *20*, 5271–5281.
- [20]. Giménez, C., De La Torre, C., Gorbe, M., Aznar, E., Sancenón, F., Murguía, J.R., Martínez-Máñez, R., Marcos M.D. and Amorós, P. Gated mesoporous silica nanoparticles for the controlled delivery of drugs in cancer cells, *Langmuir*, **2015**, *31*, 3753–3762.
- [21]. Aznar, E., Villalonga, R., Giménez, C., Sancenón, F., Marcos, M.D., Martínez-Máñez, R., Díez, P., Pingarrón, J.M. and Amorós, P. Glucose-triggered release using enzyme-gated mesoporous silica nanoparticles, *Chem. Commun.*, **2013**, *49*, 6391-6393.
- [22]. Ouyang, C., Zhang, S., Xue, C., Yu, X., Xu, H., Wang, Z., Lu, Y. and Wu, Z.S. Precision-Guided Missile-Like DNA Nanostructure Containing Warhead and Guidance Control for Aptamer-Based Targeted Drug Delivery into Cancer Cells in Vitro and in Vivo, *J. Am. Chem. Soc.*, **2020**, *142*, 1265–1277.
- [23]. Argoubi, W., Sánchez, A., Parrado, C., Raouafi, N. and Villalonga, R. Label-free electrochemical aptasensing platform based on mesoporous silica thin film for the detection of prostate specific antigen, *Sens. Actuators-B Chem.*, **2018**, *255*, 309–315.
- [24]. Llopis-Lorente, A., Lozano-Torres, L.T., Bernardos, A., Martínez-Máñez, R. and Sancenón, F. Mesoporous silica materials for controlled delivery based on enzymes, *J. Mater. Chem. B*, **2017**, *5*, 3069-3083.
- [25]. Pla, L., Xifré-Pérez, E., Ribes, À., Aznar, E., Marcos, M.D., Marsal, L.F., Martínez-Máñez, R. and Sancenón, F. A mycoplasma genomic DNA probe using gated nanoporous anodic alumina, *Chempluschem*, **2017**, *82*, 337–341.



- [26]. Ribes, À., Aznar, E., Santiago-Felipe, S., Xifre-Perez, E., Tormo-Mas, M.A., Pemán, J.P., Marsal, L.F. and Martínez-Máñez, R. Selective and sensitive probe based in oligonucleotide-capped nanoporous alumina for the rapid screening of infection produced by *Candida albicans*, *ACS Sens*, **2019**, *4*, 1291-1298.
- [27]. Goñi, J. R., Vaquerizas, J.M., Dopazo, J. and Orozco, M. Exploring the reasons for the large density of triplex-forming oligonucleotide target sequences in the human regulatory regions, *BMC Genomics*, **2006**, *7*, 63–63.
- [28]. Frank-Kamenetskii, M.D. and Mirkin, S.M. Triplex DNA structures, *Annu. Rev. Biochem.*, **1995**, *64*, 65–95.
- [29]. Goñi, J.R., De La Cruz, X. and Orozco, M. Triplex-forming oligonucleotide target sequences in the human genome, *Nucleic Acids Res.*, **2004**, *32*, 354–360.
- [30]. Aviñó, A., Frieden, M., Morales, J.C., García de la Torre, B., Güimil García, R., Azorín, F., Gelpí, J.L, Orozco, M., González, C. and Eritja, R. Properties of triple helices formed by parallel-stranded hairpins containing 8-aminopurines, *Nucleic Acids Res.*, **2002**, *30*, 2609-2619.
- [31]. Nadal, A., Eritja, R., Esteve, T. and Pla, M. "Parallel" and "antiparallel tail-clamps" increase the efficiency of triplex formation with structured DNA and RNA targets, *ChemBioChem*, **2005**, *6*, 1034–1042.
- [32]. Carrascosa, L.G., Gómez-Montes, S., Aviñó, A., Nadal, A., Pla, M., Eritja, R. and Lechuga, L.M. Sensitive and label-free biosensing of RNA with predicted secondary structures by a triplex affinity capture method, *Nucleic Acids Res.*, **2012**, *40*, e56.
- [33]. Aviñó, A., Huertas, C.S., Lechuga, L.M. and Eritja, R. Sensitive and label-free detection of miRNA-145 by triplex formation, *Anal. Bioanal. Chem.*, **2016**, *408*, 885–893.
- [34]. Wei, S., Chen, G., Jia, X., Mao, X., Chen, T., Mao, D., Zhang, W. and Xiong, W. Exponential amplification reaction and triplex DNA mediated aggregation of gold nanoparticles for sensitive colorimetric detection of microRNA, *Anal. Chim. Acta*, **2020**, *1095*, 179–184.
- [35]. Ribes, À., Santiago-Felipe, S., Aviñó, A., Candela-Noguera, V., Eritja, R., Sancenón, F., Martínez-Máñez, R. and Aznar, E. Design of oligonucleotide-capped mesoporous silica nanoparticles for the detection of miRNA-145 by duplex and triplex formation, *Sens. Actuators-B Chem.*, **2018**, *277*, 598–603.
- [36]. Pascual, L., Baroja, I., Aznar, E., Sancenón, F., Marcos, M.D., Murguía, J.R., Amorós, P., Rurack, K. and Martínez-Máñez, R. Oligonucleotide-capped mesoporous silica nanoparticles as DNA-responsive dye delivery systems for genomic DNA detection, *Chem. Commun.*, **2015**, *51*, 1414–1416.
- [37]. Oroval, M., Coll, C., Bernardos, A., Marcos, M.D., Martínez-Máñez, R., Shchukin, D.G. and Sancenón, F. Selective fluorogenic sensing of As (III) using aptamer-capped nanomaterials, *ACS Appl. Mater. Interfaces*, **2017**, *9*, 11332-11336.

- [38]. Vojkuvka, L., Marsal, L.F., Ferré-Borrull, J., Formentin, P. and Pallarés, J. Self-ordered porous alumina membranes with large lattice constant fabricated by hard anodization, *Superlattices Microstruct.*, **2008**, *44*, 577–582.
- [39]. Matsumura, Y., Tsuchido, Y., Yamamoto, M., Nakano, S. and Nagao, M. Development of a fully automated PCR assay for the detection of *Pneumocystis jirovecii* using the GENECUBE system, *Med. Mycol. J.*, **2019**, *57*, 841-847.
- [40]. Yang, S.L., Wen, Y. H., Wu, Y.S., Wang, M.C., Chang, P.Y., Yang, S. and Lu, J.J. Diagnosis of *Pneumocystis pneumonia* by real-time PCR in patients with various underlying diseases, *J. Microbiol. Immunol. Infect.*, **2019**, *5*, 785-790.
- [41]. Moodley, B., Tempia, S. and Frean, J.A. Comparison of quantitative real-time PCR and direct immunofluorescence for the detection of *Pneumocystis jirovecii*, *PLoS One*, **2017**, *12*, e0180589.
- [42]. Alanio, A., Desoubreux, G., Sarfati, C., Hamane, S., Bergeron, A., Azoulay, E., Molina, J.M., Derouin, F. and Menotti, J. Real-time PCR assay-based strategy for differentiation between active *Pneumocystis jirovecii* pneumonia and colonization in immunocompromised patients, *Clin. Microbiol. Infect.*, **2011**, *17*, 1531–1537.
- [43]. Marimuthu, S., Ghosh, K. and Wolf, L.A. Development of a Real-time PCR assay for *Pneumocystis jirovecii* on the Luminex ARIES® Platform, *Univ. Louisv. J. Respir. Infect.*, **2019**, *3*, 5.
- [44]. Cissé, O. H., Almeida, J. M., Fonseca, Á., Kumar, A.A., Salojärvi, J., Overmyer, K., Hauser, P. M. and Pagni, M. Genome sequencing of the plant pathogen *Taphrina deformans*, the causal agent of peach leaf curl, *MBio*, 2013, *4*, e00055-13.
- [45]. Rojas, P., Friaiza, V., García, E., De La Horra, C., Vargas, S.L., Calderón E.J., and Pavón, A. Early acquisition of *Pneumocystis jirovecii* colonization and potential association with respiratory distress syndrome in preterm newborn infants. *Clin. Infect. Dis.*, **2017**, *65*, 976–981.
- [46]. Kidd, S.E., Chen, S.C.A., Meyer, W. and Halliday, C.L. A new age in molecular diagnostics for invasive fungal disease: are we ready?, *Front. Microbiol.*, **2020**, *10*, 2093.

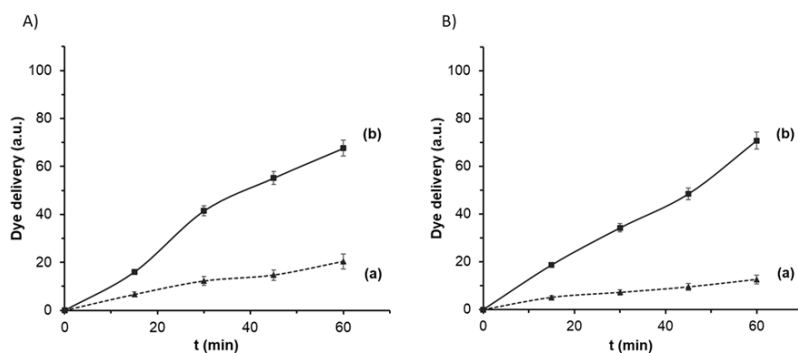
6.7. Supporting Information:  
Triplex Hybridization-based  
nanosystem for the Rapid Screening  
of *Pneumocystis pneumonia* in  
infected and colonized clinical  
samples

Luis Pla<sup>1,2,3</sup>, Anna Aviñó<sup>3,4</sup>, Ramón Eritja<sup>3,4</sup>, Alba Ruiz-Gaitán<sup>5</sup>, Javier Pemán<sup>5</sup>, Vicente Friaza<sup>6</sup>, Enrique J. Calderón<sup>6,7</sup>, Elena Aznar<sup>\*1,2,3,8</sup>, Ramón Martínez-Máñez<sup>\*1,2,3,8</sup> and Sara Santiago-Felipe<sup>1,2,3</sup>

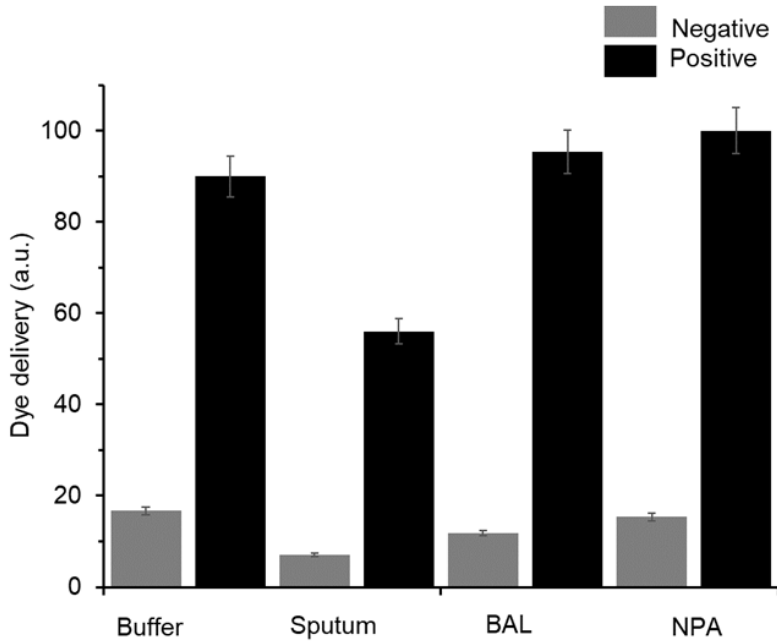
## Electronic Supplementary Material

Table S1. Mass spectrometry analysis of the oligonucleotides

Code	Name	M calculated (g/mol)	M found (g/mol)
O1	Duplex antiparallel	5575	5574
O2	Clamp antiparallel	10918	10915
O3	Control clamp antiparallel	10918	10912
O4	Target complementary	5423	5424

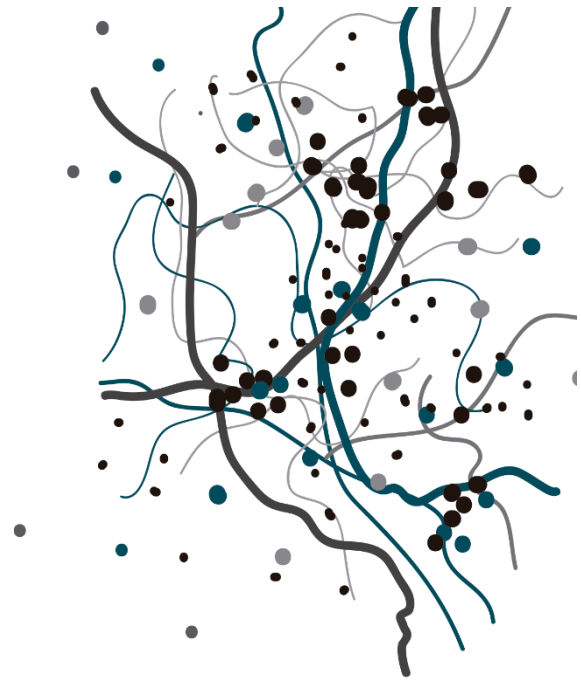


**Figure S1.** Amount of rhodamine B released from the pores of solids **S1** and **S3** when 1 nM of DNA from *P. jirovecii* was (a) present and (b) absent in a solution of hybridization buffer (20 mM Tris-HCl, 37.5 mM MgCl<sub>2</sub>, pH 7.5).



**Figure S2.** Delivery of rhodamine B from material **S2** in sputum, BAL and NPA fluids in the presence of complementary DNA from *P. jirovecii* (1 nM).





# 7

A Fluorogenic Capped  
Mesoporous Aptasensor for  
Gluten Detection





# A fluorogenic capped mesoporous aptasensor for Gluten detection

Luis Pla<sup>a,b,c,‡</sup>, M. Carmen Martínez-Bisbal<sup>a,b,c,d,e,+</sup>, Elena Aznar<sup>a,b,c</sup>, Félix Sancenón<sup>a,b,c,e,f</sup>, Ramón Martínez-Máñez<sup>a,b,c,e,f\*</sup> and Sara Santiago-Felipe<sup>a,b,c</sup>.

<sup>a</sup> CIBER de Bioingeniería, Biomateriales y Nanomedicina (CIBER-BBN), Melchor Fernández Almagro, 3, 28029, Madrid, Spain.

<sup>b</sup> Instituto Interuniversitario de Investigación de Reconocimiento Molecular y Desarrollo Tecnológico, Universitat Politècnica de València, Universitat de València, Camino de Vera s/n, 46022, València, Spain.

<sup>c</sup> Unidad Mixta de Investigación en Nanomedicina y Sensores. Universitat Politècnica de València, Instituto de Investigación Sanitaria La Fe, Avenida Fernando Abril Martorell 106, Torre A, 7<sup>a</sup> planta, 46026 València, Spain.

<sup>d</sup> Departamento de Química Física, Universitat de València, Carrer del Dr. Moliner, 50, 46100 Burjassot, València, Spain.

<sup>e</sup> Unidad Mixta UPV-CIPF de Investigación en Mecanismos de Enfermedades y Nanomedicina. Universitat Politècnica de València, Centro de Investigación Príncipe Felipe, Eduardo Primo Yúfera 3, 46012, València, Spain.

<sup>f</sup> Departamento de Química, Universitat Politècnica de València, Camino de Vera s/n, 46022, Valencia, Spain.

<sup>‡</sup> These authors contributed equally

\* Corresponding author: Ramón Martínez-Máñez // rmaez@qim.upv.es

***Submitted to Analytical Chimica Acta***



## 7.1 Abstract

Celiac disease is a complex and autoimmune disorder caused by the ingestion of gluten affecting almost 1 % of global population. Nowadays an effective treatment does not exist, and the only way to manage the disease is the removal of gluten from the diet. Owing the key role played by gluten, clear and regulated labelling of foodstuff and smart methods for gluten detection are needed to fight frauds on food industry and to avoid the involuntary ingestion of this protein by celiac patients. On that scope, the development of a novel detection system of gluten is here presented. The sensor consists of nanoporous anodic alumina films loaded with a fluorescent dye and capped with an aptamer that recognizes gliadin (gluten's soluble proteins). In the presence of gliadin, aptamer sequences displace from the surface of anodic alumina resulting in pore opening and dye delivery. The dispositive shows a limit of detection (LOD) of  $100 \mu\text{g Kg}^{-1}$  of gliadin, good selectivity and a detection time of approximately 60 min. Moreover, the sensor is validated in real food samples. This novel probe allows fast gluten detection through a simple signalling process with potential use for food control.

## Keywords

Mesoporous supports, molecular gates, aptasensor, aptamers, gluten

## 7.2 Introduction

Celiac Disease (CD) is a complex, chronic and autoimmune disorder characterised by a wide set of clinical manifestations that include gastrointestinal upset, chronic fatigue, nutrient deficiencies, poor growth in children and other derivative effects such as anaemia, dental enamel hypoplasia, reduced bone density, oral ulcers, dermatitis or also liver and biliary disease [1]. The global prevalence of CD disease is affected by different immunological, genetics [2] and environmental factors such as gender, age and geographical location, among others. In the last century, during the 1950s, gluten was pointed as the causing element of inducing CD [3] and, from that moment to date, a difficult and strict lifelong gluten-free diet has been established as the only successful treatment. For this reason, fast, accurate and low-cost

gluten detection in food is of importance, especially in those products labelled and certified as adequate for celiac patients.

Gluten is a set of macromolecules mainly found in wheat, barley, rye, oats and other varieties or hybrids of these cereals such as spelt, kamut and triticale [4]. This cluster of macromolecules is not still fully known and is matter of a deeper study [5, 6], but since standardization in 1979 by *Codex Alimentarius* it has been considered that proteins (prolamins and glutelins) are 90 % of gluten components (1:1 approximate ratio) together with lipids (8 %) and carbohydrates (2 %). The proteins in gluten are classified in two main groups according to their solubility in alcohol-water solutions: a) soluble prolamins (targeted by most of analytical techniques) that get their name from their high content in prolines and glutamines and are named as gliadins, secalins, hordeins and avenins, depending on their origin (wheat, rye, barley and oat respectively); and b) insoluble glutelins [1].

In this context, with the aim of safety and quality assessment, *Codex Alimentarius Commission* included gluten in the list of ingredients to be declared, establishing the category of “gluten-free” and “very low gluten content” foods when gluten concentration did not exceed 20 mg Kg<sup>-1</sup> and 100 mg Kg<sup>-1</sup> respectively [7–10]. The European Commission supported this regulation and promoted their control (CE Directive 2006/2014 and Regulation (EU) N° 828/2014). Canada [11], United States [12] and Australia-New Zealand [13] share the same principles. The threshold value of 20 mg Kg<sup>-1</sup> established by *Codex Alimentarius Commission*, represents the lowest level of gluten that would have no side effects on most of the CD patients.

Nowadays, available analytical methodologies for gluten detection are divided in four main groups: a) immunological techniques, b) genomics, c) proteomics and d) non-specific protein detection/quantification techniques. Several immunochemical techniques have been developed based on ELISA kits with mono- and -polyclonal antibodies against prolamins [14] relying on different types of antibodies (R5, Skerrit and G12 monoclonal antibodies) [15–18]. Other examples published implemented antibodies on quartz crystal microbalance (QCM) [19] and surface plasmon resonance (SPR) [20]. Nevertheless, and although they presented very good limits of detection (results

range from 0.3  $\mu\text{g Kg}^{-1}$  to 5  $\text{mg Kg}^{-1}$ ), all these methodologies do not fit within the needs claimed by market, in terms of cost, time and management. It is important to remark that immunoassays are not fully compatible with cocktail extractions solutions because of the easy denaturation of their components [21]. From another point of view, polymerase chain reaction (PCR) based commercial kits (SureFood® ALLERGEN QUANT), can detect gluten at concentrations as low as 0.04  $\text{mg Kg}^{-1}$  [22], despite their high cost and compromised application in highly processed or hydrolysed samples [23, 24]. Alternatively, proteomics can detect gluten at concentrations as low as 1  $\text{mg Kg}^{-1}$  [25], but require the use of expensive laboratory equipment, higher level of expertise and long analysis times [26]. Finally, non-specific protein detection/quantification methodologies, in which gluten and all present proteins are detected through Biuret reaction and/or bioluminescence adenosine triphosphate (ATP) detection, are not in general advised by the scientific community and should only be used as qualitative indicators [27].

During the last decade the detection of solubilised gliadin through specific aptamer sequences has been exploited as a new approach for the development of innovative biosensors for gluten detection. In this context, gliadin detection using aptamers G33 (against gliadin) [23] and Gli1 and Gli4 (against  $\alpha$ 2-gliadin) [28, 29] have been reported. Pinto. *et al.* (2014), developed a real-time apta-PCR technique for the specific detection of gliadin [23] with a LOD of 0.1  $\text{mg Kg}^{-1}$ . Lobo-Castañón *et al.* (2014) used Gli4 aptamer as a receptor for an electrochemical competitive assay on magnetic particles, achieving LODs as low as 0.5  $\mu\text{g Kg}^{-1}$  of gliadin [30] and continued their work with the implementation of Gli1 aptamer that provided a LOD of 49  $\mu\text{g Kg}^{-1}$  [31]. However, despite the low LODs and selectivity achieved, all these systems, in general, lack the simplicity needed for its implementation as a point of care sensing probe.

On that regard, scientific community is focusing in the development of biosensors that are portable, efficient, reliable, fast and economically affordable [32]. Nanotechnology is being a fundamental part of this development. In this field, the use of gated mesoporous supports for the development of sensing devices has resulted in the report of diverse systems with promising applications [33–35]. In this approach, capped mesoporous materials loaded

with a dye are uncapped by the presence of specific molecules allowing dye delivery, which is detected by simple optical methods [36]. Capping systems such as specific DNA sequences [37, 38], proteins [39] and nanoparticles [40, 41] have been reported. This simple sensing concept enables a host-guest interaction independent from the signaling subunit and, in addition, provides an amplifying effect since few target molecules of analyte are able to induce the release of a large quantity of entrapped signaling molecules [42].

In this scenario, we report herein a new gliadin detection system based on the synergic combination of gluten aptamers and nanoporous anodic alumina (NAA) supports. Optical signaling in response to the presence of gluten is accomplished by monitoring the fluorescence of the dye released from NAA upon aptamer binding to gluten. The system is optimized with standard PWG gliadin. In the course of the development of the sensor, three different aptamer sequences are evaluated and the sequence with the best results is used to develop a simple sensor, which is validated in real samples. The dispositive shows a limit of detection (LOD) of  $100 \mu\text{g Kg}^{-1}$  of gliadin, good selectivity and a time of detection of 60 minutes. Our results might be the basis for developing portable, simple, fast and sensitive systems for gluten detection that can be easily tuned via the use of different reporting molecules offering a great potential for point-of-care allergen testing.

## 7.3 Materials and Methods

### 7.3.1 General Techniques

Field emission scanning electron microscopy (FSEM) and Energy Dispersive X-ray spectroscopy (EDX) analyses were done under a ZEISS Ultra 55 microscope. Fluorescence spectroscopy measurements were carried out on a Synergy H1 microplate reader (BioTek, Winooski, VT, USA).

### 2.2. Chemicals

(3-isocyanatopropyl)triethoxysilane (3-ICPTS), rhodamine B, triethylamine (TEA), tris(hydroxymethyl)aminomethane (TRIS), and hydrochloric acid were purchased from Sigma-Aldrich Química (Madrid, Spain). Oligonucleotide **O1** ( $\text{NH}_2\text{-(CH}_2\text{)}_6\text{-5'-AAA AAA CCC CCC-3'}$ ) and the aptamers **O2** ( $5\text{'-TTT TGG GGG GAA ACT ACT AAC TAG GTA AGA TCA CGC AGC ACT AAA CGA CGT}$

AGT TGC CAG GGG GGT TTT-3'), **O3** (5'-TTT TGG GGG GCC AGT CTC CCG TTT ACC GCG CCT ACA CAT GTC TGA ATG CCG GGG GGT TTT-3') and **O4** (5'-TTT TGG GGG GCT AGG CGA AAT ATA GCT ACA ACT GTC TGA AGG CAC CCA ATG GGG GGT TTT-3') were acquired from Invitrogen by Thermo Fisher Scientific (Madrid, Spain). Gliadin from wheat standard was purchased from Merck-Sigma-Aldrich.

### 7.3.3 Nanoporous anodic alumina supports

NAA scaffolds were purchased from InRedox (CO, USA). They consisted on anodic aluminum oxide films grown on a 0.1 mm thick aluminum layer, with a pore density of  $9 \cdot 10^{11}$  pores·cm<sup>-2</sup>. The pores were of 5 nm in diameter and 10 μm in height.

### 7.3.4 Procedures

#### 7.3.4.1 Preparation of **S2**, **S3** and **S4**

In a typical procedure, 8 independent NAA supports were immersed in 8 mL of a solution of rhodamine B (1.0 mM) in CH<sub>3</sub>CN (30 mL). The mixture was stirred at room temperature for 24 h. Then, an excess of 3-ICPTS (1.2 mM) was added, and the final mixture was stirred at room temperature for 6 h to obtain **S0**. For the preparation of **S1**, **S0** supports were immersed in 700 μL of CH<sub>3</sub>CN with rhodamine B (1.0 mM), and 100 μL of oligonucleotide **O1** (10 μM) and 2 μL of TEA were added. Then, the mixture was stirred 3 h at room temperature and the resulting material was washed with a solution of rhodamine B (1.0 mM) in CH<sub>3</sub>CN. Finally, **S1** solids were submerged in 780 μL of TRIS buffer (pH 7.4) and 20 μL of the aptamers **O2**, **O3** or **O4** (100 μM) were added to obtain **S2**, **S3** and **S4**, respectively. Design of sequences of **O2**, **O3** and **O4** was inspired in previous studies [23, 43] and modified to link **O1** sequences attached over mesoporous support. Suspensions were stirred 2 h at 30 °C. The resulting materials were washed with hybridization buffer to eliminate the unbounded oligonucleotide.

#### 7.3.4.2 Gluten extraction

Gluten from cereals and processed foods was extracted following previously reported protocols [43]. 250 mg of food samples underwent a 30 minutes aqueous-ethanolic 40:60 (v/v) solution extraction followed by centrifugation (45

minutes, 135 g-force Thermo Scientific SL16/16R). The supernatants were then collected. Gluten-free cereals (rice and mijo-based) underwent also the same extraction protocol. Gluten food sources comprised wheat flours, strength flours, integral flours, instant outmeal, gluten-free flours, breakfast cookies, digestive cookies and gluten-free cookies. Cookies were previously homogenized through manual grinding. Extraction efficiency is expected to be in the range of 40-60 % according to reported studies [43].

#### 7.3.4.3 Detection protocol

The sensing ability of the aptasensors **S2**, **S3** and **S4** was tested using the reference *European Prolamin Working Group* (PWG) gliadin standard obtained as a reference material consisting on the extraction and mixture of gliadin proteins from 28 different European wheat cultivars. In a typical experiment, two independent **S2**, **S3** and **S4** supports were submerged in 900  $\mu\text{L}$  of TRIS buffer. Then, 100  $\mu\text{L}$  of a PWG gliadin suspension ( $100 \mu\text{g Kg}^{-1}$ ) in TRIS buffer were added to one of the supports whereas 100  $\mu\text{L}$  of TRIS buffer were added to the other (blank). Both solutions were maintained at 25  $^{\circ}\text{C}$  and aliquots were taken every 15 min for 1 hour. Cargo release was then determined by measuring the emission of the rhodamine B dye in the solution at 575 nm ( $\lambda_{\text{ex}} = 555 \text{ nm}$ ).

#### 7.3.4.4 Calibration curve

The materials with better performance in the initial delivery experiments (**S2** and **S4**) were selected for the following sensitivity experiments in ethanolic extract-buffer 15:85 (v/v) media doped with different quantities of PWG gliadin standard. For that, 100  $\mu\text{L}$  of different gliadin solutions ( $0 - 10^4 \mu\text{g Kg}^{-1}$ ) were added to **S2** and **S4** supports in a final volume of 1 mL. After 60 min at 25  $^{\circ}\text{C}$  rhodamine B released from the pores was measured at 575 nm ( $\lambda_{\text{ex}} 555 \text{ nm}$ ).

In addition, it was calculated that  $100 \mu\text{g Kg}^{-1}$  of gliadin triggered the release of an average of  $2.5 \cdot 10^{12}$  molecules of rhodamine B, which means a signal amplification of  $10^{11}$  reporter molecules per each  $\mu\text{g Kg}^{-1}$  of enzyme. Among others, geometry of the pores and probe-to-target affinity conditionate this amplification, since they determine the total amount of encapsulated cargo and the efficiency of the uncapping process, respectively.



#### 7.3.4.5 Selectivity and applicability

For selectivity and potential applicability methodology evaluation of **S4** support, 100  $\mu\text{L}$  of different cereals extracts (with and without gluten), obtained according to the procedure described in subsection 2.4.2, were diluted in 900  $\mu\text{L}$  of TRIS buffer. **S4** supports were submerged in these solutions, which were maintained at 25  $^{\circ}\text{C}$  while rhodamine B released from the pores after 60 min was measured at 575 nm ( $\lambda_{\text{ex}}$  555 nm).

In addition, the response of **S4** to different concentrations of gliadin in mijo extracts was studied. For this, 100  $\mu\text{L}$  of mijo extracts (gluten-free) doped with increasing concentrations of PWG gliadin standard (100-800  $\mu\text{g Kg}^{-1}$  gliadin) were added to 900  $\mu\text{L}$  TRIS buffer where individual **S4** supports were submerged. After 60 min. at 25  $^{\circ}\text{C}$ , the fluorescence of the rhodamine B delivered was measured at 575 nm ( $\lambda_{\text{ex}}$  555 nm).

#### 7.3.4.6 Gliadin detection in realistic samples

For these experiments, mijo ethanolic extract solutions were initially doped with PWG gliadin (250  $\mu\text{g Kg}^{-1}$ ). Then, different and increasing concentrations of PWG gliadin (0 – 600  $\mu\text{g Kg}^{-1}$ ) were spiked into the same mijo extracts and volume were completed to 1 mL with TRIS buffer. Finally, the response of individual **S4** supports submerged in each one of the solutions were studied. After 60 min. at 25  $^{\circ}\text{C}$ , the fluorescence of the rhodamine B delivered was measured at 575 nm ( $\lambda_{\text{ex}}$  555 nm). The expected initial gliadin concentration (250  $\mu\text{g Kg}^{-1}$ ) was then determined by the standard addition method.

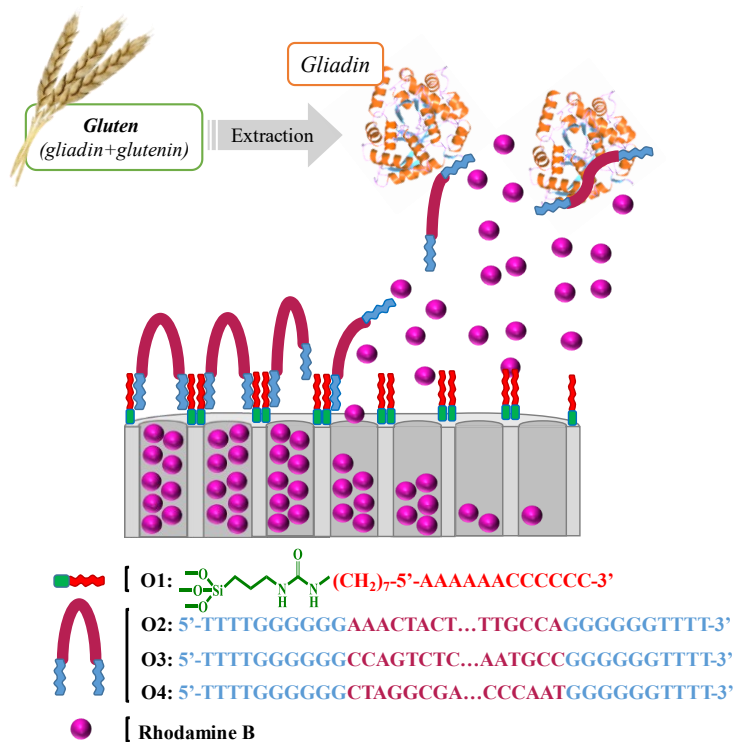
#### 7.3.4.7 Validation in gluten containing food samples

**S4** response was evaluated in real commercial samples. For that, 100  $\mu\text{L}$  of extracts of different food samples (with and without gluten), prepared according procedure detailed in 2.4.2, were added to **S4** supports in a final volume of 1 mL of TRIS buffer at 25  $^{\circ}\text{C}$ . Rhodamine B delivery from the supports was measured after 60 min at 575 nm ( $\lambda_{\text{ex}}$  555 nm). Assay was done in triplicate.

## 7.4 Results and Discussion

### 7.4.1. Preparation and characterization of the sensing supports

Commercially available NAA supports were first loaded with the fluorescent dye rhodamine B and then the external surface was functionalized 3-ICPTS resulting in the preparation of the **S0** support. Subsequently, the amino-modified oligonucleotide **O1** was attached to **S0** through the formation of a urea bond via reaction of the isocyanate active groups in **S0** and the oligonucleotide **O1**, to give **S1**. Finally, aptamers **O2-O4** [28, 44] were used as caps



**Scheme 1:** Scheme of the gated support. The material capped with the selected oligonucleotide sequences (**O2**, **O3** and **O4**) deliver the entrapped dye in the presence of gliadin.

The final solids (i.e **S2**, **S3** and **S4**) remain capped (*vide infra*) due to the steric hindrance resulting from the interaction of aptamers **O2**, **O3** or **O4** over

the **S1** support via hybridization with a short complementary sequence included in the amino-modified sequence **O1** (see Scheme 1). In the prepared final solids, the presence of the target gliadin protein is expected to displace the capping oligonucleotide chains (**O2-O4**) allowing cargo release, which finally would result in a fluorescence emission enhancement in the solution (Scheme 1). This behavior is expected to happen as consequence of the higher affinity between aptamers **O2-O4** and gliadin when compared with the affinity between **O2-O4** and the functionalized NAA support. In contrast, when gliadin is absent, the materials would keep cargo encapsulated, with no subsequent changes in fluorescence emission.

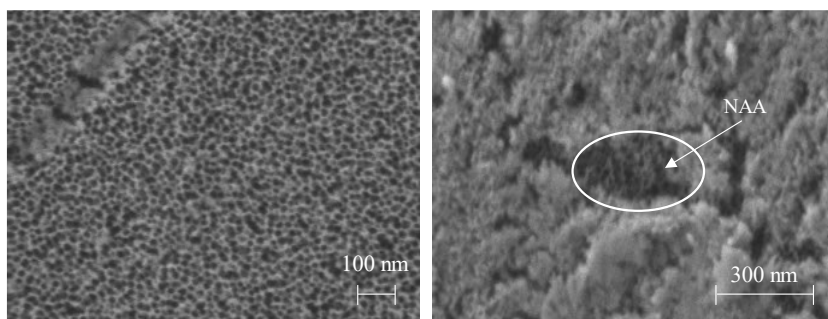


**Figure 1:** FESEM images of support **S0** and **S4**. An organic layer is observed in **S4**, whereas the characteristic porous framework of the NAA is still observed in certain areas.

NAA and the prepared supports **S0-S4** were characterized by FESEM and EDX analyses. The NAA (InRedox®) is an anodic aluminum oxide film over 0.1 mm thick aluminum layer with pore density of ca.  $9 \cdot 10^{11} \text{ cm}^{-2}$ , in which the pore entrances present a funnel-like shape that gradually narrows from sizes of 20-30 nm, at the top of the funnel, to 5 nm size at the bottom. This gradual decrease in size from top to bottom represents a profundity of approximately 3 times the pore diameter, and below this depth, the pore structure becomes uniform along 10  $\mu\text{m}$ . The FESEM images of the starting NAA confirmed the porous structure and revealed, for solids **S1-S4**, the presence of an organic layer on the top of the pores, in which the characteristic porous framework can still be visualized in certain areas, confirming the preservation of the nanoporous structure in the final supports after the functionalization and capping processes (Figure 1).

Moreover, organic content in **S0-S4** was analyzed by energy dispersive X-ray spectroscopy (Table 1). A high carbon C/AI ratio was found in solid **S1**, due to the high loading capacity of NAA material, which increases in solids **S2**, **S3** and **S4** as consequence of the addition of the capping oligonucleotides **O2**, **O3** and **O4**, respectively. Solids **S2-S4** also show a significant increase in the N/AI and P/AI ratios attributed to the presence of the oligonucleotides. In addition, from extraction experiments, the concentration of rhodamine B in the final materials was calculated to be 4 mg/g NAA.

**Table 1.** C/AI, N/AI and P/AI ratios from EDX studies for **S0**, **S1**, **S2**, **S3** and **S4**.

<b>Solids</b>	<b>C/AI</b>	<b>N/AI</b>	<b>P/AI</b>
<b>S0</b>	1.00	-	-
<b>S1</b>	0.52	0.03	0.01
<b>S2</b>	0.65	0.17	0.06
<b>S3</b>	0.60	0.11	0.03
<b>S4</b>	0.75	0.14	0.04

#### 7.4.2 Delivery kinetics

In a first step, the response of the **S2-S4** supports in the presence of PWG gliadin standard was studied. In a typical experiment, two independent supports were submerged in TRIS buffer. Then, a gliadin suspension ( $100 \text{ mg Kg}^{-1}$ ) was added to one of the supports whereas TRIS buffer was added to the other. Both solutions were maintained at  $25 \text{ }^\circ\text{C}$  and aliquots were taken at scheduled times (0, 15, 30, 45 and 60 min). Cargo release was then determined by the emission of the rhodamine B dye in the solution at 575 nm ( $\lambda_{\text{ex}} = 555 \text{ nm}$ ). Typical delivery profiles for **S2**, **S3** and **S4** are shown in Figure 2a, 2b and 2c, respectively. The best results were obtained for **S2** and **S4**. In these cases, there was a poor cargo release in the absence of the PWG gliadin standard, whereas in its presence a sustained payload delivery was observed. For **S3** an enhanced cargo release was also observed in the presence of gliadin, however in this case, the oligonucleotide was unable to significantly inhibit cargo delivery in the absence of the protein. These different behaviours in the capping and delivery ability of the oligonucleotides are most likely related to differences in their 3D conformation adopted when attached on the NAA surface and in the relative

affinity of the **O2-O4** oligonucleotides for the NAA surface and gliadin. Taking into account these results, further optimization assays were carried out only with supports **S2** and **S4**.

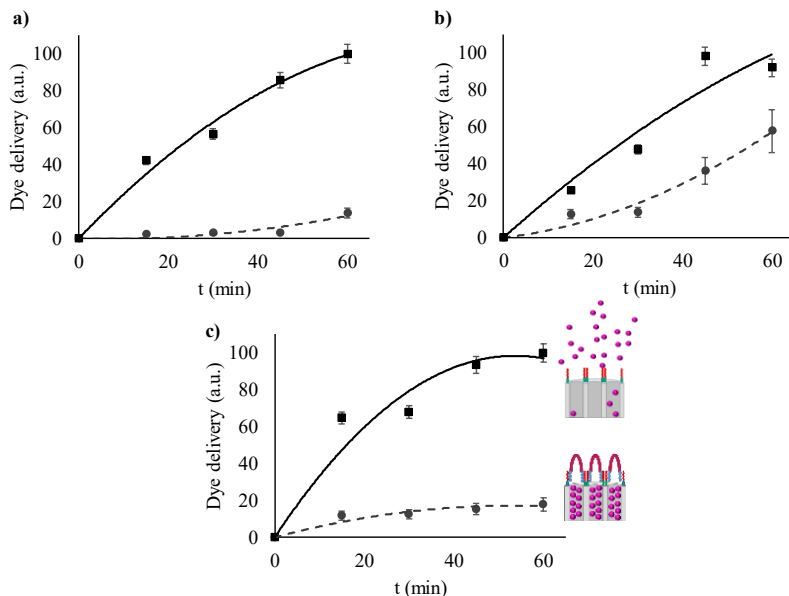


**Figure 2.** Release profile of rhodamine B from functionalized NAA in the presence (solid line) and the absence (dotted line) of gliadin protein in hybridization buffer for a) **S2**, b) **S3** and c) **S4**.

#### 7.4.3 Analytical performance: Sensitivity and specificity studies

In a further step, an evaluation of the sensitivity of supports **S2** and **S4** was undertaken. For this, the response of the materials to different and growing concentrations of PWG gliadin standard in a mixture of ethanol - TRIS buffer 15:85 (v/v) was studied. The limit of detection (LOD) was established at the intersection of the two regression lines that defined the amount of delivered rhodamine B from the sensor in the concentration range tested (Figure 3a, 3b). LOD which was calculated to be  $100 \mu\text{g Kg}^{-1}$  for both **S2** and **S4**, is two orders of magnitude lower than the threshold value of  $20 \text{ mg Kg}^{-1}$  established by the *Codex Alimentarius Commission* (*vide ante*) and in agreement with other commercially available methodologies [22]. Although obtained LODs are higher than those obtained for the above cited ELISA, QCM analysis and SPR

sensors, the simplicity provided by the developed materials positions **S2** and **S4** as good alternatives for gluten point-of-care detection. According to the results obtained, **S4** shows a better behaviour in terms of a minor and stable residual leakage (*vide ante*).

In addition, it was calculated that for **S4**  $100 \mu\text{g Kg}^{-1}$  of gliadin triggered the release of an average of  $2.5 \cdot 10^{12}$  molecules of rhodamine B, which means a signal amplification of  $10^{11}$  reporter molecules per each  $\mu\text{g Kg}^{-1}$  of enzyme. Among others, geometry of the pores and probe-to-target affinity conditionate this amplification, since they determine the total amount of encapsulated cargo and the efficiency of the uncapping process, respectively.

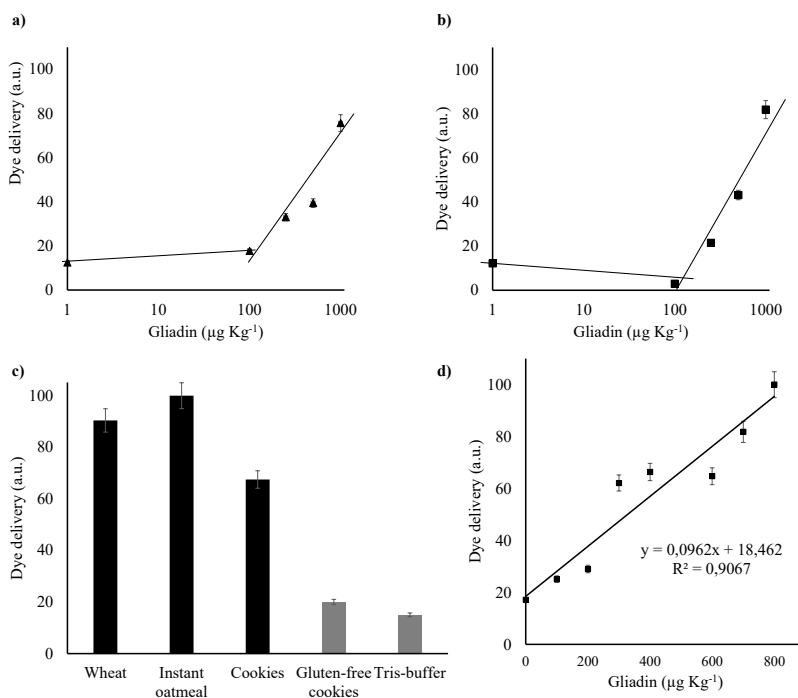


**Figure 3.** a) **S2** and b) **S4** materials response in the presence of growing concentrations of gliadin at 60 min; c) Delivery of rhodamine from **S4** in extracts of different commercially available products at 60 min; d) Response of **S4** to the presence of mijo extracts doped with different concentration of gliadin.

Further experiments with real samples from food extracts were undertaken with **S4**. In a typical experiment, different food extracts (flours, flour-mixtures,

instant oatmeal and cookies with and without gluten) were diluted in TRIS buffer and **S4** was submerged in these solutions. Rhodamine B after 60 min was then measured (Figure 3c). A poor dye delivery (less than 20 %) was observed from **S4** in TRIS buffer or with extracts of gluten-free cookies, whereas a clear signal was found for extracts of gluten-containing samples (i.e. wheat, instant oatmeal and cookies). It is important to remark the high selectivity of the developed system, since there is only response in the presence of gliadin protein, which are not affected by the presence of other proteins present in food extracts. This is for instance demonstrated by the equal response observed by gluten-free cookies extract and bare TRIS hybridization buffer (Figure 3c).

#### **7.4.4 Gliadin detection in realistic samples and validation in commercial food supplies**

Afterwards, **S4** ability for gliadin detection and quantification in a more realistic sample was studied. With this aim, gliadin determination in mijo extracts (gluten free) doped with PWG gliadin standard was evaluated employing a standard addition method. For this, independent **S4** materials were submerged in separated mijo extracts, previously doped with 250  $\mu\text{g Kg}^{-1}$  of PWG gliadin standard, that were additionally spiked with different known amounts of a PWG gliadin standard solutions (0, 100, 200, 300, 400, 600, 700 and 800  $\mu\text{g Kg}^{-1}$ ). As it could be seen, the dye delivered is proportional to the amount of gliadin in the 0 - 800  $\mu\text{g Kg}^{-1}$  range and fits the linear equation  $y = 0.0962 \cdot x + 18.462$  with  $R^2$  of 0.9067 (Figure 3d), and confirm both that dye delivery from **S4** is consequence of the presence of gliadin and that **S4** is able to respond to gliadin concentration in realistic samples. From the interception of the curve with the x axis, an initial gliadin concentration in the gliadin-doped mijo extracts of 200  $\mu\text{g Kg}^{-1}$  was determined, achieving 80 % recovery.

Besides, and as a particularity of these systems that is worth mentioning, previous studies demonstrated the re-usability of the NAA support by calcination of already used gated-NAA systems [46, 47]. In this present work, regeneration of used gated-NAA was undertaken through calcination to remove organic matter, and the calcinated NAA were used as starting materials to prepare new gated NAA for gluten detection. The NAA supports were reused up to 3 times obtaining similar results. Moreover, preliminary stability studies

carried out with aptamer-gated nanomaterials have demonstrated that this type of nanosensors can be stored up to 12 weeks without any changes in their sensing performance [48].

**Table 2:** Results from extracts obtained from gluten and gluten-free commercial products analysed using the gated material S4 compared with labelling information.

#Sample	Origin	RIDA®QUICK Gliadin <sup>a</sup>	S4 <sup>b</sup>
1	Wheat flour 1	+	+
2	Wheat flour 2	+	+
3	Strength flour 1	+	+
4	Strength flour 2	+	+
5	Integral flour 1	+	+
6	Integral flour 2	+	+
7	Instant oatmeal 1	+	+
8	Instant oatmeal 2	+	+
9	Digestive cookies 1	+	+
10	Digestive cookies 2	+	+
11	Breakfast cookies 1	+	+
12	Gluten-free cookies 1	-	-
13	Gluten-free cookies 2	-	-
14	Gluten-free mix flours 1	-	-
15	Gluten-free mix flours 2	-	-

a) Samples were considered positives (+) when two coloured bands (the blue control and the red test band) were visible in the result window.

b) Samples were considered positives (+) when the fluorescence intensity at 575 nm ( $\lambda_{ex} = 555$  nm) was higher than the average fluorescence of the negative controls plus three times their standard deviation.

Encouraged for the results above the presence of gluten or not in gluten-containing and gluten-free commercial products was determined using **S4**. For this, mijo, rice, oat and wheat-based food stuff were extracted according reported procedures [43] and **S4** was submerged in these solutions for gluten detection. In these experiments, samples were considered positives (+) when



the fluorescence intensity at 575 nm ( $\lambda_{\text{ex}} = 555$  nm) was higher than the average fluorescence of the negative controls plus three times their standard deviation. Gliadin was also assessed in the complete set of food extracts using a commercially available immunochemical test for the detection of gliadin (RIDA@QUICK Gliadin, R-Biopharm, License num. 101702) to validate the results obtained with **S4**.

An excellent correlation was observed between the RIDA@QUICK Gliadin results and those obtained when using **S4**. From these data, a 100 % of selectivity, sensitivity and accuracy was found for **S4** as a simple system to detect gluten in food samples. Sensitivity and selectivity parameters were calculated according the statistical definition provided in bibliography through the successes and errors regarding the gluten content data provided by RIDA@QUICK Gliadin validating test [49]. The developed sensor differs greatly from the commercial RIDA@QUICK Gliadin test used as a validation technique. One of the major differences is that developed **S4** sensor consists of a reusable NAA support and an aptamer. In contrast, the RIDA@QUICK Gliadin test uses antibodies that are more expensive and complex to prepare. On the other hand, RIDA@QUICK Gliadin uses visible colorimetric signalling, unlike the **S4** sensor, which currently requires the use of a fluorescence spectrometer. Both require sample extraction processes and, according to the results obtained in Table 2, both present identical results in terms of real samples analysis. Therefore, it can be affirmed that the presented **S4** sensor, even though it is in an initial development phase, has great potential as a reference food control tool, to become a real, rapid, accurate and simple approach for food safety applications.

## 7.5 Conclusions

A new aptasensor designed for the detection of gluten water soluble protein gliadin is developed. The sensing system consists of a NAA support loaded with rhodamine B and capped with a specific aptamer for gliadin recognition. The presence of this protein results in a displacement of the capping aptamer and in the subsequent pore opening and release of the entrapped fluorophore. The resulted LOD ( $100 \mu\text{g Kg}^{-1}$ ), selectivity and time response (60 minutes) demonstrate the potential application of the probe for the detection of gluten.

The obtained response is proportional to gliadin concentration in the range 100-800  $\mu\text{g Kg}^{-1}$  and the aptasensor has been validated in real food samples. Moreover, the simplicity, rapidness and cost of the presented sensor make it a potent alternative for traditional gluten detection tools. We believe our system opens new concepts for the development of simple sensors with the capability of being used at sites without infrastructure or specialized personnel for the detection of gluten. Further implementation of this system could provide a reliable detection kit to be used by CD patients and for the control of gluten-free products and gluten contamination.

## 7.6 Acknowledgments

The authors want to thank the Spanish Government RTI2018-100910-B-C41 (MCUI/AEI/FEDER, UE) and the Generalitat Valenciana (project PROMETEO/2018/024) for support. L.P. thanks to Ministerio de Economía, Industria y Competitividad for his FPI grant. S.S.-F. thanks CIBER and ISCIII for her Sara Borrell contract. The authors also thank the Electron Microscopy Service at the UPV for support.

### Declaration of competing interest

The authors declare that they have no known competing financial interests or personal relationships that could have appeared to influence the work reported in this paper.

### CRedit authorship contribution statement

Luis Pla: Investigation; Methodology; Writing - original draft, Elena Aznar: Investigation; Funding acquisition, Félix Sancenón: Investigation; Supervision, M. Carmen Martínez-Bisbal: Conceptualization; Funding acquisition, Writing - review & editing, Ramón Martínez-Máñez: Conceptualization, Funding acquisition, Writing - review & editing, Sara Santiago-Felipe: Investigation; Methodology; Writing - original draft.

## References

- [1] J.A. Tye-Din, H.J. Galipeau, D. Agardh, Celiac disease: A review of current concepts in pathogenesis, prevention, and novel therapies, *Front. Pediatr.* 6 (2018) 1–19.

- [2] R. Kuja-Halkola, B. Lebwohl, J. Halfvarson, C. Wijmenga, P.K.E. Magnusson, J.F. Ludvigsson, Heritability of non-HLA genetics in coeliac disease: A population-based study in 107 000 twins, *Gut*. 65 (2016) 1793–1798.
- [3] M.S. Losowsky, A history of coeliac disease, *Dig. Dis.* 26 (2008) 112–120.
- [4] J.R. Biesiekierski, What is gluten?, *J. Gastroenterol. Hepatol.* 32 (2017) 78–81.
- [5] F. Rasheed, Structural architecture and solubility of native and modified gliadin and glutenin proteins: non-crystalline molecular and atomic organization, *J. Am. Dent. Assoc.* (1939) 4 (2014) 2051.
- [6] B.G. Thewissen, I. Celus, K. Brijs, J.A. Delcour, Foaming properties of Wheat Gliadin, *J. Agric. Food Chem.* 59 (2011) 1370–1375.
- [7] A. Codex Stan, Codex standard for foods for special dietary use for persons intolerant to gluten, *Codex Alimentarius*. (2015) Codex Stan 118-1979. Amendment: 1983 and 2015. Rev.
- [8] B. Neuenahr-Ahrweiler, Report of the 29th session of the Codex Committee on nutrition and foods for special dietary uses, Geneva, 2008.
- [9] A. Codex Stan, General standard for the labelling of prepackaged foods, Rome, 1985.
- [10] E. Commission, Commission Implementing Regulation (EU) 828/2014, 2014. [https://eur-lex.europa.eu/eli/reg\\_impl/2014/828/oj](https://eur-lex.europa.eu/eli/reg_impl/2014/828/oj) (accessed April 15, 2020).
- [11] H.P. and F.B. Bureau of Chemical Safety, Food Directorate, Health Canada's Position on Gluten-Free Claims, Canada, 2012.
- [12] Food and Drug Administration, HHS, Food labeling: gluten-free labeling of foods. Final rule., *Federal Register*. 78 (2013) 47154–79.
- [13] A.N.Z.F. Standards, Australia New Zealand Food Standards Code – Standard 1.2.7 – Nutrition, health and related claims, Attorney-General's Department, 2016.
- [14] N. Gujral, M.R. Suresh, H.H. Sunwoo, Quantitative double antibody sandwich ELISA for the determination of gliadin, *J. Immunoassay Immunochem.* 33 (2012) 339–351.

- [15] M.C. Mena, M. Lombardía, A. Hernando, E. Méndez, J.P. Albar, Comprehensive analysis of gluten in processed foods using a new extraction method and a competitive ELISA based on the R5 antibody, *Talanta*. 91 (2012) 33–40.
- [16] Allergen Control Group Inc. (Canadian Celiac Association), White Paper : The Current State of Scientific Knowledge about Gluten, Milton (Ontario), 2018.
- [17] Joint FAO/WHO Codex Alimentarius Commission. Session (26th : 2003 : Rome), Joint FAO/WHO Food Standards Programme., Food and Agriculture Organization of the United Nations., World Health Organization., Report of the Twenty-Sixth Session, Rome, 30 June - 7 July 2003, World Health Organization, Food and Agriculture Organization of the United Nations, 2003.
- [18] C.D. Peter Koehler, Theresa Schwalb, Ulrike Immer, Markus Lacorn, Paul Wehling, AACCI Approved Methods Technical Committee Report: Collaborative Study on the Immunochemical Determination of Partially Hydrolyzed Gluten Using an R5 Competitive ELISA, *Cereal Food World*. 58 (2013) 113-117.
- [19] P.T. Chu, C.S. Lin, W.J. Chen, C.F. Chen, H.W. Wen, Detection of gliadin in foods using a quartz crystal microbalance biosensor that incorporates gold nanoparticles, *J. Agric. Food Chem*. 60 (2012) 6483–6492.
- [20] M. Soler, M.C. Estevez, M. de L. Moreno, A. Cebolla, L.M. Lechuga, Label-free SPR detection of gluten peptides in urine for non-invasive celiac disease follow-up, *Biosens. Bioelectron*. 79 (2016) 158–164.
- [21] V. V. Doña, C.A. Fossati, F.G. Chirido, Interference of denaturing and reducing agents on the antigen/antibody interaction. Impact on the performance of quantitative immunoassays in gliadin analysis, *Eur. Food Res. Technol*. 226 (2008) 591–602.
- [22] SureFood® ALLERGEN Gluten - Food & Feed Analysis, (n.d.). <https://food.r-biopharm.com/products/surefood-allergen-gluten-2/> (accessed April 16, 2020).

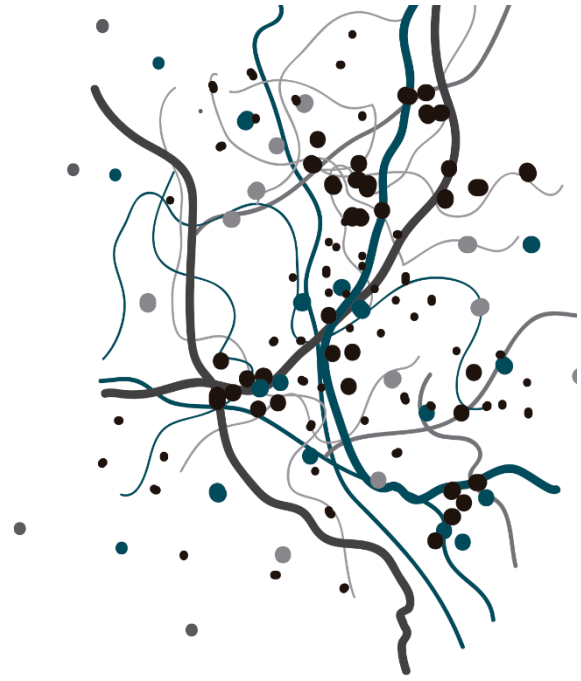
- [23] A. Pinto, P.N. Polo, O. Henry, M.C.B. Redondo, M. Svobodova, C.K. O'Sullivan, Label-free detection of gliadin food allergen mediated by real-time apta-PCR, *Anal. Bioanal. Chem.* 406 (2014) 515–524.
- [24] J.R. Mujico, L. Dekking, Y. Kooy-Winkelaar, R. Verheijen, P. Van Wichen, L. Streppel, N. Sajic, J.W. Drijfhout, F. Koning, Validation of a new enzyme-linked immunosorbent assay to detect the triggering proteins and peptides for celiac disease: Interlaboratory study, *J. AOAC Int.* 95 (2012) 206–215.
- [25] K.L. Fiedler, S.C. McGrath, J.H. Callahan, M.M. Ross, Characterization of grain-specific peptide markers for the detection of gluten by mass spectrometry, *J. Agric. Food Chem.* 62 (2014) 5835–5844.
- [26] C. Diaz-Amigo, B. Popping, Labeling Regulations, Detection Methods, and Assay Validation, *J. AOAC Int.* 95 (2012) 337–348.
- [27] M. Soler, M.C. Estevez, M. de L. Moreno, A. Cebolla, L.M. Lechuga, Label-free SPR detection of gluten peptides in urine for non-invasive celiac disease follow-up, *Biosens. Bioelectron.* 79 (2016) 158–164.
- [28] S. Amaya-González, N. de-los-Santos-Álvarez, A.J. Miranda-Ordieres, M.J. Lobo-Castañón, Aptamer-based analysis: A promising alternative for food safety control, *Sensors.* 13 (2013) 16292–16311.
- [29] Y.S. Kim, M.B. Gu, Advances in aptamer screening and small molecule aptasensors, *Adv. Biochem. Eng. Biotechnol.* 140 (2014) 29-67.
- [30] S. Amaya-González, N. De-Los-Santos-Álvarez, A.J. Miranda-Ordieres, M.J. Lobo-Castañón, Aptamer binding to celiac disease-triggering hydrophobic proteins: A sensitive gluten detection approach, *Anal. Chem.* 86 (2014) 2733–2739.
- [31] S. Amaya-González, N. de-los-Santos-Álvarez, A.J. Miranda-Ordieres, M.J. Lobo-Castañón, Sensitive gluten determination in gluten-free foods by an electrochemical Aptamer-based assay, *Anal. Bioanal. Chem.* 407 (2015) 6021–6029.
- [32] B.B. Tasbasi, B.C. Guner, M. Sudagidan, S. Ucak, M. Kavruk, V.C. Ozalp, Label-free lateral flow assay for *Listeria monocytogenes* by aptamer-gated release of signal molecules, *Anal. Biochem.* 587 (2019) 113449.

- [33] F. Sancenón, L. Pascual, M. Oroval, E. Aznar, R. Martínez-Máñez, Gated Silica Mesoporous Materials in Sensing Applications, *ChemistryOpen*. 4 (2015) 418–437.
- [34] L. Pla, B. Lozano-Torres, R. Martínez-Máñez, F. Sancenón, J. V. Ros-Lis, Overview of the Evolution of Silica-Based Chromo-Fluorogenic Nanosensors, *Sensors*. 19 (2019) 5138.
- [35] C. Hofmann, A. Duerkop, A.J. Baeumner, Nanocontainers for Analytical Applications, *Angew. Chem. Int. Ed.* 58 (2019) 12840–12860.
- [36] C. Coll, R. Casasús, E. Aznar, M.D. Marcos, R. Martínez-Máñez, F. Sancenón, J. Soto, P. Amorós, Nanoscopic hybrid systems with a polarity-controlled gate-like scaffolding for the colorimetric signalling of long-chain carboxylates, *ChemComm.* (2007) 1957–1959.
- [37] A. Ribes, E. Aznar, S. Santiago-Felipe, E. Xifré-Pérez, M.A. Tormo-Más, J. Pemán, L.F. Marsal, R. Martínez-Máñez, Selective and sensitive probe based in oligonucleotide-capped nanoporous alumina for the rapid screening of infection produced by *Candida albicans*. *ACS Sensors*. 4 (2019) 1291-1298.
- [38] L. Pla, S. Santiago-Felipe, M.Á. Tormo-Mas, J. Pemán, F. Sancenón, E. Aznar, R. Martínez-Máñez, Aptamer-capped nanoporous anodic alumina for *Staphylococcus aureus* detection, *Sensor. Actuat. B-Chem.* 320 (2020) 128281.
- [39] R. Bhat, I. García, E. Aznar, B. Arnaiz, M.C. Martínez-Bisbal, L.M. Liz-Marzán, S. Penadés, R. Martínez-Máñez, Lectin-gated and glycan functionalized mesoporous silica nanocontainers for targeting cancer cells overexpressing Lewis X antigen, *Nanoscale*. 10 (2018) 239–249.
- [40] R.R. Castillo, M. Vallet-Regí, Functional mesoporous silica nanocomposites: Biomedical applications and biosafety, *Int. J. Mol. Sci.* 20 (2019) 929.
- [41] G. Xu, Q. Xie, Z. Chen, F. Luo, B. Qiu, L. Guo, Z. Lin, A smart and sensitive sensing platform to monitor the extracellular concentration of hydrogen peroxide in rat brain microdialysates during pathological processes based on mesoporous silica nanoparticles, *Anal. Methods*. 10 (2018) 4361-4366.

- [42] E. Climent, D. Gröninger, M. Hecht, M.A. Walter, R. Martínez-Máñez, M.G. Weller, F. Sancenón, P. Amorós, K. Rurack, Selective, sensitive, and rapid analysis with lateral-flow assays based on antibody-gated dye-delivery systems: The example of triacetone triperoxide, *Chem. Eur. J.* 19 (2013) 4117–4122.
- [43] E. García, M. Llorente, A. Hernando, R. Kieffer, H. Wieser, E. Méndez, Development of a general procedure for complete extraction of gliadins for heat processed and unheated foods, *Eur. J. Gastroenterol. Hepatol.* 17 (2005) 529–539.
- [44] S. Amaya-González, N. de-los-Santos-Álvarez, A. Miranda-Ordieres, M. Lobo-Castañón, Aptamer-Based Analysis: A Promising Alternative for Food Safety Control, *Sensors.* 13 (2013) 16292–16311.
- [45] A. Pinto, P.N. Polo, O. Henry, M.C.B. Redondo, M. Svobodova, C.K. O'Sullivan, Label-free detection of gliadin food allergen mediated by real-time apta-PCR, *Anal. Bioanal. Chem.* 406 (2014) 515–524.
- [46] À. Ribes, E. Xifré-Pérez, E. Aznar, F. Sancenón, T. Pardo, L.F. Marsal, R. Martínez-Máñez, Molecular gated nanoporous anodic alumina for the detection of cocaine, *Sci. Rep.* 6 (2016) 1–9.
- [47] L. Pla, E. Xifré-Pérez, À. Ribes, E. Aznar, M.D. Marcos, L.F. Marsal, R. Martínez-Máñez, F. Sancenón, A *Mycoplasma* Genomic DNA Probe using Gated Nanoporous Anodic Alumina, *ChemPlusChem.* 82 (2017) 337–341.
- [48] À. Ribes, S. Santiago-Felipe, A. Bernardos, M.D. Marcos, T. Pardo, F. Sancenón, R. Martínez-Máñez, E. Aznar, *ChemistryOpen.* 6 (2017) 653–659.
- [49] R. Trevethan, Sensitivity, Specificity, and Predictive Values: Foundations, Pliabilities, and Pitfalls in Research and Practice, *Front. Public Health.* 5 (2017) 307.







# 8

## Summary of the Results and General Discussion



Summary of the results and general discussion:

The research carried out in this PhD thesis has aimed the development of versatile and innovative nanodevices for sensing applications in diagnosis and food control by the implementation of molecular gates over nanostructured alumina supports. All described systems share a general structure in terms of preparation and working. This is, a mesoporous support accurately functionalized for the attachment (covalently or electrostatically) of oligonucleotide sequences that act like gatekeepers and modulate the diffusion of an entrapped indicator, whether the target is present or not. In addition, the proper working of these sensing probes have been successfully validated in real samples, taking a step forward in its potential application. These are the developed sensing systems:

## » Diagnosis application:


1. Development of a sensing system for the detection of *Mycoplasma fermentans* bacterium.
2. Optimization and validation of a gated nanomaterial for a rapid and reliable detection of bacterium *Staphylococcus aureus* bacterium.
3. Development of a new *Pneumocystis jirovecii* fungus detection nanoprobe for rapid analysis of clinical samples.

## » Food control application:

4. Development of a tool for gluten control in processed and non-processed food products.

Table 7 summarizes main features of the developed sensing systems and Table 8 collects all the oligonucleotide chain sequences employed

**Table 7:** Summary of the developed systems with the most remarkable sensing features.

System	Target	LOD	Sensitivity	Specificity	Temp. °C	Real Samples	Sample Pretreatment	Patent
1	<i>Mycoplasma fermentans</i>	20 DNA copies· $\mu\text{L}^{-1}$	-	-	25	1	No	-
2	<i>Staphylococcus aureus</i>	2-5 CFU (buffer&blood)	100 %	100 %	25	25	No	
3	<i>Candida auris</i>	-	-	-	-	-	-	-
4	<i>Pneumocystis jirovecii</i>	0.001 $\mu\text{M}$	100/70 %	100/78 %	37	12/21	No	-
5	Gluten	100 ppb	100 %	100 %	25	16	Yes	-

**Table 8:** List of the whole oligonucleotide sequences used.

Target	Name	5'→3' Sequence	Num. bp.
<i>Mycoplasma fermentans</i>	O1	NH <sub>2</sub> -(CH <sub>2</sub> ) <sub>6</sub> -GACTACCAGGGTATC	15
	O2	AAGCGTGGGGAGCAAACAGGATTAGATAC CCTGGTAGTC	39
<i>Staphylococcus aureus</i>	O1	NH <sub>2</sub> -(CH <sub>2</sub> ) <sub>6</sub> -AAAAACCCCC	12
	O2	TTTTGGGGGGTCCCTACGGCGCTAACCCC CCCAGTCCGTCTCCAGCCTCACACCGC CACCGTGCTACAACGGGGGGTTTT	82
<i>Candida auris</i>	-	-	-
	-	-	-
	-	-	-
<i>Pneumocystis jirovecii</i>	O1	GAAGGGAAACAGCCCAG	17
	O2	GACAAAGGGAAAG-TTTT- GAAAGGGAAACAGCCCAG	35
	O3	AGAGCAGAAAGGA-TTTT- GAAAGGGAAACAGCCCAG	35
	O4	CTGGGCTGTTCCCTTTC	18
<i>Gluten</i>	O1	NH <sub>2</sub> -(CH <sub>2</sub> ) <sub>6</sub> -AAAAACCCCC	12
	O2	TTTTGGGGGGAACTACTAAGTAAG ATCACGCAGCACTAAACGACGTAGTTGCC AGGGGGGTTTT	69
	O3	TTTTGGGGGGCCAGTCTCCC GTTACCGC GCCTACACATGTCTGAATGCCGGGGGTT TT	60
	O4	TTTTGGGGGGCTAGGCGAAATATAGCTAC AACTGTCTGAAGGCACCCAATGGGGGGTT TT	60

Nowadays techniques used in the health system for diagnosis are based, mainly, on the direct identification of a disease through the patient's clinical or symptomatic picture. Moreover, many diseases present wide and variable symptomatology, so validated analysis techniques are additionally and commonly used. Besides, processes to obtain samples are usually associated to invasive interventions (in greater or minor grade). Unfortunately, results provided for some of these techniques are certainly ambiguous and are obtained, generally, after long analytical processes, which could be definitive for the surveillance and recovering of the patient. This is also so for diseases caused by a specific microorganism and, in particular, experts have expressed the decline in the number of expertise personnel needed for the identification of microorganisms as well as the lack of available technologies for their accurate detection.<sup>142</sup> Techniques currently used for the identification of pathogenic microorganisms can be divided in the following groups (Figure 31):

- » Immunologic and serologic detection. Antibodies are widely used in diagnosis techniques through ELISA techniques. Along the last decades, several analytical kits have been developed for the specific detection of targets of interest. However, these techniques require experience and are associated with expensive reagents. Serologic methodologies, by their side, present other important inconveniences. In one hand, organism needs some time to adopt a significant response since the infection moment; and in the other hand, the null response induced by immunosuppressed patients.
- » Microbiological culturing: Liquid media (broth) or solid (solid agar). A number of organisms require specific environmental conditions for their proliferation. Incubation times range from 12 hours to 6-8 weeks, and some of them need aerobic conditions. Detection is visually accomplished, it is not specific and depends largely on personnel experience. Identification needs, in many scenarios, a second confirmation through other validated technique or a specific culture.
- » Genetics. It is based on the detection of unique nucleotide sequences (DNA or RNA) of a specific microorganism that causes a determined

---

<sup>142</sup> L. B. Wickes and N. P. Wiederhold, *Nature communications*, **2018**, 9, 5135-5148.

disease. The technology developed for PCR analysis (qualitative and quantitative) allows amplification and identification of specific DNA and RNA sequences. Their main advantages are sensitivity and specificity, nevertheless analysis time are very long, the equipment and reagents are expensive, and processes demand highly experienced personnel.

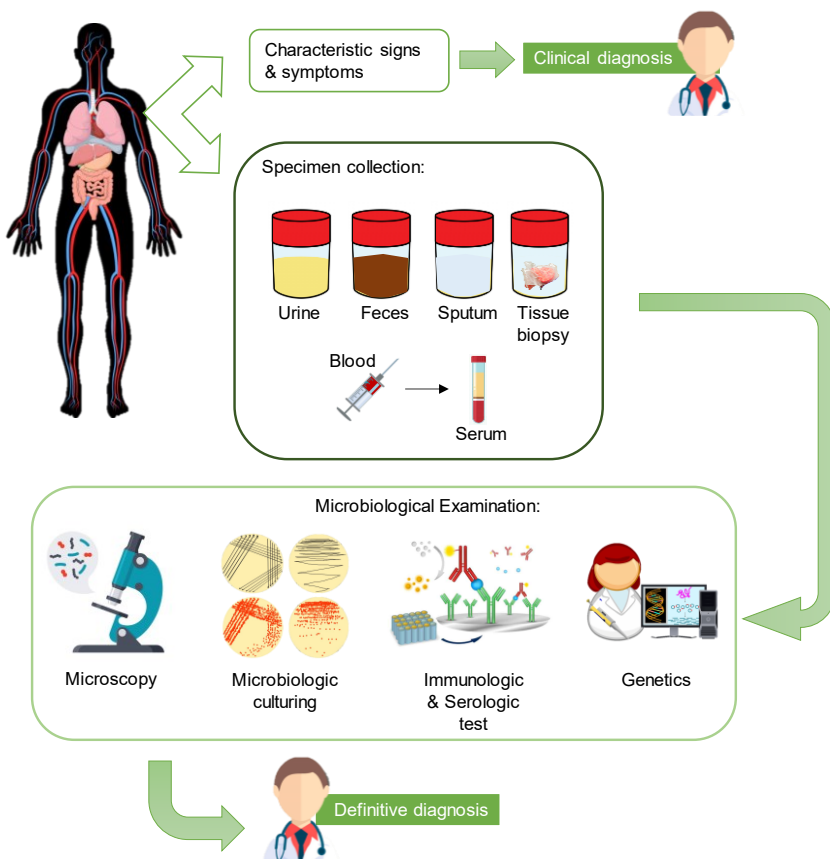


**Figure 31:** Laboratory procedures used in confirming a clinical diagnosis of infectious disease. <sup>143</sup>

<sup>143</sup> Medical Microbiology. 4th edition. Baron S, editor. Galveston (TX): University of Texas Medical Branch at Galveston; 1996.

To sum up, the development of early, easy-to-use and low-cost diagnosis tools for bacterial and fungal detection are critical to manage effective treatments.<sup>144</sup>

Analogously to diagnosis, food control is considered one of the basis of the healthcare system. In EU, although citizens feel protected, around 71 % questioned citizens thought that EU authorities must work harder to guarantee security in alimentary products and said that food safety is among their concerns.<sup>145</sup> The good condition of the products consumed, as well as the absence of toxics and/or allergens, are presupposed in developed countries, however, this is not always the case.

It is known that there are companies that voluntarily cheat consumers looking for economic benefits provided by a particular labelling. This is the case of low-gluten and gluten free products, which are directed to gluten sensitive and celiac population and are, generally, more expensive. Several cases of label fraud come to light usually were products present greater gluten quantities than expressed. Consequently, celiac suffers the lack of a suitable and rapid tool for the detection of this allergen in the industry, but also in the domestic ambit.

Nowadays, gluten detection is mainly accomplished by three different techniques (see Figure 32):<sup>146</sup>

- » Immunologic: ELISA tests based on mono-and polyclonal antibodies against prolamin proteins. These assays are complex and relatively expensive as antibodies are not cheap.
- » Genetics: Amplification and replication of specific DNA/RNA fragments. Do not target proteins, but the gene that encodes the protein. DNA content may not correlate with gluten concentration. Useful when immunochemical methods are not suitable.

---

<sup>144</sup> T. R. Kozel and B. Wickes, *Cold Spring Harb Perspect. Med.*, **2014**, *4*, 1-14.

<sup>145</sup> Special Eurobarometer Wave EB91.3, **2019**. EFSA – European Commission

<sup>146</sup> M. A. Bustamante, E. Simón, I. Churrua, M. P. Fernández-Gil, *Nutricional and Analytical Approaches of Gluten-Free Diet in Celiac Disease*, Chapter 3, *SpringerBriefs in Food, Health and Nutrition*, **2017**.



» Proteomics: Nonspecific techniques. Based on separation of proteins and their individual identification.

In all these techniques and due to the complexity of gluten protein matrix, samples have to be subjected to an extraction process to simplify the analysed sample. Basically, this treatment consists on the separation of gliadin protein, the soluble part of gluten, since most of the developed analytical techniques are undertaken in liquid phase.

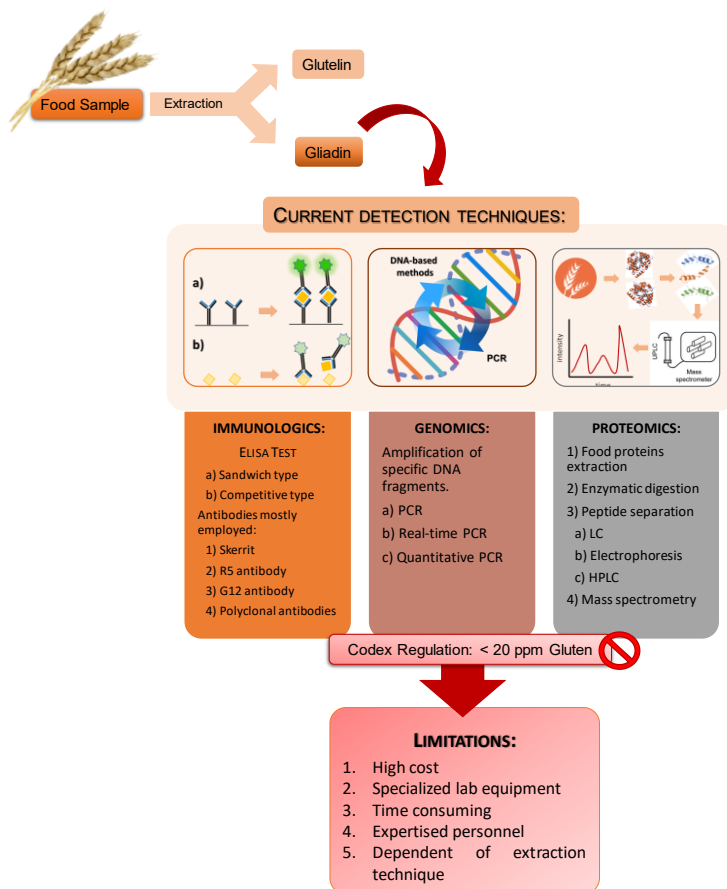


**Figure 32:** Schematic summary of nowadays developed gluten detection techniques.

Although these techniques present several advantages, such as sensitivity or selectivity, there exist numerous disadvantages that make necessary the

development of new detection systems. The commercialized test, besides, are not considered 100 % reliable. Thus, there is a growing need of rapid, reliable and cost-competitive detection techniques in order to assure the consumer security in a globalized market with products that are processed, in a greater or a lesser grade, in countries that do not necessarily share our strict food control systems or by companies that superimpose the economic benefits to the health of the celiac population.

Despite the good qualities shown by traditional techniques employed in diagnosis and food control, the development of new protocols and sensing nanodevices are of importance and this thesis has aimed to contribute in this field. Some of the characteristics of the sensing solids prepared in this thesis are the following:

- » Signal amplification: Few analyte molecules induce the release of a great number of fluorescent reporter molecules (some systems show 1:10<sup>8</sup> analyte:reporter enhancement ratio). This self-amplification allows avoiding long and previous DNA amplification and/or replication processes, which are required for other analytical techniques.
- » Fastness: Gate opening and cargo diffusion, that is, recognition and signaling, are undertaken in less than one hour. Faster response, besides, contributes to a better evaluation.
- » Robustness: Developed systems have been validated in real samples, with a proper working unaffected by complex matrixes.
- » Versatility: Systems have been subtly modified for detecting different species. This means that, it would be possible to prepare multiplexed systems through the combination of mesoporous supports functionalized by different DNA sequences for multi-analyte detection.
- » Cost and easy use: Materials and reagents required are cheap, which improve their potential as an analytical routine tool. These sensing systems are easy to handle, portable and do not require experienced personnel nor expensive instrumentations.

Individually, the developed systems introduced in this thesis present several advantages in comparison with nowadays established methodologies. The

performance of the developed sensing systems are gathered in Table 7 and a brief summary of the results are detailed below.

Dealing with the *Mycoplasma fermentans* nanoprobe our objective was to develop a new platform for an easier use based in a previous work. For this purpose, the mesoporous nanoparticles used in a previously reported work<sup>147</sup> were changed by a NAA film. The recognition mechanism relies in the high affinity between a highly conservative DNA sequence in *M. fermentans* and the oligonucleotide sequence employed as gatekeeper. The presence of *M. fermentans* genomic DNA induces pore opening and delivery of the fluorescent reporter. The sensitivity and selectivity of the new nanoprobe were not affected by the scaffold substitution. Besides, we demonstrated that the NAA support can be reused. The obtained LOD is analogous that reported for other detection procedures based on more sophisticated technologies.

The diagnosis probe for the detection of *Staphylococcus aureus* uses an aptamer as molecular gate, whose structural conformation recognizes the aforesaid bacteria. Savings on time (from typical 3 days culturing to less than 1 hour), as well as its sensitivity in real samples, makes this sensing nanodevice an attractive alternative to nowadays established *Staphylococcus aureus* detection techniques. The system is specific and recognizes *S. aureus* from a great variety of similar *Staphylococcus* species such as *S. conhii*, *S. capitis*, *S. epidermidis*, *S. carnosus*, *S. saprophyticus*, *S. chromogenes*, *S. xylosus*, *S. haemolyticus*, *S. lugdunensis*, *S. hominis* and *S. warneri*, with LOD in the 2-5 range CFU without the need of sample processing. Finally, a validation with 25 real samples from patients provided by the Hospital Universitari I Politènic La Fe de València, showed 100 % sensitivity and specificity.

Given the excellent results obtained, the developed diagnosis system for both *S. aureus* and *C. auris*, have been object of protection by patents.

Lastly, a detection system for fungus *Pneumocystis jirovecii* was prepared. For this purpose, 3 different oligonucleotide sequences that entailed two different structural conformations, *duplex* and *triplex*, when bound to *Pneumocystis* DNA were studied as capping units in NAA supports. The *triplex*

---

<sup>147</sup> L. Pascual, I. Baroja, E. Aznar, F. Sancenón, M. D. Marcos, J. R. Murguía, P. Amorós, K. Rurack, R. Martínez-Mañez, *Chem. Commun.*, **2015**, 51, 1414-1416.

sequence resulted in a more competitive pore closing, and further studies were undertaken with this sequence. The *Pneumocystis jirovecii* pathogen is difficult to detect and, furthermore, there is no culturing process capable of reproducing this fungus, which makes its study difficult. The sensitivity achieved (LOD 1 nM) with the capped sensing material is lower than the concentration usually found in infected patients, while selectivity was successfully validated with other organisms such as *Aspergillus spp.*, *C. albicans*, *C. auris* and *C. tropicalis*. The sensor was tested in 16 real samples from patients provided by Hospital La Fe de València. Moreover, the system is simple and fast.

Finally, and in an attempt to diversity the bunch of application available for these new gated systems, a gluten sensitive nanodevice was developed. As well as in other examples detailed above, the design of the system is based on the highly sensitive and specific interaction between gliadin protein (the soluble part of gluten) and a selected aptamer. A LOD of 100 ppb (much lower than nowadays regulation limits) was achieved and the sensing device was successfully tested in real samples. The cost, analysis time and easiness make this nanoprobe a potential tool for celiac and gluten sensitive consumers.

The obtained sensing nanodevices developed in this thesis are the result of an ambitious multidisciplinary project that cover aspects of materials science, chemistry, biology and clinical. The developed nanodevices demonstrate that the synergistic implementation of molecular gates over nanostructured materials constitutes a potential tool for the detection of analytes of interest, such as bacterium, fungus and allergens. Their performance makes them a realistic and highly competitive alternative against current standard techniques generally used.